

Evaluation Methods for Porous Silicon Gas Sensors

A Thesis
Presented to
The Academic Faculty

by

John DeBoer

In Partial Fulfillment
Of the Requirements for the Degree
Master of Science in Mechanical Engineering

Georgia Institute of Technology
August, 2004

Evaluation Methods for Porous Silicon Gas Sensors

Approved by:

Dr. P. Hesketh, Advisor

Dr. S. Graham

Dr. J. Gole

Dr. L. Degertekin

Date Approved: May 3, 2004

ACKNOWLEDGEMENT

I would first like to thank the members of my committee Professor Peter Hesketh, Professor Sam Graham, Professor James Gole, and Professor Levant Degertekin for their time, effort, and insight that enable this opportunity. I would also like to thank Professor Gole, Professor Hesketh, and Dr. Ocha for their advice and guidance during the development of this project. Additionally I would like to thank Dr. Degertekin for his rapid and generous help under short notice.

This project would not be possible without the work of Stephen Lewis. He personally manufactured over 450 porous silicon gas sensors, helped with numerous tests, and provided valuable ideas during the experimental process. Erica Parra, an undergraduate research assistant, and Benjamin Kirk, a high school intern, provided much appreciated assistance in the day-to-day experimentation necessary to characterize the device.

I would also like to thank all the members of the MEMS Research group. Their collective pool of knowledge is an incredible opportunity to experience. The facilities at Georgia Tech were of profound benefit in this project. In particular, thanks are due to the staff of the Georgia Tech Machine Shop, the Mechanical Engineering Electronics Lab, and MiRC for their skills and supplies.

Finally I would like to thank my parents for their support and guidance, and my wife Emily for her insightful encouragement and criticism throughout the process.

TABLE OF CONTENTS

Acknowledgements	iii
List of Tables	vii
List of Figures	viii
Summary	xii
Chapter 1 Background Information	1
1.0 Introduction	1
1.1 Gas Sensing	1
1.1.1 Classification of gas sensors	2
1.1.2 Measures of performance	3
1.1.3 Applications for gas sensors	8
1.1.4 Industries	9
1.1.5 Current gas sensing technologies	11
1.2 Signal Processing	15
1.2.1 Classification of signal processing for gas sensors	16
1.2.2 Preprocessing	18
1.2.3 Current signal processing applications	20
1.3 Evaluating the Porous Silicon Gas Sensor	23
References	24
Chapter 2 Preliminary Results	27
2.0 Introduction	27
2.1 Setup and Procedure	27
2.1.1 Gas experiments	28
2.1.2 Environmental experiments	33
2.1.3 Additional fixtures	39
2.2 Environmental Tests	40
2.2.1 Temperature	40
2.2.2 Pressure	44
2.2.3 Humidity	48
2.2.4 Baseline drift	49
2.2.5 Conclusions from environmental testing	51
2.3 Electrical Behavior	53
2.3.1 Resistance and impedance of the gas sensor	53
2.3.2 I/V plots for contact assessment	55
2.3.3 I/V plots assisting a manufacturing decision	58
2.3.4 I/V plots through the device	60
2.3.5 Conduction in a second path	62

2.3.6	Gold adhesion	63
2.4	Gas Response Measurement	64
2.4.1	Sensor #6	65
2.4.2	Sensor #7	66
2.4.3	Sensor #17	67
2.4.4	Preliminary signal processing	68
2.5	Performance Characteristics for Sensor 17	73
2.5.1	Lower onset of detection to NO _x	73
2.5.2	Transient analysis	75
2.6	Motivation for a Novel Testing Technique	76
	References	78
Chapter 3	Gas Pulsing Method	79
3.0	Introduction	79
3.1	Experimental Conditions	79
3.1.1	Experimental setup	79
3.1.2	Environmental factors	85
3.1.3	Review of discrete analysis	87
3.1.4	Selection of operating frequency	89
3.2	The Gas Pulsing Method	91
3.2.1	How gas pulsing works	91
3.2.2	Refuting the alternatives	94
3.3	Signal Processing for the Gas Pulsing Method	96
3.3.1	FFT analysis module	97
3.3.2	Time delay module	101
3.3.3	Solution extraction module	104
3.3.4	An example	105
3.4	Issues Associated with the Gas Pulsing Method	110
3.4.1	Windowing	110
3.4.2	The effect of manual switching	112
3.5	Applications of the Method	114
3.5.1	Benefits and costs of method	114
3.5.2	Additional applications	116
3.6	Conclusions	118
	References	119
Chapter 4	Applications of the Gas Pulsing Method	121
4.0	Introduction	121
4.1	Rapid / Reliable Method for Gas Sensitivity Screening	122
4.1.1	Alternative screening techniques	124
4.1.2	Screening attributes within the gas pulsing method	127
4.1.3	Sample matrix and gas pulsing	132
4.1.4	Results	137
4.2	Cleaning and Metallization of Porous Silicon	141
4.2.1	Historical impetus for method	142
4.2.2	Equipment and procedure	143

4.2.3 Results	147
4.3 Device Characterization	150
4.3.1 Lower onset of detection	151
4.3.2 Thermal and gas fluctuations	153
References	155
Chapter 5 Conclusions	156
Appendix A: Fabrication Process	157
Appendix B: Propagation of Uncertainty Analysis	159
Appendix C: Features of Test Matrix	160
Appendix D: Original Test Matrix	162
Appendix E: List of Successful Electroless Coatings	163

LIST OF TABLES

Table 1-1	Examples of a) excellent and b) poor selectivity for an array of three sensors	6
Table 2-1	Normalized temperature sensitivity of select devices	41
Table 2-2	Moisture response of porous silicon	49
Table 2-3	Comparison of noise parameters for several sensors	52
Table 2-4	Initial resistance of various gas sensitive devices	54
Table 4-1	Results from test signals	129
Table 4-2	Results from untreated sensor testing (bold indicates a strong response)	137
Table 4-3	Outline of common cleaning recipes	146
Table 4-4	Recipes for common electroless metal deposition	146
Table 4-5	Results from elevated temperature testing of a porous silicon gas sensor	154

LIST OF FIGURES

Figure 1-1	Illustration of sigmoid shape and the linear operating range	4
Figure 1-2	Illustrative plot of sensitivity	5
Figure 1-3	Schematic for lower onset of detection based upon a known deviation of signal response (σ)	7
Figure 1-4	Pictures of two porous silicon structures with varied etch parameters	14
Figure 1-5	Example of PCA clusters	17
Figure 2-1	Flow through experiment with thermostating bath	29
Figure 2-2	Bubbling flow through experiment	30
Figure 2-3	Delay in the original flow through system (delay is 190 seconds)	31
Figure 2-4	Reduced length flow through experiment	31
Figure 2-5	Reduced response time associated with shorter piping	32
Figure 2-6	Schematic of Gas Testing in an a) pad-to-pad configuration and b) through wafer configuration	34
Figure 2-7	Example of a wirebond breaking during the heating process	35
Figure 2-8	Experimental configuration for temperature testing	36
Figure 2-9	Schematic of localized heater for porous silicon gas sensor	37
Figure 2-10	Image of Pressure testing setup	38
Figure 2-11	Test cell used for vacuum evacuation	39
Figure 2-12	16 pin TO-8 to BNC connector	40
Figure 2-13	Example of irreversibility and nonlinearity in temperature sensitivity of a device	42
Figure 2-14	Temperature burst for a) a proportional sensitivity and b) an inversely sensitive device	43
Figure 2-15	Impulses associated with mass flow rate change	45
Figure 2-16	Pressure effects on an ammonia sensitive sensor	46

Figure 2-17	Effects of two vacuum evacuations on the porous silicon gas sensor	47
Figure 2-18	Opening and closing of bubbler that exposed porous silicon device to saturated nitrogen	48
Figure 2-19	3.5 hour response of a sensor with several apparent frequencies of noise	51
Figure 2-20	Three examples of localized high magnitude instability in a sensor over a three hour time-span	51
Figure 2-21	Variations in the I/V characteristics of gas sensors fabricated with an evaporated gold contact pad	56
Figure 2-22	I/V plots of three devices formed with the electroless metallization method	57
Figure 2-23	a) Normal porous silicon sensor b) porous silicon sensor with misalignment c) detail section of probe configuration for gold-gold I/V test d) detail section of probe configuration for gold-step I/V test	59
Figure 2-24	Detrimental effect of intentional misalignment	59
Figure 2-25	I/V plot of highly non-ohmic but gas sensitive device	60
Figure 2-26	I/V plot of through-contact on a porous silicon gas sensor	62
Figure 2-27	Schematic of 1) current path across porous silicon and 2) path through bulk of device and along backside aluminum contact	63
Figure 2-28	Picture of a porous silicon device with a large gold band that directly grounds the two gold connections together	64
Figure 2-29	Response of sensor #6 to a six minute pulse of NH ₃ at 50 ppm	65
Figure 2-30	Two tests performed on sensor #7 at 7.5 ppm NO	66
Figure 2-31	response of sensor #17 with a shorter recovery time	68
Figure 2-32	Raw sensor output of device 6 to 50 ppm NH ₃ at 20 SCCM	69
Figure 2-33	Temperature variations during experiment	69
Figure 2-34	Sensor output after linear temperature compensation	69
Figure 2-35	Results for sensor #6 after three different exposures	70
Figure 2-36	Indication of how data points were recorded for Sensors #7 & #17	71
Figure 2-37	Processed gas responses for sensor #7	71
Figure 2-38	Illustration of difficulty in determining “actual” delta R on drifting baseline	72
Figure 2-39	Gradual onset of gas response in sensor #17	73

Figure 2-40	36 data points with linear regression scheme for response of sensor #17	74
Figure 2-41	Sensor 17 reactivity at 70 ppm for various widths of NO at 20 SCCM	76
Figure 3-1	Configuration for all gas pulsing experiments	80
Figure 3-2	Uncertainty of experimental gas concentration for a test cylinder at a concentration 1000 ppm and a N ₂ flow-rate of 100 SCCM	82
Figure 3-3	Experimental validation of delay in system	84
Figure 3-4	Picture of periodic pressure waves (frequency of 1.50 mHz)	86
Figure 3-5	Impedance spike due to external laboratory disturbance	87
Figure 3-6	The available spectrum for gas pulsing	91
Figure 3-7	The output signal of a) a non-responsive device and b) a functioning gas sensor	92
Figure 3-8	Example of a developing gas response (system error)	93
Figure 3-9	Flow chart for gas pulsing method	96
Figure 3-10	Example of a strong gas response with low noise	98
Figure 3-11	Example of non-linear effects on signal	100
Figure 3-12	a) plot of raw data file and b) filtered data with artificial oscillation in the early response	100
Figure 3-13	Time delay illustrating strong response and zero drift	104
Figure 3-14	Example of raw data that illustrates rapid convergence between positive and negative delta R	105
Figure 3-15	a) Raw impedance response and b) filtered impedance response	106
Figure 3-16	a) FFT of sensor response b) detail of “spread” of gas pulse	107
Figure 3-17	Time delay module for the example signal	108
Figure 3-18	a) Positive delta R gas response b) Negative delta R or recovery of gas response	109
Figure 3-19	Discrete transform of the impulse function with side lobes	111
Figure 3-20	Reduced amplitude of middle pulse due to operator error	113
Figure 4-1	Illustration of a false signal (drift) under only a nitrogen flow and a gas signal under preliminary results for exposure to 50 ppm NH ₃	123

Figure 4-2	Time constant for two devices turned on until saturation	126
Figure 4-3	a) FFT of a highly responsive device and b) a detail in the area of interest	127
Figure 4-4	a) FFT of nitrogen only pulsing of a device and b) a detail of the FFT in the area of interest	128
Figure 4-5	a) Non-responsive device output in the frequency domain and b) detail of area of interest	130
Figure 4-6	Mass flowrate study with rate variation from 80 to 100.4 SCCM N ₂	132
Figure 4-7	The experimental setup	135
Figure 4-8	Illustration of the signal and noise band regions for a device that passes the screening process	136
Figure 4-9	Response of device to 10 ppm NH ₃ at 100 SCCM	139
Figure 4-10	a) The case of a weak response ratio of 1.6. (2.0 is the cutoff standard)	139
Figure 4-11	Results from applying the test signal to the signal processing algorithm	140
Figure 4-12	I/V sweep of a device before and after drying	143
Figure 4-13	Response plots for an electroless gold treated device	148
Figure 4-14	Response plots for an electroless tin coated device	149
Figure 4-15	Comparison of impedance response to 20 ppm of test gas at 100 SCCM	150
Figure 4-16	Lower onset of detection for an electroless gold coated gas sensor	151

SUMMARY

This study investigated the behavior of porous silicon gas sensors under exposure to CO, NO, and NH₃ gas at the part per million level. Parameters of interest in this study included the electrical, environmental, and chemi-resistive performance associated with various porous silicon morphologies. Based upon the variability of preliminary results, a gas pulsing method was combined with signal processing in order to analyze small impedance changes in an environment of substantial noise. With this technique, sensors could be effectively screened and characterized. Finally this method was combined with various post-treatments in order to improve the sensitivity and selectivity of individual sensors.

CHAPTER ONE

BACKGROUND INFORMATION

1.0 Introduction

Porous silicon gas sensors offer a technology platform for rapid, low cost, portable gas measurement. When defining the operating characteristics of porous silicon, it is critical to benchmark device performance against the current state of the art. In this chapter, technologies for both gas sensing and signal processing will be described, and attributes of the existing technologies that are significant to porous silicon and its characterization will be detailed.

1.1 Gas Sensing

The motivation for improved gas sensing capabilities for ammonia (NH_3), carbon monoxide (CO), and nitrogen oxide (NO) is predominantly driven by the risk of these gases to humans. Exposure to gaseous ammonia at concentrations of 50-100 parts per million (ppm)ⁱ can cause severe burns to the skin, eyes, throat, and lungs. In the case of exposure at or above 5,000 ppm, blindness, lung damage, and death are possible. Even at low concentrations, ammonia exposure causes coughing and irritation. Persons with asthmatic conditions are particularly prone to these effects.ⁱⁱ At concentrations around 25 ppm, chronic exposure can lead to damage of the eyes, liver, kidneys, and lungsⁱⁱⁱ.

The threat of exposure to carbon monoxide is considerably greater. CO is a byproduct of incomplete combustion reactions. Exposure at concentrations around 30 ppm can result in the weakening of heart contractions, reduction in ability to perform

manual tasks, and general drowsiness.^{iv} For individuals with heart conditions, exposure to concentrations as low as 10 ppm can cause similar effects on the body. At concentrations greater than 35 ppm for extended durations (>24 hrs), carbon monoxide exposure can result in headaches, irritability, blurred vision, lack of coordination, nausea, dizziness, and death. According to United States government regulations, the threshold level value for CO is 50 ppm for an eight hour exposure.^v

Nitrogen oxide gas, at 1-5 ppm, is a general irritant of the respiratory system as well as the eyes. Exposure over time results in fluid build-up in the lungs, nausea, and fatigue. Higher concentration exposures cause swelling of the throat, reduced oxygenation in the blood, and in severe cases, death.^{vi}

Based upon these symptoms, considerable attention has been given to the monitoring of these gases in the environment. Automotive congestion elevates the presence of these gases in urban locations. In rural settings, gas concentrations can become elevated due to fertilizers or excessive density of livestock byproducts.^{vii}

1.1.1 Classification of gas sensors

According to Sensor Business Digest, the market for chemical gas sensors in the United States was \$750 million in 2002.^{viii} The European market for chemical gas sensors has grown to a \$154 million industry in 1997 and is expect to exceed \$221 million by 2004.^{ix} In direct association with the size of the market, a vast array of chemical sensing devices have emerged from both research and commercialization efforts. Associated with this proliferation is a convoluted set of terminology associated with gas measurement. In this section, the important criteria for a gas sensor will be

defined. These criteria include the specific performance attributes, the functional applications for the device, and a brief market analysis.

The specifications of a gas sensor are intimately related to the proposed applicability of the device. Chemical sensors are principally divided according to their sensing mechanism. Within the literature, the terminology for the collective set of gas sensing mechanisms is somewhat inconsistent. Common terms that are used to describe the collective sensing mechanism are device classes, operating principles, modes of operation, and sensing modes. Regardless of the terminology of how one classifies the set, the mechanisms themselves are more clearly described. Some common mechanisms that can be used for gas sensing include conductometric, potentiometric, capacitive, calorimetric, gravimetric, optical, resonant, and fluorescent.

1.1.2 Measures of performance

After determining the class of a sensor, the gas specific parameters of sensitivity, selectivity, dynamic range, response time, lower onset of detection (LOD), and coefficient of variance (CV) should be defined. By properly defining these parameters, one can determine the operating condition for which the device is ideally suited.

The first parameter, sensitivity, is the ability to detect small concentrations of an analyte. Typically sensitivity is measured as the slope of the response curve (also known as the calibration curve). The response curve is a plot of the device response versus concentration of gas (Figure 1-1). The linearity of the device can be determined from the response curve. If the device is non-linear, advanced signal processing techniques are required to interpret the sensor's output. In the case of non-linearity, methods are often

imposed to force the response to a linear manner in order to ease analysis. Examples of these techniques will be provided in the signal processing section of this chapter.

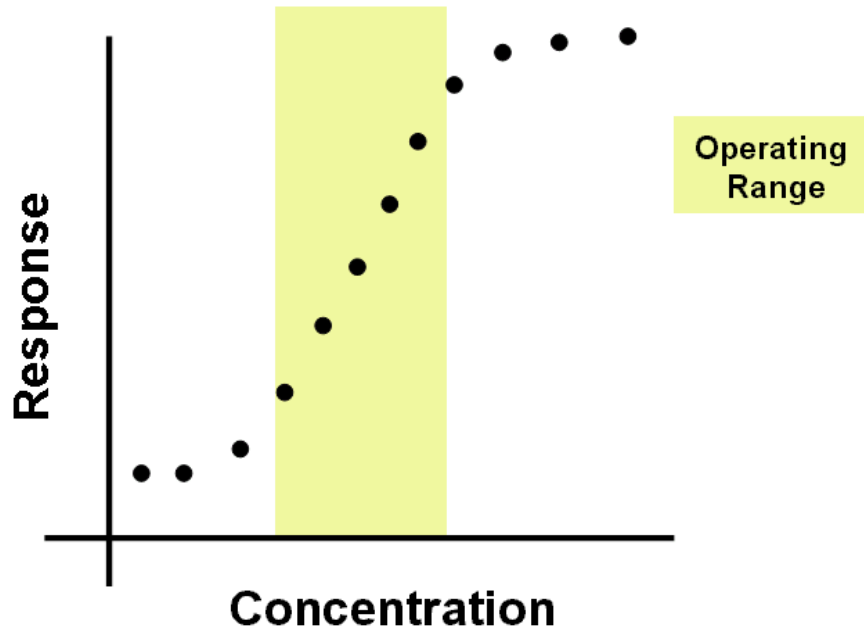


Figure 1-1: Illustration of sigmoid shape and the linear operating range

Occasionally, the sensitivity of a gas sensor is reported as a normalized ratio of the response signal over the baseline. This method, often referred to as R/R_0 or $\Delta R/R_0$, is the standard for reporting performance of microphones and some pressure transducers. Because of the prevalence of both reporting methods, it is important to ascertain the specific definition of sensitivity within a given application. Within this investigation of porous silicon, sensitivity will be defined as the slope of the response curve.

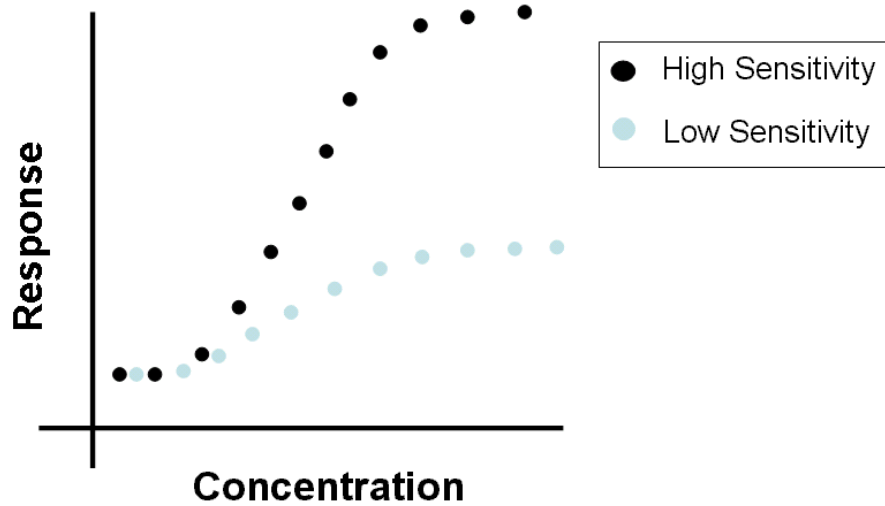


Figure 1-2: Illustrative plot of sensitivity

Selectivity, or the ability to distinguish between gases, is the second parameter that defines a sensor. Selectivity, in general, is not uniformly represented within literature. Qualitatively, selectivity implies a capability to distinguish between two given gases. Within published literature, the exact definition is highly dependant upon the mode of signal processing. A generalized, quantifiable metric associated with selectivity is the false positive probability. In medical applications, this metric is commonly referred to as specificity. In both cases, this term refers to the measured probability that a combined sensor and signal processing system will incorrectly indicate the presence of an analyte when that analyte is not present. Minimization of false positive probability is of considerable interest in areas such as inline process control and medical diagnosis where substantial costs are incurred for a single error.

Table 1: Examples of a) excellent and b) poor selectivity for an array of three sensors

a)		NH3	NO	CO
	Sensor 1	Response	X	X
	Sensor 2	X	Response	X
	Sensor 3	X	X	Response

b)		NH3	NO	CO
	Sensor 1	Response	Response	X
	Sensor 2	Response	X	X
	Sensor 3	X	Response	X

Dynamic range is simply defined as the spectrum over which the sensor operates. While the term “operates” is nondescript, the range is often further restricted according to a range of linear operation or reversibility. This parameter is useful for defining specific applications of the device. Often the dynamic range is referred to as the region of the response curve over which the response is linear (Figure 1-1). Saturation effects often dictate the upper threshold of absorption for a gas sensor. Since many gas responses appear as a sigmoid shape, the dynamic range is both lower and upper limit bound.

The next parameter of interest is the response time. For national security and fire detection applications, this parameter is of paramount importance. The response time is a measure of the exposure time of a gas that is required in order to reach a specific percentage of the steady state value. Often the time constant of a sensor is defined as the time to reach 90% of steady state response. Sensors possess a wide array of transient response shapes. Two common approximations for the shape of the transient response are a logarithmic curve and the error function. Modeling of transient analysis is often closely interrelated to either diffusion or mass transport limited absorption. The boundary and initial conditions are additional factors that are critical for the projected shape of the solution.

As previously mentioned, the response signal of a gas sensor is often a sigmoid shape with a non-zero value at lower concentrations. This factor, in combination with the

variability of the response curve, suggests that the lower limit of detection is not the point when one sees “zero” signal from the device. Instead the lower limit of detection is a statistically significant point where one can say with certainty that the observed response of the device is genuine. The quantification of this issue is known as the lower onset of detection. The LOD is the measured or extrapolated response signal to zero analyte plus two (or three) standard deviations. Figure 1-3 illustrates how the LOD is determined.

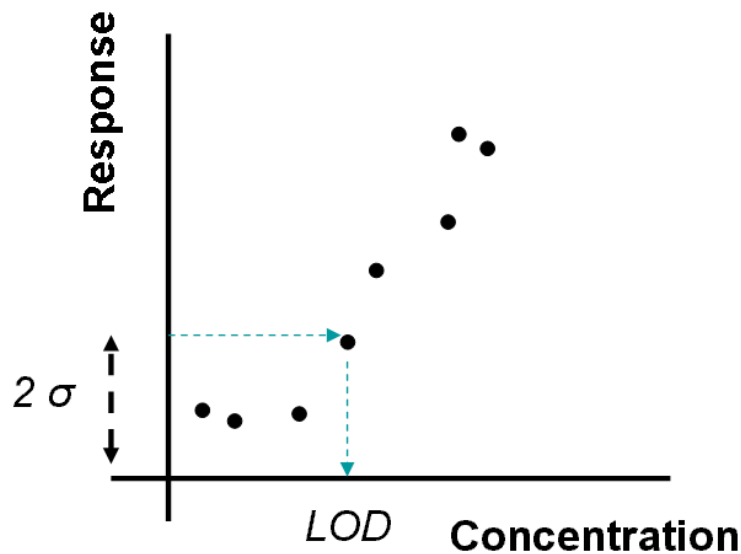


Figure 1-3: Schematic for lower onset of detection based upon a known deviation of signal response (σ)

Figure 1-3 also highlights an important issue with respect to determining the LOD. At lower concentrations, the response of the device often shifts in a non-linear manner. Therefore, when determining the LOD, it is critical to test a device to this cutoff threshold. If one instead assumes a linear extension of the trend as observed at the higher concentration, the LOD approximation will be better (lower) than the actual detection limit of the device.

The final parameter of interest is the coefficient of variance (C_σ). This parameter is a measure of the reproducibility of the device's response at a given operating point. In this equation σ_r represents the standard deviation of the responses. The mean (r_{bar}) is a measure of the mean response at the given operating point. The coefficient of variance is defined as:

$$C_\sigma = \frac{\sigma_r}{r_{bar}}$$

[Equation 1-1]

1.1.3 Applications for gas sensors

With the increasing breadth and capability of gas sensors as well as the proliferation of inexpensive electronics, the applications for gas sensors have rapidly expanded. The application is closely correlated to the performance, electrical, and environmental parameters that describe the gas sensor.

Gas sensors are used in many roles. For portable applications, the sensor must have low power consumption, be lightweight, and be simple in operation. Sensitivity requirements are application specific. At the same time, the portable nature of the device implies that the device will be exposed to a wide variety of chemical species. Therefore selectivity is a driving factor in the design of most portable systems. Examples of portable applications include portable military lab-on-chip systems, on-board automotive exhaust monitors, and the electronic nose.^x

For monitoring applications, the requirements are somewhat different. In this application, power is a moderate concern because many devices are either powered with a 9V battery or are connected to 120V terminals. In the case of the monitoring station, selectivity and sensitivity are of paramount importance. Some examples of monitoring

applications include emissions inspection stations, urban air quality monitoring stations, fire alarms, CO detectors, laboratory applications, and industrial process/quality control systems.

1.1.4 Industries

Four industries have demonstrated the greatest interest in the development of chemical sensors. These industries include automotive, household appliances, food/agriculture, and medical. In the automotive industry, the objective of chemical sensors is to ensure air-cabin quality and monitor emissions to the environment. Within the environmental dimension, two potential applications exist. The first application is on-board diagnostics. Within this application, sensitivities must exist with respect to reducing gases, volatile organics, polymers, and sulfur compounds. On-board systems are constrained to a low price point, high reliability, and ease of integration into existing car architectures. A second application is emission inspection. With this application, the required breadth of selectivity is reduced a limited list of known byproducts of combustion in automobiles. At the same time, however, sensitivity requirements are considerably increased. Currently in the state of Georgia, sensors for emission stations^{xi} must be sensitive and selective to CO, NO_x, and hydrocarbons at the low ppm level. According to a market study conducted by the Capteur, a European gas sensor manufacturer, the world wide market for chemical gas sensors in automobiles will have grown from 115,000 units in 1999 to 7.1 million units by 2003.^{xii} Furthermore, according to the Freedonia Group, semiconductor gas sensor sales are projected to grow at a rate of 10.6% annually through 2006.^{xiii}

Within the household appliance industry, there is a considerable demand for sensitivity to carbon monoxide and ammonia. Watson and Davies describe the need for carbon monoxide sensing for analysis of incorrectly adjusted gas-fired heaters.^v Bernhard describes the use of a work function TiN sensor for room temperature measurement of ammonia for the leakage control in commercial and residential refrigeration and air conditioning applications.^{xiv} The future growth potential of these applications is directly dependant upon the nature of government regulation on air quality in residential settings.

In the food/agriculture industry, ammonia is a common cleaning agent for food lines. In this application, ammonia monitoring is needed to ensure the safety of the food for end user consumption. According to Bernhard, the detection range for this application is around 1 ppm. Similarly for the agricultural industry, sensitive measurement of ammonia is typically necessary in the 5-20 ppm range.

Finally within the medical community there is a broad set of potential applications. In general gas sensor are being applied to improve the diagnostic process for medical physicians. Under the current system, many physicians are forced to culture bacteria for several days in order to diagnose disease. The objective of the chemical sensing systems is to reduce the time for diagnosis. Ammonia exhalation is a common sign of hepatic encephalopathy which is due to cirrhosis of the liver.^{xv} Ilona Koronczí describes the benefit of culturing human breath for oral bacteria with tin oxide arrays^{xvi}. Finally, Gardner applied chemical sensor arrays for analysis of *S. Aureus* and *E. Coli* bacteria as well as other diseases associated with the ear, nose, and throat.^{ix}

Although not an industry at the forefront of technology acclimation, the construction industry has a considerable need for the detection of hazardous gases.^{xvii} Works who operate in confined spaces such as sewer repair, telecommunication vaults, and bridge/tunnel construction are at a heightened risk for exposure to carbon monoxide, hydrogen sulfide, nitric oxide, nitrogen dioxide, methane, and other combustible gases. Similarly, construction workers who operate near automobiles such as paving crews and earthmoving teams are at a heightened risk for CO, NO, and NO₂ exposure. Market growth for these applications, however, will likely be closely correlated with governmental regulation.

1.1.5 Current gas sensing technologies

An abounding quantity of gas sensors exist within the market. There are over 4000 patents alone for gas sensors within the United States.^{xviii} Furthermore, several technologies have the potential to displace the need for chemical gas sensors. According to D.M. Wilson:

With the advance of chromatographic and spectroscopic analysis microsystems, the role of physical sensors that directly interact with the chemical stimulus ... has been increasingly questioned in the crowded chemical sensors market.^{xix}

While the sensor market is crowded, many of the aforementioned needs have not yet been resolved. Penetration into these markets will require disruptive technologies that operate with lower energy and higher sensitivity. The porous silicon gas sensor is an example of a device that could address specific niche market needs not met by more sophisticated chemical sensing equipment.

In order to properly quantify the unique need addressed by the porous silicon gas sensor, a review of existing chemical gas sensors is necessary. The results of this technology survey will be divided into two groups. The first group will include non-porous silicon chemical sensors that detect similar gases. This group will help define the current status of alternative technologies, and the subsequent technology risk that porous silicon faces. The second group describes porous silicon structures derived from alternative fabrication processes. This study will help indicate the diverse potential associated with unique fabrication approaches with porous silicon.

Many gas sensors besides porous silicon provide exceptional sensitivity and selectivity to NH_3 , CO , and NO_x . T. Le, *et al.*^{xx} developed a highly sensitive NO_x gas sensor manufactured from a Au/n-Si Schottky diode. The gold surface on one end of the diode was actually a 1 mm dot of thermally evaporated gold/antimony alloy. With this system, the dynamic range was stated from 750 parts per billion (ppb) to 30 ppm. For concentrations from 750 ppb to 1.5 ppm, the system was considered reversible. Additionally the device was insensitive to ammonia. For portable applicability, however, the device had one fundamental flaw. The barrier height in this case was 0.81 V. Due to this fact, energy requirements were excessive for portable applications.

For automotive applications, a zeolite coated interdigitated platinum electrode^{xxi} was used to detect ammonia. This heated device used capacitive sensing to detect ammonia concentrations in a range of 5 to 100 ppm. Drawbacks of this design for portability included a need to heat the zeolite film and a cross sensitivity to hydrocarbons.

E. Williams^{xxii} described a carbon monoxide sensor based upon an ohmic chemiresistive thin film tin oxide platinum sensor. The device has a dynamic range for

carbon monoxide from 0.2 to 8%. The principle drawback of the design was the poor lower limit of the dynamic range and corrosion in the operating environment. Another example of CO detection was the Figaro^v 203 tin oxide device. This low level CO monitor combated cross contamination with an activated charcoal filter that blocked NO_x. M. Martin demonstrates improved sensitivity to CO^{xxiii} through an artificial network. In this case, levels of 2-45 ppb NO can be distinguished from 125 ppb CO. The device was based upon sintered and thick tin oxide films operating at an elevated temperature. Again, the heating requirement of the device put a design constraint on its applicability for portable systems.

Porous silicon is also an effective platform for the sensing of NH₃, CO, and NO_x. In fact, the high volume/area ratio of porous silicon makes the substrate an ideal candidate for gas detection. A wide range of manufacturing techniques have been developed for the construction of gas sensitive porous silicon. In each case, the sensing parameters of porous silicon were highly dependant upon the manufacturing process. Critical steps within the manufacturing process include the etching solution, the electrical potential of the etch, and the etch time. Additionally factors such as the silicon's orientation and the geometry of the etching cell are critical in the formation of the porous silicon. The collective effect of these parameters enables many different porous silicon formations.

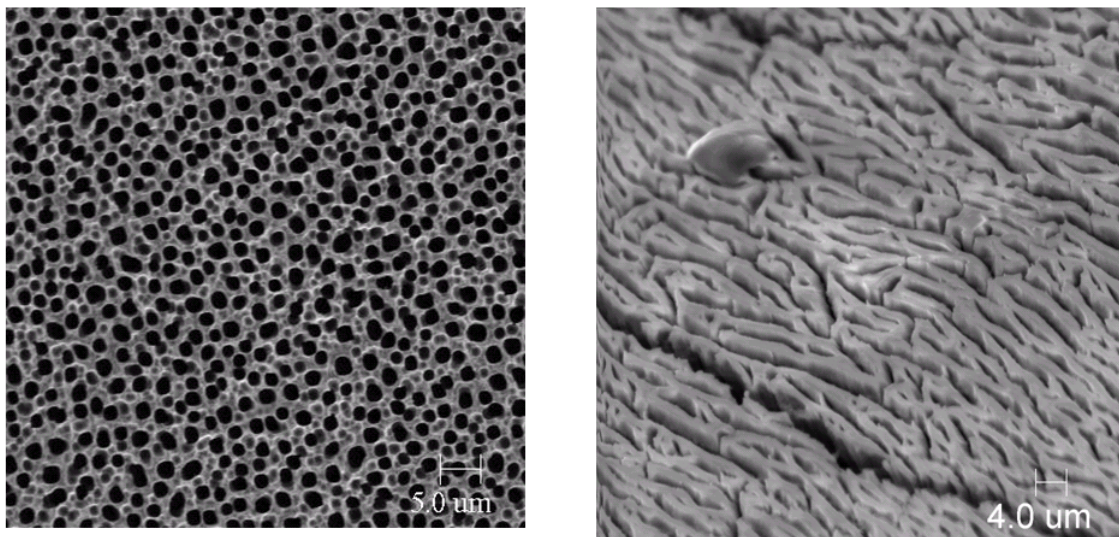


Figure 1-4: Pictures of two porous silicon structures with varied etch parameters

The most applicable example of porous silicon formation for chemical sensing is the two contact rapidly reversible porous silicon gas sensor.^{xxiv} The two contact design is a precursor to the device investigated in this paper. The basic fabrication process for this device is given in Appendix A. The porous silicon gas sensor has low energy consumption. This attribute is achieved through low resistance ohmic contacts that are formed on the device's surface. Furthermore, the reduction of the Schottky barrier between the metal and silicon resulted in improved detection of HCl, NH₃, and NO_x. Evaluated limits of the original design were 100 ppm at room temperature.

Several other gas sensing porous silicon structures have been demonstrated. S. Green demonstrated the effects of oxygen on the surface conductance of porous silicon at room temperature.^{xxv} In that study, a four point porous silicon device was fabricated with aluminum pads. Gas was delivered onto the surface at partial pressures of 1 to 100 torr. The device required a potential of at least 10 volts for minimal detection of oxygen.

L. Pancheri^{xxvi} manufactured a sensitive NO₂ sensor from meso-porous silicon. The resistivity of the wafer for this process was 0.006-0.015 ohm-cm. Etching conditions included 30% volumetric fraction of 48% wt HF and an etching density of 50 mA/cm². The porous silicon device manufactured by this process had a stated dynamic range of 12-240 ppb NO₂ in dry air. Downsides of the sensor design included reduced sensitivity in the presence of moisture and substantial baseline drift.

S. Zangoie^{xxvii} demonstrated the vapor sensitivity of a 111 p-type porous silicon gas sensor. Using a spectroscopic ellipsometry technique, 1000 ppm of ethanol and 12-1500 ppm acetone were distinguished. The response time of the device was approximately 20 seconds, with a slow but unspecified recovery time. Zangoie proposed that the variation between the response and recovery times of a porous silicon gas sensor were related to the “ink bottle” structure common to porous silicon. A final example of the diverse “tuning” capabilities of porous silicon is Ting Gao’s^{xxviii} development of a mesoporous silicon gas sensor that is sensitive to ethanol, methyl ethyl ketone, and n-hexane made from (100) p⁺⁺ wafer.

As one can see, there are many opportunities for selective formation of porous silicon to accomplish gas sensitivity in an array of structures and device configurations. In this research, an emphasis will be placed upon the design of porous silicon for a low cost, lower power device.

1.2 Signal Processing

In order to distinguish an analyte of interest at low concentrations, most gas sensors require a form of systematic signal processing. In this section, the common

classifications and terminology for signal processing will be detailed. After a discussion on the general classifications of signal processing, the details of preprocessing, or methods used to improve the signal analysis process will be discussed. Finally, existing technologies that reflect the general classifications will be discussed.

1.2.1 Classification of signal processing for gas sensors

Signal processing is classically divided in two manners: parametric versus non-parametric and linear versus non-linear. These parameters actually reflect both the technical understanding of the device and the fundamental nature of the response. Because of the broad set of tools available for each combination, the classification of a given sensor and signal is an advantageous activity. It should be noted, however, that a system is never bound to a given definition. In fact, with specific perturbations to a system, parametric relationships can be derived from a nonparametric system. This concept is fundamental to the gas pulsing method, a concept discussed in chapter 3. For the cases where such manipulations are not possible, the use of highly generalized algorithms can be used to characterize the response of the system. With this technique, however, extensive training and programming efforts are required.

Parametric systems are defined by the ability to closely link a gas sensitive variable (known as a parameter) to the gas species and concentration observed. In a parametric system, this linkage must be associated with a knowledge or prior insight relating the output to the predictable behavior of the device. With this knowledge, an algorithm is customized and a high degree of functionality can be obtained. If such knowledge is not available, the system is known as non-parametric. In a non-parametric

system, the relationship among the parameters cannot be understood. In this case, pattern recognition techniques are used to manage the unpredictable, complex, gas sensing system.

For either parametric or non-parametric systems, a set of linear techniques are available. The ability to utilize a linear system is dependant upon the fundamental nature of the gas response, the acceptable error tolerance, and the dimension in which the sensors are separated. One example of linear analysis is the principal component or cluster analysis. In this system, the n^{th} dimensional sensing space is reduced to either a 2-D or 3-D space where particular clusters are separated.^{xvii} The n^{th} dimensional space is typically based upon arrays of sensors or multiple attributes of a gas response (i.e. average response, normal distribution, frequency of noise, etc.). The term clusters refers to the behavior where similar gases produce solutions (in close proximity) in the 2-D or 3-D space. An example of PCA clusters is given in Figure 1-5.

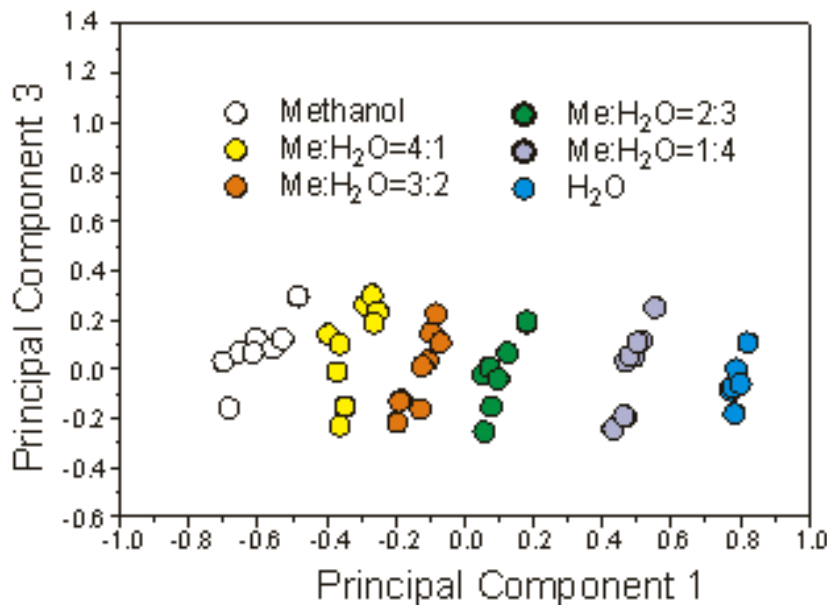


Figure 1-5: Example of PCA clusters^{xxix}

A second linear method is discriminant functional analysis. In this technique, the results of a gas sensor are organized in a multidimensional space based upon several measured behaviors from the devices. A discriminant functional algorithm is one which attempts to group the solutions of the multi-dimensional space into clusters. These clusters are interpreted by the algorithm with appropriate weighing function.^{xvii} The linearity aspect of the discriminant functional analysis is an essential component of the matrix manipulations needed to define clusters. In the end, the groups tagged with a label and a band of for this group is defined. Discriminant functional analysis, as a technique, becomes less efficient for increased sensor array sizes.

For situations in which the physical response cannot be reduced, non-linear methods are applied. The most common class of nonlinear techniques is the artificial neural network. In this system, processing elements, or parameters that are measurable within the system, are defined. Next the elements are interconnected into a network of relations by defining generalized equations. In order to solve the relationship vectors, a training set is performed. The ability of the training set to capture all probable situations dictates the effectiveness of the method. Three common node configurations are multi-layer perception, radial basis function, and Elman.

1.2.2 Preprocessing

Preprocessing is the process of modifying a raw gas response in order to prepare the signal for data analysis. Typically tacit knowledge of the sensor or system is applied

to the signal in order to screen against noise, non-functioning sensors, and drift.

Resolution and robustness are the end objectives of preprocessing.

The most common preprocessing techniques are associated with noise identification and reduction. The first practice is to assess the noise associated with the sensor. Apparent noise can occasionally be used as a point of differentiation for situations. Such effects are common when a gas is non-responsive to the primary mode of detection but perturbs the humidity or temperature of a device. If the noise provides no added value, either numeric algorithms or lock-in amplifiers can be used to remove noise components with specific frequency dependence. Normalization is often performed in situations of sensor arrays in order to minimize random noise effects.

The second potential function of preprocessing is to separate healthy sensors from non-functioning devices. This activity is critical to large arrays where the probability of one or more non-functioning devices is increased. This activity is accomplished with many approaches, but the method is always dependant upon an ability to define specific limits for operating sensors. These limits can either be derived empirically from the performance of the device or through parametric knowledge of the device in its environment. In devices where there is substantial drift or non-linear effects, this differentiation becomes highly non-trivial.

Two other common methods of preprocessing are scaling and feature extraction. Scaling is applied in situations to compensate for drift or aging. For example if the precise temperature sensitivity of a device is known, the overall signal can be scaled prior to analysis. Feature extraction is a generalized term for preprocessing activities that attempt to align the data within “distinguishable classes.”^{xvii} With feature extraction,

attributes besides the primary mode of analysis are first used to separate the group. Within the smaller groups, greater sensitivity is achieved.

1.2.3 Current signal processing applications

Signal analysis algorithms are extensively applied both academically and commercially. The following examples provide an infinitesimal sampling of the diverse applications of signal processing for gas sensors. Whenever possible, signal processing algorithms that resolved the measurement of CO, NO_x, and NH₃ gas was studied. Additionally, applications related to porous silicon surfaces were sought. The results of this study included parametric, non-parametric, linear, and non-linear systems.

Parametric analysis was previously described as a signal processing method where specific tacit knowledge about the system was used for differentiation in the signal. One form of parametric analysis is modulation of a well documented parameter associated with the sensor. If this parameter behaves uniformly over the operating range, an effective means for signal analysis has been found.

The first example of a parametric technique is Ortega's work toward the measurement and discrimination between CO and methane.^{xxx} In this method, a DSP-based hardware was connected to a tin oxide gas sensor. The DSP hardware generated a modulated thermal effect on the surface of the sensor. Since the thick tin oxide's gas sensitivity was exponentially related to temperature, the shape of the gas sensor's response could be specifically mapped and trained. The use of on-chip architecture increased the signal fidelity and subsequently reduced the training time for the device.

This similar temperature modulation approach was performed by Roth for the case of organic coated gas sensors.^{xxxix} In this method the periodic modulation of the sensor's temperature actually triggered periodic absorption and desorption on the thin-film surface of the interdigitated capacitive sensor. With on-chip integration of a heating element, the pulsing time was reduced from 300 seconds to 30 ms. As a secondary beneficial effect, the temperature modulation method appeared to lengthen the lifetime of the device by reducing irreversible saturation effects. Finally signal normalization was utilized to minimize the effect of aging and poisoning on the device. Additional examples of parametric routines include work by the NIST on the optimization of metal oxide arrays for reducing gases^{xxxix} and Kato's^{xxxix} work on extracting the Fourier transform in the frequency domain for gas analysis. This sinusoidally heated metal oxide sensor was used to distinguish ethanol, methanol, diethyl ether, acetone, ethylene, ammonia, isobutene, and benzene at the 100 ppm level.

Non-parametric systems tend to exhibit highly complex relationships. In application, however, non-parametric systems have been used for many practical applications. Martin^{xxii} used non parametric signal processing architectures to differentiate CO and NO₂ using a 12 element tin oxide sensor array. Work done by Abdel-Aty-Zohdy^{xxxiv} utilized a VLSI system approach for the classification of chemical compounds using an electronic nose with no systemic parameters. The framework for this system was based upon automated pattern recognition, classification, and distinction among multi-component chemicals.

In one example of linear methods, Dickert^{xxxv} used multivariate data analysis to distinguish devices and compensate for drift in the analysis of volatile compounds with a

mass sensitive sensor. For the case of high variant humidity conditions, network training was also applied to account for the highly non-linear change in polarity of the device.

In the case of the Kamina,^{xxxvi} a linear discriminant analysis was used with a PCA algorithm to detect low acetone and methyl mercaptane at a lower exposure limit of 10 ppm. To aid in the processing of data, the value of the steady state response of the device to the pulsed gas was averaged. This value was then used as a reference for normalization. An analysis of the normalized signals demonstrated characteristics of variation between pure gas exposures and ensembles.

Linear PCA and DFA methods applied to array configurations have gained widespread success in the distinction between similar components. Gardner^{ix} *et al.* present sufficient separation of a toxic and non-toxic cyanobacteria with a principle component method. Similarly, Gibson^{xxxvii} categorized the quality of olive oil by applying a linear PCA method. Finally, for refrigeration applications, Sarry^{xxxviii} differentiated CO₂ from forane R134A through the use of DFA on a metal oxide array.

Non-linear solution sets tend to be highly specific toward the sensor and application for which the optimization has occurred. Regardless, these methodologies indicate possible solutions for problematic resolution between analytes.

In one example of non-linear modeling, Pardo^{xxxix} explores the use of an inverse system identification problem applied to the dynamic performance of a gas sensor. With this technique the erroneous gas response of a Bulk acoustic wave quartz crystal was minimized for cases where the error source was of a time scale proportional to the time constant of the sensor.

Carey's^{x1} work on eight Taguchi gas sensors was used to analyze two and three component mixtures of toluene, benzene, acetone and trichloroethylene. The model itself require a non-linear partial with a least-squares approximation. The result of the method was compared to a dual linear technique and found to reduce the prediction error by 50%.

The aforementioned list is in no way an exhaustive representation of existing signal processing technologies. Instead this section highlights a common thread to signal processing techniques, customized solutions based upon empirical information and the demands of the application.

1.3 Evaluating the Porous Silicon Sensor

This chapter highlights fundamentals of gas sensing and signal analysis. Given the number of parameters that influence a gas sensor, experimentation must be used to prioritize an algorithm to solve the problem of interest. In the following sections, extensive preliminary experiments will be performed on an early state sensor design, the porous silicon gas sensor. With this preliminary information, the need for a signal processing technique will be motivated. This signal processing technique will be customized to the porous silicon gas sensor, and the limitations of the solution will be explored. Finally the signal processing technique will be applied to the porous silicon gas sensor in a range of applications. The results of this effort will lead the design improvements of the sensor and a new technique for small amplitude signal discernment.

REFERENCES

- ⁱ Toxicology Facts for Ammonia, Agency for Toxic Substances and Disease Control, September (2002) <http://www.atsdr.cdc.gov/tfacts126.html>
- ⁱⁱ Toxic Air Contaminant Identification List Summaries: Ammonia, California Air Research Board (September 1997)
<http://www.arb.ca.gov/toxics/tac/factshts/ammonia.pdf>
- ⁱⁱⁱ Chemical Profile: Ammonia, Children's Health Environmental Coalition (2001)
<http://www.chechnet.org/healthehouse/chemicals/>
- ^{iv} Health Facts: Carbon Monoxide, Wisconsin Department of Natural Resources, March 2003, <http://www.dnr.state.wi.us/org/aw/air/HEALTH/carbon.htm>
- ^v J Watson and G. Davies, A low level carbon Monoxide monitor, Sensors and Actuators B 2 (1990) 219-222
- ^{vi} J. B. McCammon, W. D. Wagner, D. Groth, G. Hatfield, and L. Reed, Current Intelligence Bulletin 50: Carcinogenic Effects of Exposure to Diesel Exhaust, CDC Publication, August 1988, <http://www.cdc.gov/>
- ^{vii} R. Venterea, D. Rolston, Nitric and nitrous oxide emission following fertilizer application to agricultural soil, biotic and abiotic mechanisms and kinetics, Journal of Geophysical Research, 105, (2000) 15117-15129
- ^{viii} P. Andrian, Nanosensors targeted at the right markets could generate big business opportunities, Sensor Business Digest, 12 (July 2003)
- ^{ix} Bogue, Robert, The UK gas sensor industry, Sensor Review, 21 (2001) 98
- ^x J. Gardner, H. Shin, E. Hines, An electronic nose system to diagnose disease, Sensors and Actuators B 70 (2000) 19-24
- ^{xi} Repairs and Passing, Georgia's Clean Air Force: Georgia Environmental Protection Division (2004) <http://www.cleanairforce.com/passing2.htm>
- ^{xii} Ward's Auto World, Primedia Business Magazines, 35 (January 1999) 21
- ^{xiii} P. Andrian, MEMS gas sensors are beginning to make inroads in diverse high-volume applications, Sensor Business Digest, 11 (November 2002)

- ^{xiv} B. Ostrick, R. Pohle, M. Fleisher, H. Meixner, Sensors and Actuators B 68 (2000) 234-239
- ^{xv} Robbins, A Pathological Basis of Disease, 6th Edition, W.B. Saunders Company (1999)
- ^{xvi} I. Koronczi, K. Ziegler, U. Kruger, J. Goschnick, Medical Diagnosis with the Gradient Microarray of the Kamina, IEEE Sensors Journal, 2 (June 2002) 254
- ^{xvii} Manning, Gretchen, Lewis, Kimberly Atmospheric hazards in construction work, Occupational Health and Safety, 71-8 (August 2002) 52-54
- ^{xviii} United States Patent and Trade Office (April 2004) <http://www.uspto.gov>
- ^{xix} D. Wilson, T. Roppel, Signal Processing Architectures for Chemical Sensing Microsystems.
- ^{xx} T. Le, V. Dang, K. Phan, and G. Gerlach, Highly sensitive NO_x gas sensor based on an Au/n-Si Schottky diode, Sensors and Actuators B 84 (2002) 226-230
- ^{xxi} R. Moos, R. Muller, C. Plog, A. Knezevic, H. Leye, E. Irion, T. Braun, K. Marquardt, K. Binder, Selective ammonia exhaust gas sensor for automotive applications, Sensors and Actuators B, 83 (2002) pg 181-189
- ^{xxii} E. Williams, N. Tomlinson, M. Cheney, A. Keeling, A thin-film tin oxide carbon monoxide sensor for exhaust gas analysis, Journal of Material Science: Materials in Electronics, 11 (June 2000) 369-372
- ^{xxiii} Miguel A Martin, JP Santos, JA Agapito, Application of artificial neural networks to calculate the partial gas concentrations in a mixture, Sensors and Actuators B 77 (2001) 468-471
- ^{xxiv} L. Seals, J. Gole, A. Tse, P. Hesketh, Rapid, reversible, sensitive porous silicon sensor, Journal of Applied Physics, 91 (February 2002) 2519-2523
- ^{xxv} S. Green, P. Kathirgamanathan, Effects of oxygen on the surface conductance of porous silicon towards room temperature sensor applications, Materials Letters 52 (2002) 106-113
- ^{xxvi} L Pancheri, C. Oton, Z. Gaburro, G. Soncini, L. Pavesi, Very sensitive porous silicon NO₂ sensor, Sensors and Actuators B, 97 (2003) 1-3
- ^{xxvii} S. Zangoie, R. Bjorklund, H. Arwin, Vapor Sensitivity of thin porous silicon layers, Sensors and Actuators B 43 (1997) 168-174

- ^{xxviii} Ting Gao, Jun Gao, Tuning the response and stability of thin film meso-porous silicon vapor sensors by surface modification, University California San Diego (2003)
- ^{xxix} H. Lang, M. Baller, R. Berger, C. Gerber, J. Gimzewski, F. Battiston, P. Fornaro, J. Ramseyer, E. Meyer and H. Güntherodt, An artificial nose based on a micromechanical cantilever array, *Analytica Chimica Acta*, 393 (1999) 59-65
- ^{xxx} A. Ortega, S. Marco, A. Perera, T. Sundic, A. Pardo, J. Samitier, An intelligent detector based on temperature modulation of a gas sensor with a digital signal processor, *Sensors and Actuators B*, 78 (2001) 32-39
- ^{xxxii} M. Roth, R. Hartinger, R. Faul, H. Endres, Drift reduction of organic coated gas-sensors by temperature modulation, *Sensors and Actuators B* 36 (1996) 358-362
- ^{xxxiii} McAvoy, TJ, *Engineering Technology Sustainable World*, 3 (1996) 9-10
- ^{xxxiv} K. Kato, Y. Kato, K. Takamatsu, T. Udaka, T. Nakahara, A. Matsuura, K. Yoshikawa, Toward the realization of an intelligent gas sensing system utilizing a non-linear dynamic response, *Sensors and Actuators B* 71 (2000) 192-196
- ^{xxxv} H. Abdel-Aty-Zohdy., M. Al-Nsour, Reinforcement learning neural network circuits for electronic nose, *ISCAS'99 Proceedings of the 1999 IEEE International Symposium on Circuits and Systems: VLSI*, (1999) 379-382
- ^{xxxvi} FL Dickert, O Hayden, Detection of Volatile Compounds with mass-sensitive sensor arrays in the Presence of Variable Ambient Humidity, *Analytical Chemistry* 1999, 71, 1338-1341
- ^{xxxvii} I. Koroncz, Z. Karlheinz, U. Kruger, J. Goschnick, Medical Diagnosis with the Gradient Microarray of the Kamina, *IEEE Sensors Journal*, 2 (June 2002) 254-259
- ^{xxxviii} T. Gibson, O. Prosser, J. Lubert, R. Marshall., P. Corcoran, P. Lowery, E. Ruck-Keene, S. Heron, Detection and simultaneous identification of microorganisms from headspace samples using an electronic nose, *Sensors and Actuators B*, 44 (1997) 413-422
- ^{xxxix} F. Sarry, M. Lumbreras, Discrimination of carbon dioxide and forane R134a using Figaro-type sensors TGS 832, *Sensors and Actuators B*, 57 (September 1999) 142-146
- ^{xl} A. Pardo, S. Marco, J. Samitier, Dynamic Measurements with Chemical Sensor Arrays Based on Inverse Modeling, *IEEE Instrumentation and Measurement Technology Conference* (June 1996) 570-574
- ^{xi} W. Carey, S. Yee, Calibration of nonlinear solid-state sensor arrays using multivariate regression techniques, *Sensors and Actuators B*, 9 (1992) 113-122

CHAPTER TWO

PRELIMINARY RESULTS

2.0 Introduction

Analysis of chemical sensors involves many parameters beyond the gas concentration delivered to the surface. Characterization involves parameters of the device's performance as well as its ability to operate in various environmental conditions. In this chapter, preliminary characterization and methods of evaluation will be described. In order to characterize the device for its intended application of gas sensing, the analysis will include gas testing, environmental investigations, and electrical analysis. Based upon these three types of tests, deficiencies will be identified and the requirements for a resolution to these deficiencies will be proposed.

2.1 Setup and Procedure

The characterization process for porous silicon involved many experimental apparatus with varying procedures. These apparatus have been divided into two categories: environmental and gas experiments. Environmental experiments involved temperature, pressure, and humidity. In all cases the effect of external factors associated with the laboratory environment were also considered.

Gas experiments include analysis of CO, NO_x, NH₃, CH₄, dry N₂, and saturated nitrogen. These experiments were conducted in both packaged devices (TO-8 header package) and diced fragments of one or more sensors. Variability in these experiments

included the mass flow-rate, the electrical signal applied to the device, and the environment in which the experiment was conducted.

2.1.1 Gas experiments

The experimental setup for the PS gas sensor is illustrated in Figure 2-1. The objective of this configuration was to deliver a continuous flow of test gas that could be tuned to a desired concentration. To obtain the proper concentration level, the mass flow rate of the high purity carrier nitrogen and the fixed concentration of test gas were varied. These streams were mixed together and then proceeded to the surface of the sensor. To obtain the required precision, test gas cylinders and nitrogen cylinders of a calibrated concentration were connected to calibrated mass flow controls (1179A, MKS) via ¼ inch stainless steel tubing. The gas in this system was thermostated by traveling through a 5 ft section of 1/8" stainless steel tubing wound in a Branson 5510 heated bath. A total of approximately eight feet of stainless steel tubing with eighteen 90° turns was necessary to deliver the gas from the cylinders to the sensor's test chamber. The test chamber was a 1 cm³ stainless steel cylindrical well that housed the packaged gas sensor. The entire setup was enclosed in a convection oven (1410M, VWR) where the temperature was monitored. Thermocouples (5TC K-type, Omega) entrained in the gas flow and positioned on the backside of the sensor package monitored the temperature variations throughout the tests. The sensor was connected to an impedance analyzer (Model 1260, Solatron). Impedance sweeps were performed with a range of drive voltages and frequencies depending upon the specific experiment. The drive voltages investigated ranged from 5mV AC to 500 mV AC. The DC biasing was varied from -1 Volt to 1 Volt.

In general, however, DC biasing was not supplied to the device during gas experiments. In all cases, the sampling rate of the impedance analyzer was either 0.1 Hz for overnight analysis or 1 Hz for all other experiments.

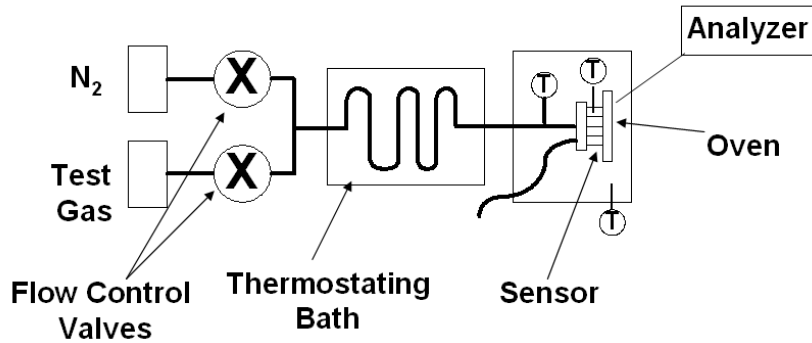


Figure 2-1: Flow through experiment with thermostating bath

For moisture testing of the device, a pair of 3-way valves (SS-43X-S4, Swagelok) replaced the thermostating bath. On one side of the valve junction, a glass beaker bubbled water vapor into the nitrogen flow. In the other direction, a normal length of tubing with an area equivalent to the bubbler carried dry gas. The bubbler and 3-way valve were placed directly outside the oven, and as a consequence, a more rapid response to the environment change was noticed. Figure 2-2 illustrates the modifications made to the setup.

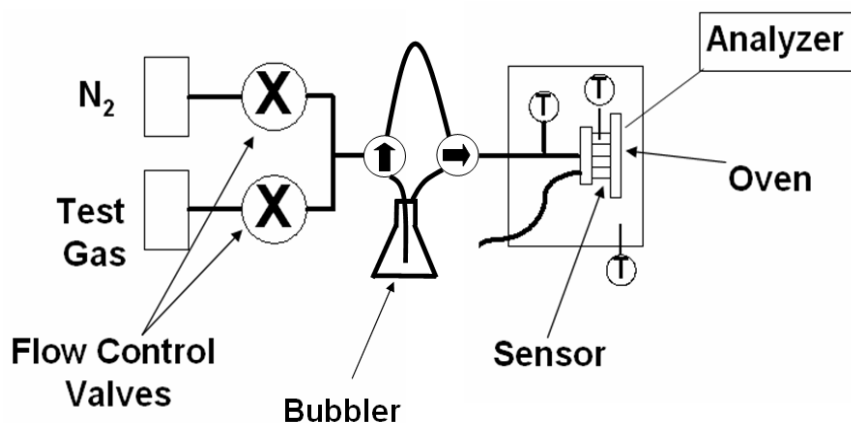


Figure 2-2: Bubbling flow through experiment

After the evaluation of approximately 6 generations of porous silicon, a mass flow rate for experimentation was standardized at 20 SCCM. At this flow rate the effect of travel time in the pipe was investigated. The travel time investigation was motivated by two effects. First, a delay in the system existed, and the cause of this delay needed to be ascertained. Secondly, a problematic diffusion effect existed for experiments with pulses of gas of short time duration (less than 60 seconds). In these cases, it often appeared that no gas was being delivered to the surface.

Empirically it was shown that the packet of gas took 2.5 - 3.0 minutes to reach the sensor (Figure 2-3). While this effect could be related to the time constant of the sensor, experimentation revealed that reducing the length of tubing reduced the response time. This information demonstrated that modifications to the system were necessary.

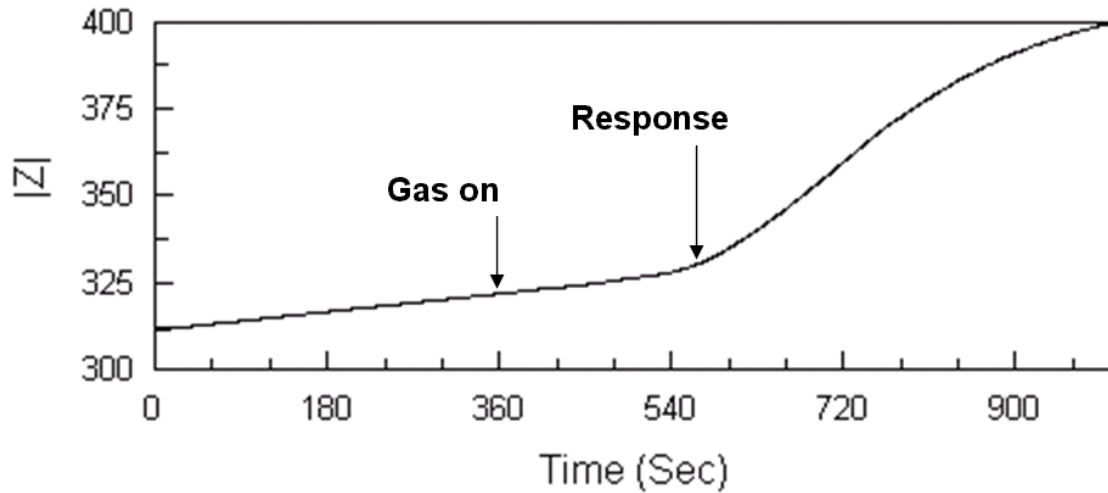


Figure 2-3: Delay in the original flow through system (delay is 190 seconds)

In order to reduce the travel time of the gas, the thermostating bath, oven, and over 9 feet of tubing in total were exchanged for approximately 1.5 feet of tubing (Figure 2-4). For all possible locations, the $\frac{1}{4}$ " tubing was replaced with $\frac{1}{8}$ " tubing. Also the pipe length from the mixing point of the two gases to the surface of the sensor was reduced from 7.5 feet to 9 inches. Finally, to provide heat to the sensor, a thin strip resistive heat source (Model 0039C, Watlow) was placed over the test cell area as well as along the piping that leads into the test chamber.

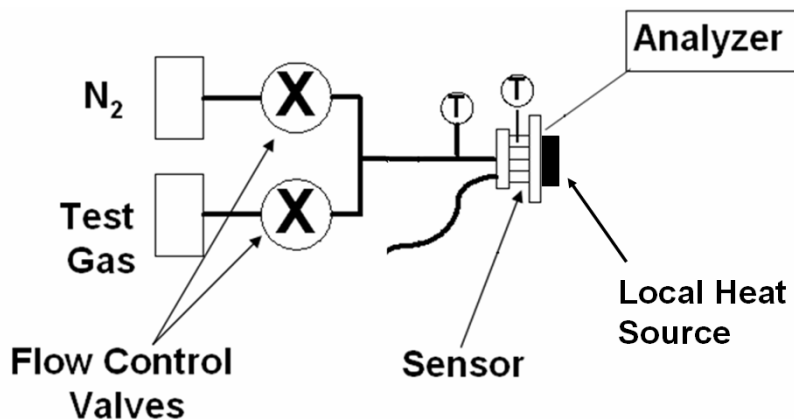


Figure 2-4: Reduced length flow through experiment

As a result of these changes, several changes in the system were observed. The time constant of the system dropped to around 27 seconds (Figure 2-5). This result was repeatedly observed in over 20 different sensors from 7 different manufacturing runs. Secondly noise issues in the system appeared to decrease. Finally the time to change sensors and prepare experiments was greatly reduced.

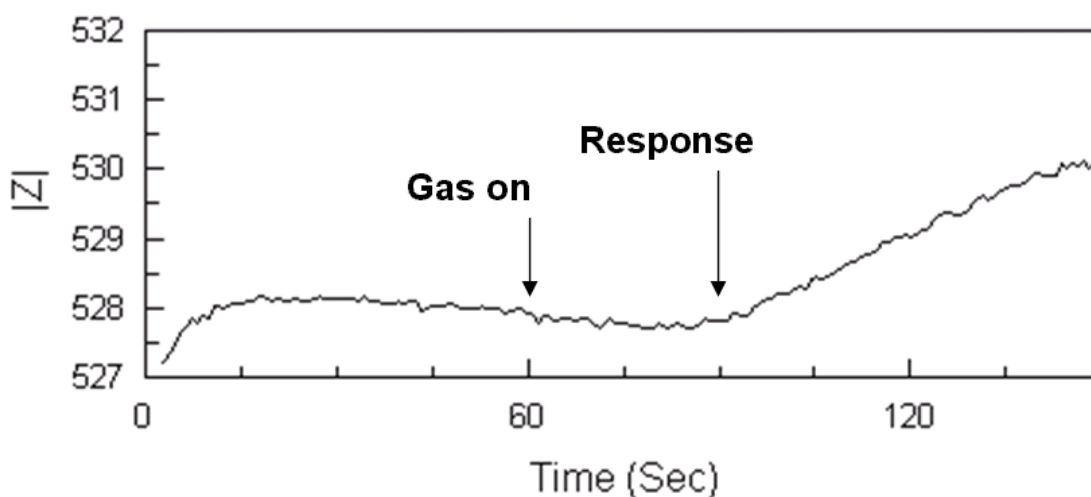


Figure 2-5: Reduced response time associated with shorter piping

During the course of the three iterations on the gas delivery system, some variability was introduced into the standard operating procedure for the experiment. Pertinent variations, when they occurred, will be provided for the discussion of specific gas experiments. In general, however, the following steps were performed:

1. *System validation* – Ensure that mass flow controllers are properly opening and closing. Validate that the state of all valves. If the first run on the day, perform 30 minute run to purge contaminants from downstream piping. If first run after system modification, run electrical analysis with a bare resistor or grounded piece of metal.

2. *Record Pre-test data* - Record the temperature of the room, the intended operating voltages (DC, AC, and frequency), the device number, the test number, the test gas of interest, and the intended operating concentrations.
3. *Run warm-up file* (Optional) - Measure the impedance of a device only under nitrogen flow. Validate the stability and reasonable operating range of the device (Impedance should be less than 100 kilo-ohms and fluctuations should be less than 10% of full scale).
4. *Run experiment* – Start the timer and data acquisition system. Introduce gas concentrations as appropriate. Periodically record temperature, concentration, and operational notes.
5. *Document Results* – Stop program, initiate a nitrogen purge for a range of two minutes to five hours depending upon the nature of the experiment. (Optional) Track impedance of device on a separate file to ensure the system is returning to an equilibrium position.

2.1.2 Environmental experiments

The process of environmental analysis for porous silicon gas sensors was an essential benchmark to determine their real-world applicability. Given the unstable and highly variable nature of the manufacturing process, it was essential that all environmental experiments were “rapid” in nature. With rapid testing techniques and short machine down time, large quantities of sensors could be analyzed in a relatively short period. Once this process was in place, a method for rapidly tuning the sensors to the necessary configuration could be obtained.

The experimental configurations for the analysis of environmental factors included a current / voltage (I/V) probe station, a temperature analysis, and a pressure test rig. The I/V probe station had two configurations in order to analyze both packaged devices and diced wafer fragments. Due to the need to seal the sensor in a pressurized environment, the pressure test rig could only accommodate packaged and wire bonded devices.

The I/V probe station was simply comprised of a Hewlett Packard multi-meter (3478A), a Tektronix power supply (PS2520G), and a pair of Microtech probes. In the case of packaged devices, the probes were replaced with a pair of shielded banana plugs.

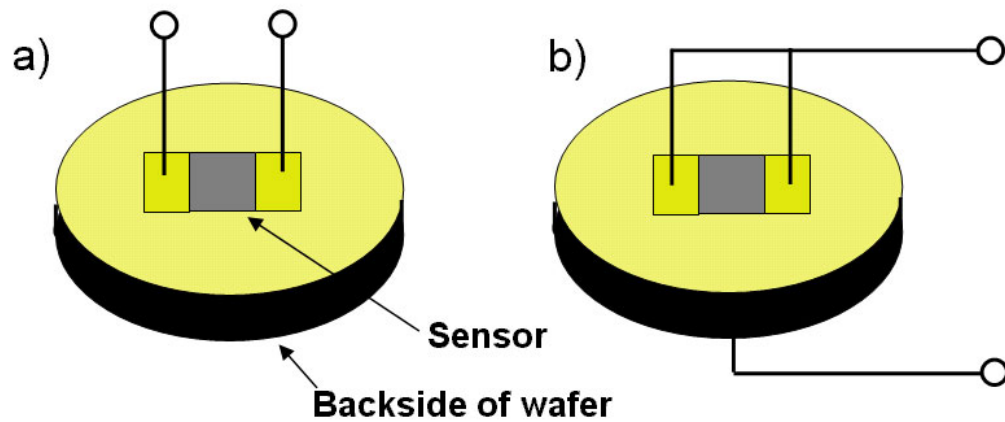


Figure 2-6: Schematic of Gas Testing in an a) pad-to-pad configuration and b) through wafer configuration

I/V analysis began with a simple calibration and validation with a 1000 Ohm resistor. Once conductivity was ascertained, the voltage and current were recorded for 0.1 V increments for a range from zero to one Volt. The device was tested in a pad-to-pad configuration (Figure 2-6). Since the terminal was only capable of supplying positive voltages, the connections at the power supply were inverted. The test was then repeated from 0 Volts to -1 Volt. In the case of apparent instability, this I/V sweep was repeated up to three times. The entire process was analogous for the probe station configuration. The notable exception was that calibration was not quantified against a known value, but rather the probe tips were positioned on top of a gold pad in direct

contact with one another. If a resistance greater than 15 ohms was detected on the gold surface, the configuration of the probe tips was realigned and the experiment repeated.

The second environmental experiments were temperature analysis of porous silicon sensors. In these experiments a packaged and wire bonded sensor was placed in a 1 cm³ test chamber. The test chamber, which was identical to the configuration used on gas test experiments, was placed into a convection oven. Initially the temperature was ramped from room temperature to 105° C. During repeat testing, however, instability was noted for temperature increases greater than 80° C (Figure 2-7). Additionally, the connection between the wire bond and the porous silicon surface tended to separate at these elevated temperatures. During experimentation this failure occurred with five out of eight wirebonded devices. As a result of these failures, the range of the temperature experiment was often restricted from 22.5 to 60 ° C.

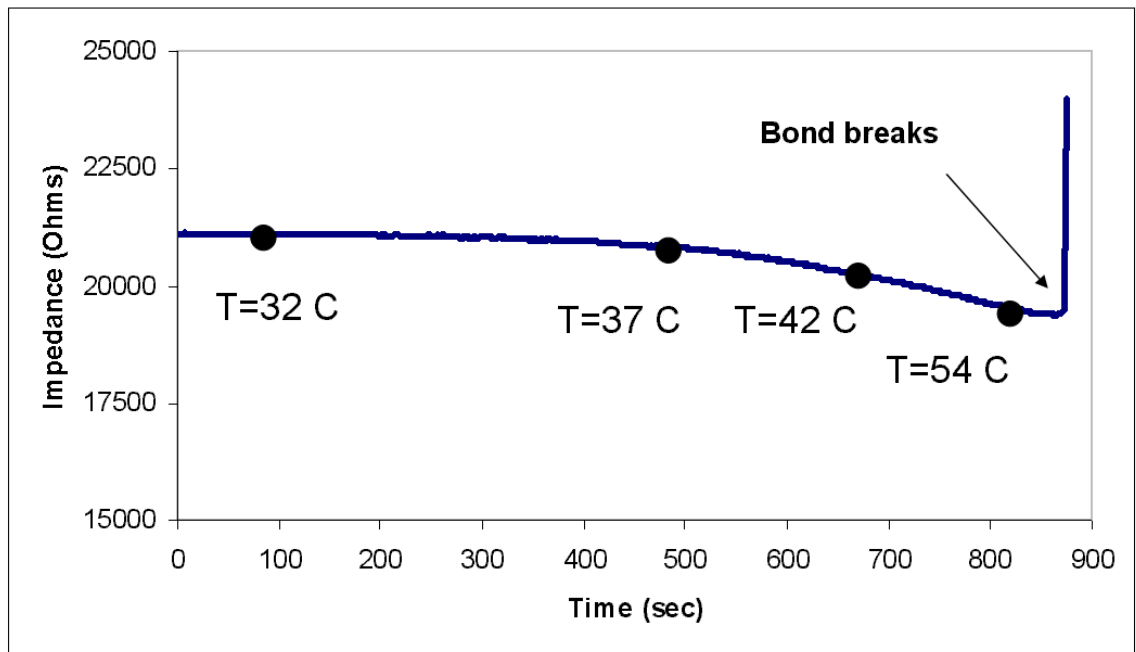


Figure 2-7: Example of a wirebond breaking during the heating process

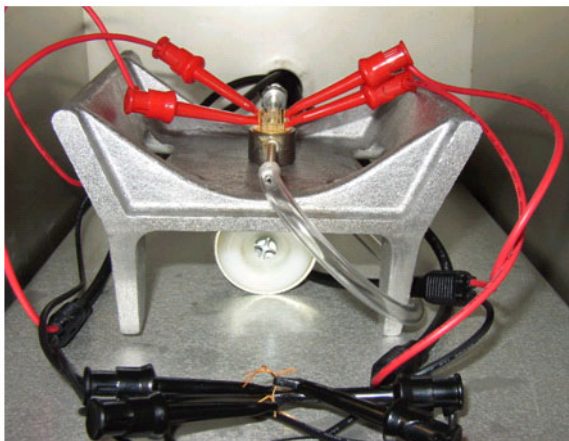


Figure 2-8: Experimental configuration for temperature testing

A similar temperature test was also designed as a quick screen for sensors. At the time, no specific methodology existed for the evaluation of functioning gas sensors. Additionally, due to impurities on the gold surface, the process of wire-bonding met with a success rate of less than 10%. In order to maximize the probability that a device of value would be properly wire-bonded, a quick temperature test was devised. In this case, a sensor was placed in a 100 °C oven for approximately one minute with the impedance analyzer running. With thermocouples placed on the back surface of the gas sensor and in proximity of the surface, the device's temperature was tracked for approximately one minute. During this time an impedance sweep was taken on the device. Once the minute elapsed, the sensor was removed from the oven, and a rough estimate of the temperature dependence was ascertained.

A final variation on the temperature test was introduced with the addition of a localized heater instead of the oven. This configuration was invaluable for rapid ramping of the device without the need to wait for uniform heating in the oven. Due to a lower thermal mass of the test system, a cyclical heating and cooling of the device was possible.

This method was applied in the continued analysis of porous silicon's temperature sensitivity.

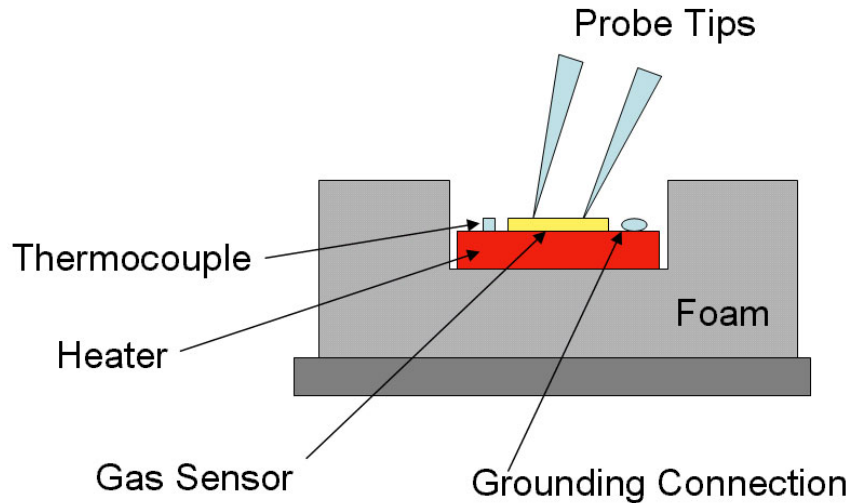


Figure 2-9: Schematic of localized heater for porous silicon gas sensor

The final environmental experiment performed on porous silicon was a pressure sensitivity analysis. In this experiment a glass bulb filled with a test gas of a prescribed composition was bled into an initially evacuated test chamber. The pressure was recorded with an MKS 121AA pressure transducer. Impedance measurements were simultaneously taken with a Solartron 1260 Impedance analyzer. In order to further fix the sensor at a given pressure, a fast acting valve (South Bend Controls, 2-way NC inert valve) that was located between the porous silicon sensor and the gas bulb could be actuated. For higher pressure measurements (>3 PSIG), the glass bulb was alternatively replaced with a cylinder of research grade nitrogen. Due to dynamic range limitations of the 121AA pressure transducer, it was also replaced with an Omega PX302 pressure transducer. In this configuration, pressure measurements could be taken up to 15 PSIG.

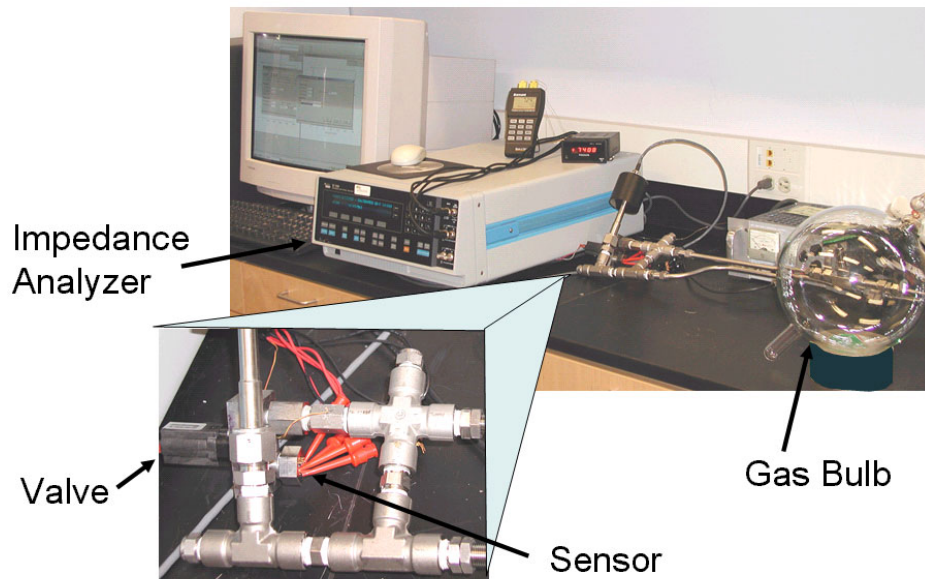


Figure 2-10: Image of Pressure testing setup

As a final pressure experiment, a configuration utilized by L. Sealsⁱ was repeated. In this configuration, both gas composition and pressure were varied during the course of an experiment. The operating premise was that a porous silicon device could be made reversible by increasing the pressure gradient for desorption. To accomplish this objective, a porous silicon gas sensor was initially placed in a flow through test setup and the setup was purged with a vacuum pump (Figure 2-11). Next nitrogen was pumped into the evacuated volume until the pressure was returned to 14.7 PSIG. Once the baseline had settled, a test gas of known composition was delivered onto the sensor's surface. Once a steady equilibrium was obtained, the test gas is turned off and the system was evacuated again.

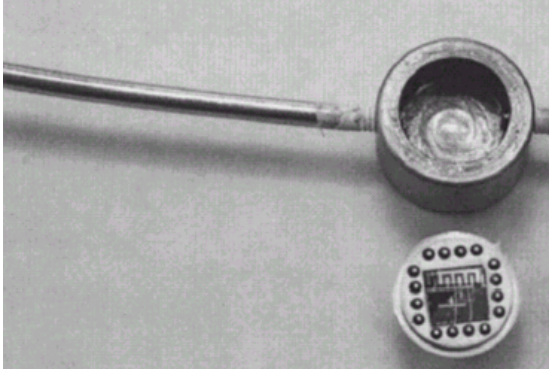


Figure 2-11: Test cell used for vacuum evacuation

2.1.3 Additional Fixture

In order to reduce changeover time between experiments, a 16 pin TO-8 to BNC PCB board was constructed (Figure 2-12). With this board, the data from multiple wirebonded sensors on one package could be extracted from the test area. This functionality would be critical for simultaneous analysis of multiple components on one chip. Electrical validation on the 16 pins of the connector with a 1000 ohm resistor demonstrated sufficient precision in the manufacturing of the connector. A variation of less than 0.5 ohms existed for the resistance of all connections, and the variance was less than 0.3 ohms for six of the sixteen connections. Drawbacks of this fixture included difficulty in initially loading a packaged sensor and thermal limitations in materials used in the construction of the adaptor.

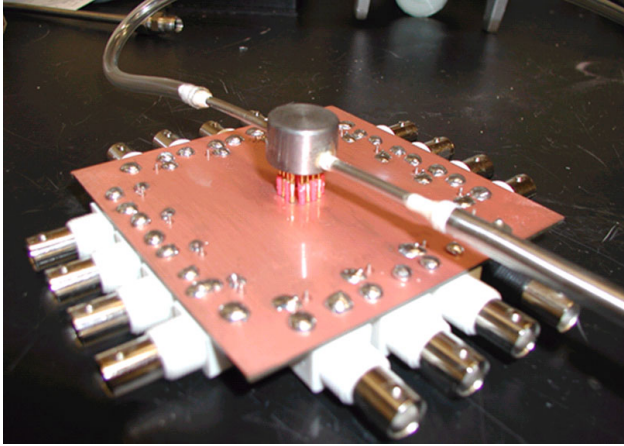


Figure 2-12: 16 pin TO-8 to BNC connector

2.2 Environmental Tests

Environmental testing on porous silicon was conducted for two principal reasons. The first objective in evaluating porous silicon under variable environmental conditions was to ascertain its sensitivity to explicit parameters that are commonly encountered in real world environments. The second object of this form of testing was to seek a mechanism through which gas sensors could be screened.

2.2.1 Temperature

The temperature sensitivity of porous silicon gas sensors is based upon two specific issues. The first issue is the temperature sensitivity (in $\Omega/^{\circ}\text{C}$) of both the bulk silicon and the porous silicon. The effect of heating on silicon's resistance is widely known as an inversely proportional relationship. The effect of temperature of the resistance of porous silicon continues to be a studied effect. The second issue that is related to the temperature sensitivity of the device is the effect of temperature on

diffusion kinetics. Devices based upon this operating principle were described in Chapter two.

The temperature dependence of porous silicon demonstrated results that were both proportional and inversely proportional to temperature depending upon the specific batch of porous silicon. Table 2-1 indicates some examples of thermal sensitivity. In general, a device's temperature sensitivity had no direct bearing on its gas sensitivity. Both devices 6 and 7 were gas sensitive while devices 8, 10, and 15 were not. As a result it was concluded that a measurement of temperature sensitivity would not serve as a sufficient means for gas sensitivity screening.

Table 2-1: Normalized temperature sensitivity of select devices

Device	6	7	8	10	15
$\Delta\Omega/\Omega/^{\circ}\text{C}$ (E-3)	-11.17	5.9	6.62	1.44	-33.48

A degree of hysteresis was noted after a small thermal heating of a porous silicon device. Figure 2-13 indicates the hysteresis for device number 7 after its first heating. Similar results were observed in other sensors with a predominantly proportional response. Error sources associated with baseline drift potentially account for the section of inversely proportional response observed in the onset of test 2 of Figure 2-13.

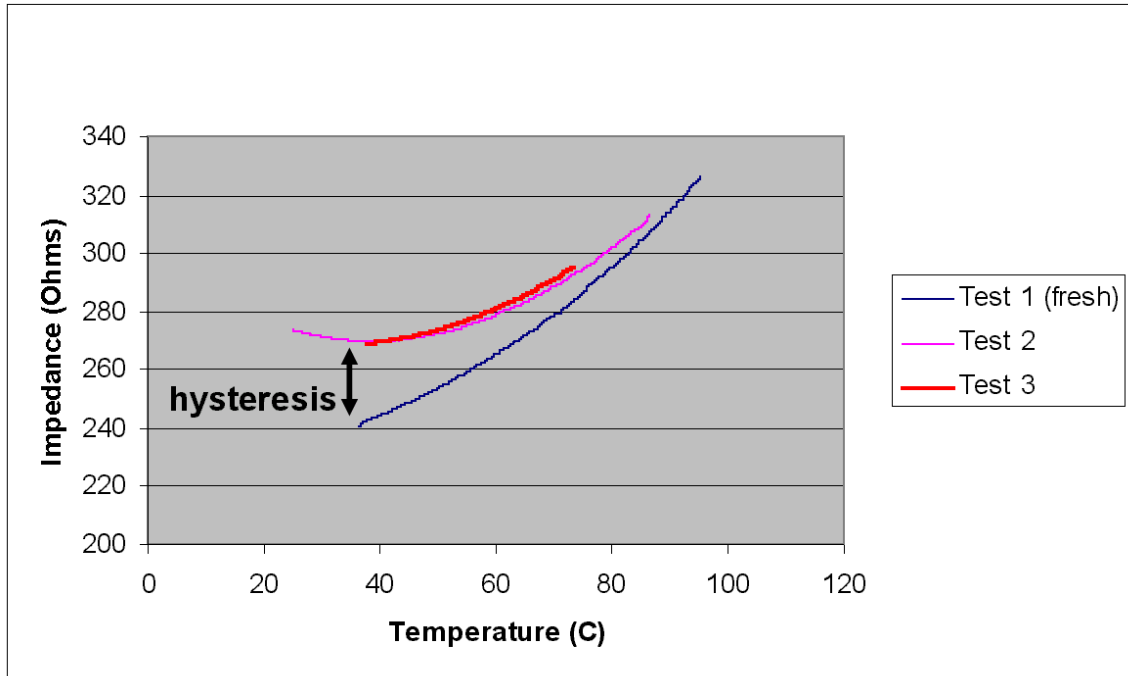


Figure 2-13: Example of irreversibility and nonlinearity in temperature sensitivity of a device

After noting the wide discrepancy between the magnitude and direction of temperature sensitivity, a quick temperature test was devised. In this analysis, a packaged device was placed into a 100 °C oven for only 2 minutes. A thermocouple mounted on the surface of the sensor extracted the transient temperature information which was compared to the impedance response. An example of this procedure is given in Figure 2-14. It should be noted that when wirebonding of devices was discontinued, this procedure was replaced with localized heating experiments of a sinusoidal form.

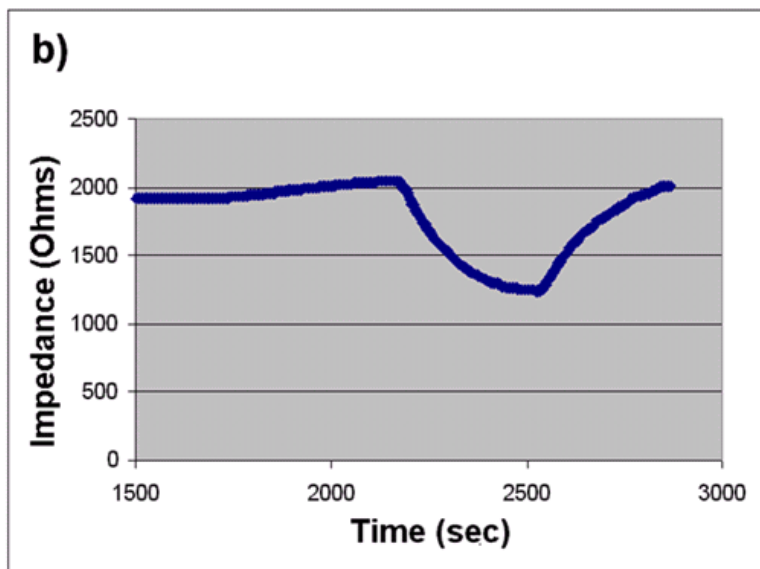
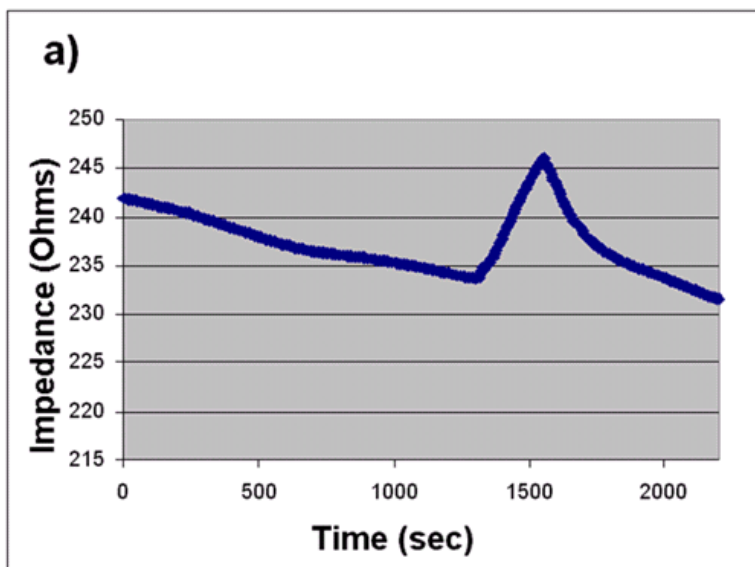


Figure 2-14: Temperature burst for a) a proportional sensitivity and b) an inversely sensitive device

2.2.2 Pressure

The attempt to analyze pressure effects produced predominantly trivial and suspect results. For the two initial pressure testing configurations, negative pressure leakage problems in the experimental fixtures were unresolved at the interface between NPT fittings, at the fast action valve, and in the interface between the TO-8 package and the surrounding housing. Regardless of these issues, both positive pressure and vacuum pressure effects were studied in a qualitative manner with several configurations.

The need for a pressure study was actually based upon results from varying the mass flow rate in an experiment. Figure 2-15 illustrates the effect of a dramatic mass flow change on the surface and the resulting impedance change. Originally these impedance changes were believed to be a gas response. By running nitrogen as the test gas, it was discovered that these pulses were actually the result of mass flow rate change. A secondary indicator that this response was not related to gas sensitivity was a capacitance shift in the system. In fact, the imaginary component of impedance was a dramatic portion of the overall response (20-30%). These results, when combined with a physical inspection of the device after testing, suggested that the impedance change was associated with delamination of the gold from the gold/porous silicon interface. Future manufacturing changes included the addition of a Ti layer between the gold and porous silicon as well as modifications to the gold thickness in order to prevent metal contact delamination.

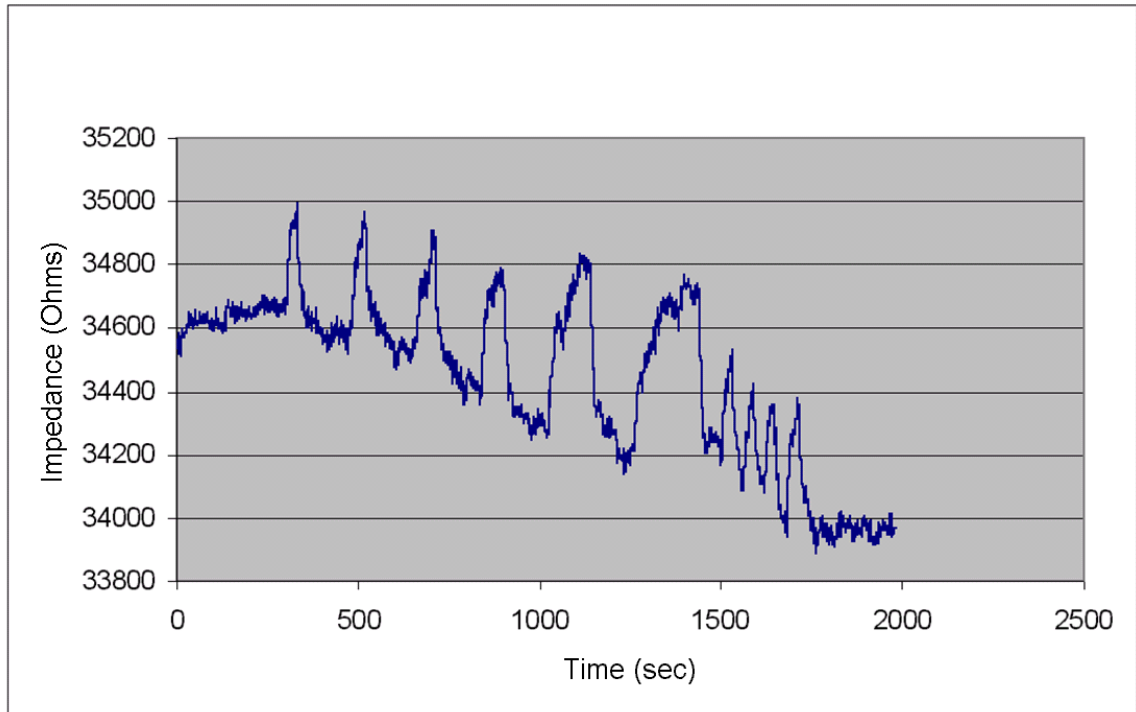


Figure 2-15: Impulses associated with mass flow rate

After realizing the effect of mass flow rate, the apparatus shown in Figure 2-10 was reconfigured to evaluate the pressure sensitivity of devices. In this experiment, a positive nitrogen pressure was varied from 0 to 5 PSIG. In order to load a wafer into this experimental configuration while maintaining a leak-proof seal, a packaged and wirebonded device was necessary. As previously noted, the adhesion of wire bonds was quite poor. At the time, only three devices were available for testing that had wire bonds on them. The test could potentially damage either the bond or the device itself. As a consequence of these concerns, only one device was evaluated with this experiment. The result of the experiment is given in Figure 2-16.

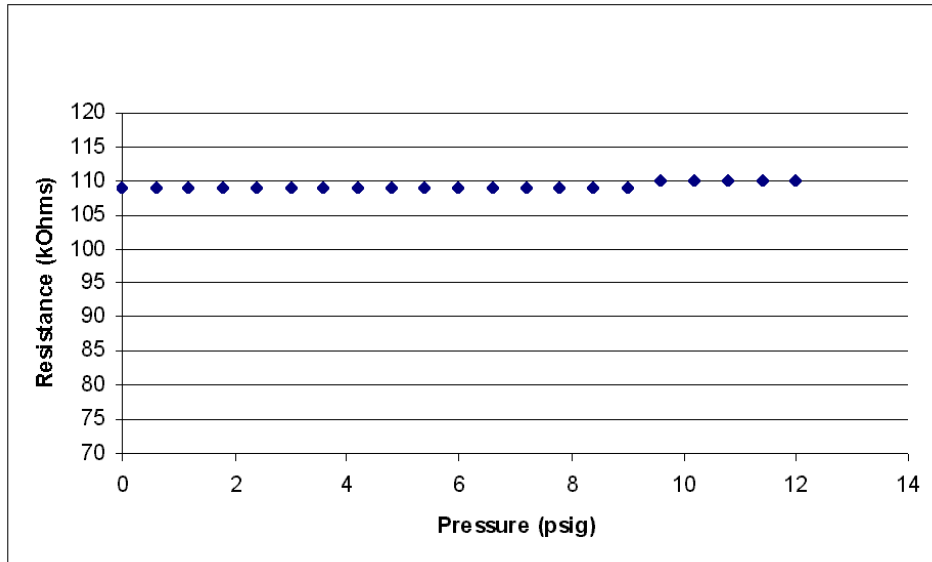


Figure 2-16: Pressure effects on an ammonia sensitive sensor

From these results, one should note that the device is, in general, insensitive to pressure. These results are somewhat suspect, however, given the extremely high impedance value of the device. While this device is 110 kilo-ohms, most porous silicon gas sensors possess impedance in the range of 200-5000 ohms. As a result, noise information in the 10-500 ohm range is suppressed by the relative impedance of this device.

As a final evaluation of pressure on porous silicon, a vacuum pressure test was necessary. In order to repeat the experiments of L. Sealsⁱⁱ, a vacuum pump was added at the end of the gas flow experiment originally described in Figure 2-1. With the vacuum system, a gas sensor was pulsed with a known gas, allowed to reach a saturation level and then purged with the activation of a down-stream vacuum. Figure 2-17 gives an example of one gas pulse followed by two vacuum evacuations of the device. In this example one should notice the timescale for both the gas experiment (approximately 500 seconds) as

well as the pressure changes (unsettled after 5000 seconds). Immediately after the pump was turned off, the impedance reversed direction and drifted at a new baseline.

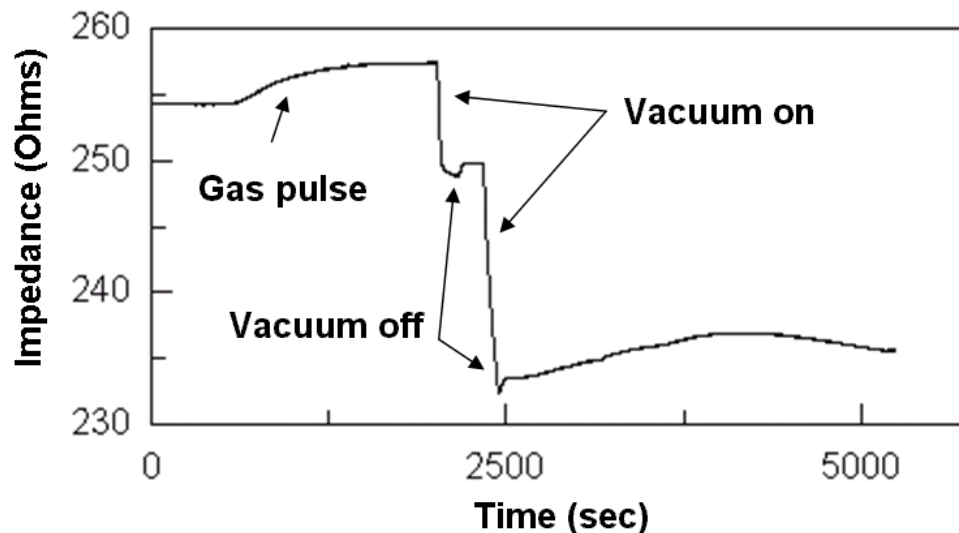


Figure 2-17: Effects of two vacuum evacuations on the porous silicon gas sensor

Based upon this experiment, fundamental flaws of pressure recovery were noted. First the pressure recovery had a long relaxation time as noted by the behavior from 2500-5000 seconds. In fact, the time necessary to recovery from a pressure change exceeded the three hour duration of the experiment. Attempts to more closely ascertain the exact time constant for this recovery were confounded by the effects of baseline drift. The second result from this pressure testing was the apparent change in the operating point of the device. Since the impedance was driven downward, one might theorize that improved sensitivity could result from vacuum purging the device before experimentation. This action however resulted in heightened instability in the impedance of the device and created a situation where the gas response was more difficult to

ascertain. Additionally the feasibility of implemented an on-chip vacuum evacuation system for the sensor is highly non-trivial. As a result, pressure purging was shown to increase system complexity and was ineffective at purging the device in a stable, repeatable manner.

2.2.3 Humidity

During preliminary testing, the moisture response of the porous silicon gas sensor was analyzed with respect to a dry nitrogen background. In the experiment, an initial flow of dry nitrogen was used to establish a baseline for the device. A set of manual three way valves was rapidly adjusted in approximately one second in order to switch the flow the dry to a saturated flow of high purity nitrogen. A example of a moisture test is given in Figure 2-18.

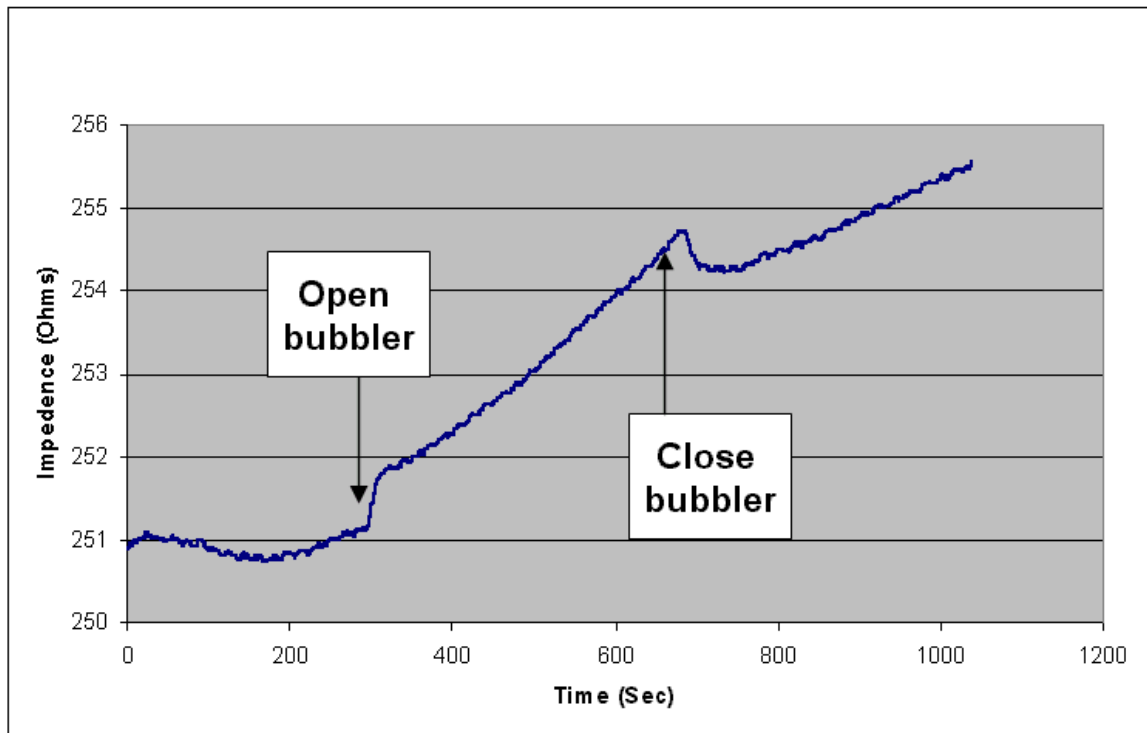


Figure 2-18: Opening and closing of bubbler that exposed porous silicon device to saturated nitrogen

One should note the drastic baseline drift that was commonly associated with moisture response experiments. Some sources of error that may generate increased drift are general contamination in the bubbler system and the residual existence of moisture in the tubing after the conclusion of an experiment.

Baseline stability for moisture analysis was acquired after 6-8 hours for both room temperature and 50 °C experiments. This time for stabilization suggested that a moisture analysis was not an effective method for rapidly screening gas sensors in order to optimize geometry or pore structure. The results of the moisture analysis are given in Table 2-2.

Table 2-2: Moisture response of porous silicon

	Response (ohms)	Response time (sec)	Return (sec)
Test 1 (Room)	0.8	45	90
Test 2 (Room)	1.3 - 4.5	150	24
Test 3 (50 C)	0.75	15	18
Test 4 (50 C)	0.75	17	18

2.2.4 Baseline drift

The final environmental method that was sought for rapid screening of gas sensors was an analysis of baseline drift. This measurement technique was essentially an aggregate analysis of all aforementioned environmental factors as well as measure of the electrical stability of the device. In this procedure the baseline was tracked for time-lines from 3 hours up to 2 days. In the analysis, three components were analyzed. The first component was the average and deviations of the baseline. This analysis was a valuable

metric for characterization because it gave a first pass screen for the variability that was commonly encountered during testing. By comparing this variability to the observed magnitude change due to a gas or environmental factor, one could acquire a qualitative sense for the validity of the experiment. Furthermore, since one had a qualitative understanding of noise sources and frequencies, an improved ability to discern noise from a genuine gas response was obtained.

The second analysis of baseline drift was a qualitative assessment of localized high-magnitude instability in a sensor. This form of noise was highly problematic for the accurate measurement of a sensor. If devices with this error were implemented in real-world applications, a substantial false positive rate would result. For the purposes of experimentation, this error was also highly problematic. If the localized instability occurred during the course of a gas, pressure, or temperature experiment, it would be difficult to distinguish the behavior from the parameter of measure in the experiment (Figure 2-20). The final measure of baseline drift was a frequency analysis of the noise sources. This method would help correlate reoccurring sources of error.

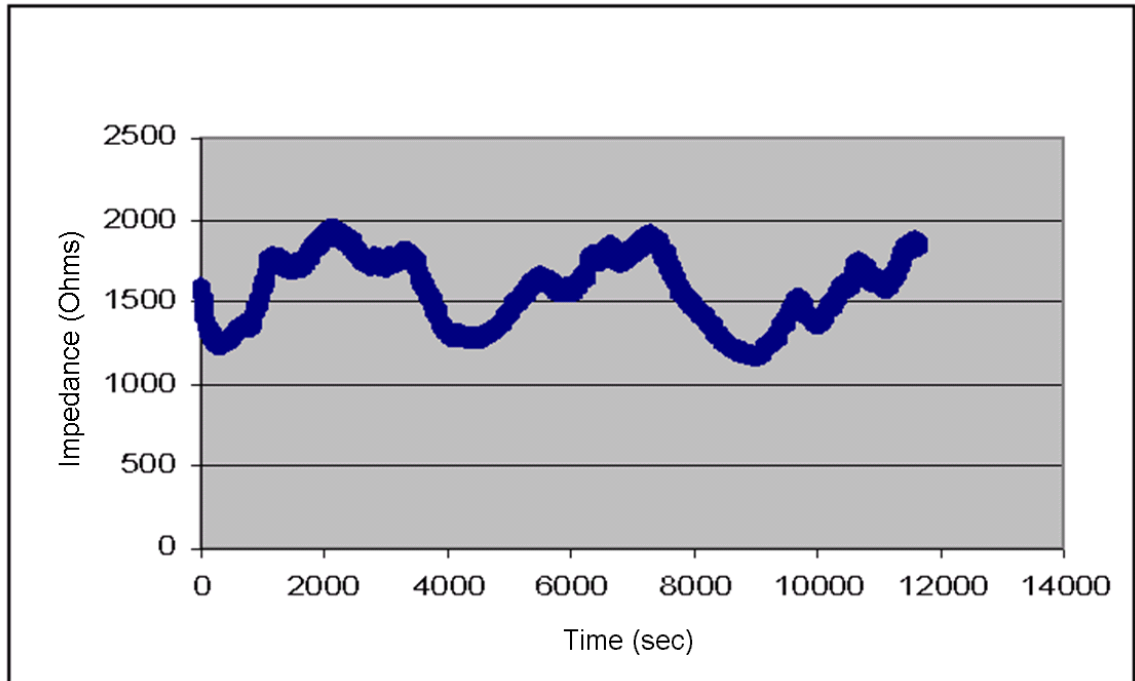


Figure 2-19: 3.5 hour response of a sensor with several apparent frequencies of noise

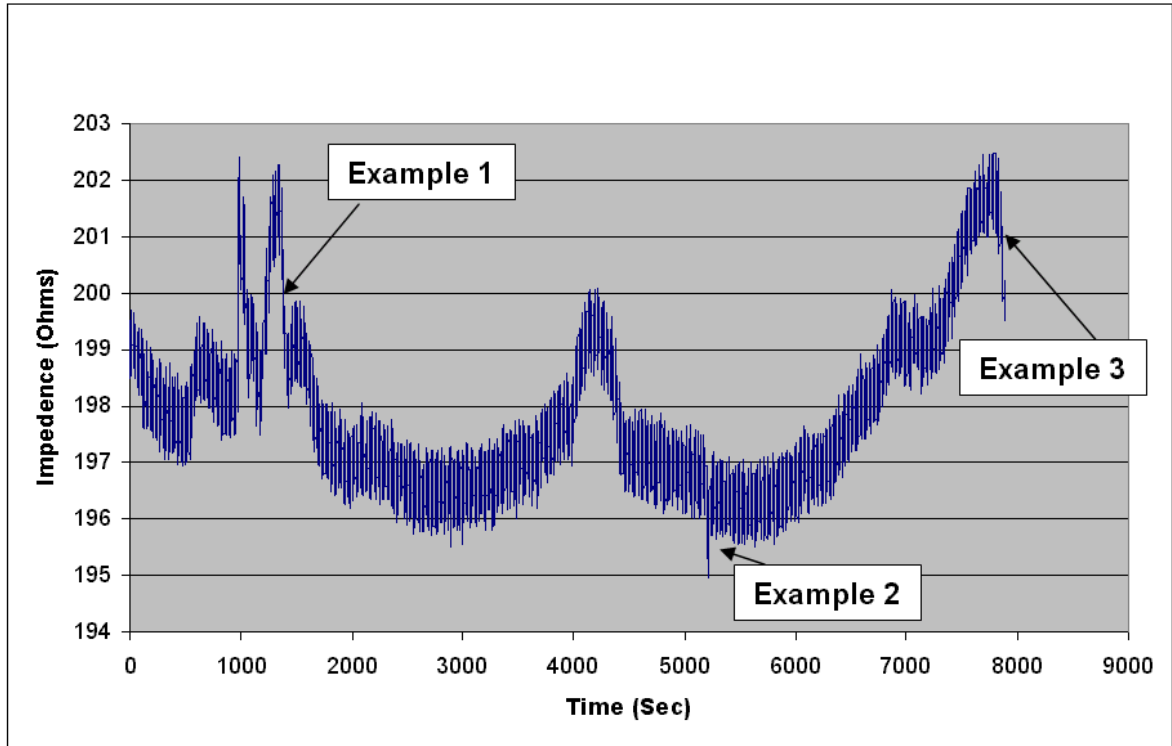


Figure 2-20: Three examples of localized high magnitude instability in a sensor over a three hour time-span

Finally, Table 2-3 provides a side-by-side comparison of several gas sensors and their relative noise sources. All tabulated values are for a sensor under dry nitrogen for a time period of 2.5 hours. Within the table, the average column is the total impedance averaged during the course of the entire experiment. Similarly, the standard deviation column is the deviation of the signal during this period. The third column is simply a ratio of the deviation over the signal. If localized high magnitude errors were present, “Y” was the answer given in the fourth column. Finally if repetitive frequencies were present in the signal, the frequency of the oscillation is provided in the fifth column. The mechanism for extracting the frequency of this noise (as well as gas signals) is given in Chapter 4.

Table 2-3: Comparison of noise parameters for several sensors

PS Type	Average	St. Dev.	Dev/Avg (E-3)	Localized Errors	Dominant Frequencies
Sensor #7	221.5	3.33	15.02	N	1.6 mHz
Sensor #12	266.7	3.63	13.61	N	1.55 mHz
Sensor #19	979.0	101.05	103.21	Y	.06 mHz
3.2.3 #2	4746.7	161.62	34.05	N	1.65 mHz
3.2.1 A	1893.0	23.98	12.67	N	1.65 mHz, 3.2 mHz, 4.9 mHz

2.2.5 Conclusions from environmental testing

The results from environmental testing revealed that no single measure was predicting a gas sensitive device. Furthermore, the process of identifying a device that was stable from the standpoint of environmental factors often also led to a device that

was not responsive to reducing gases. As a result, the attempt to correlate gas sensors against a simple environmental parameter was shifted to a study of electrical properties.

2.3 Electrical Behavior

Within this section, both the basic electrical properties and methods to screen sensors based upon their electrical properties will be introduced. Electrical screening for performance analysis is a critical requirement for rapid quality control analysis of gas sensors. The challenge that resulted from this study, however, was that non-ohmic electrical characteristics often identically led to improved gas sensitivity. In this section preliminary results of electrical analysis will be introduced and some key issues associated with performance differentiation based upon this metric will be described.

2.3.1 Resistance and impedance of the gas sensor

The first parameter of interest was the fundamental resistance of the device between the two gold contacts on the device's surface. Efforts to minimize this parameter would result in a lower power device that was better suited for portable applications. During the evaluation process, resistance was originally suggested as the criteria by which to screen gas sensors. If this were an effective technique, devices could be rapidly screened and poor devices could be removed. Unfortunately, this theory was refuted by both the results of gas testing and the observed behavior of the device when poisoning occurred.

Table 2-4: Initial resistance of various gas sensitive devices

Device #	6	7	17	3.2.1 H	3.2.4 #4	3.2.5 #4	3.2.3 #7
Resistance (ohms)	1460	203.6	117	1400	1990	771	275

Although specific manufacturing processes can create a highly ohmic device, this parameter does not necessarily dictate a propensity to gas sensitivity. Table 2-4 tabulates some devices with gas sensitivity and their respective baseline resistance. In order to acquire the resistance, a multimeter, which provided a 10mV DC signal, probed the device in a pad-to-pad configuration (Figure 2-6). These results were later verified with an impedance analyzer. This experiment demonstrated that the impedance of the device was resistive. The imaginary component of impedance accounted for less than one percent of the observed signal. Furthermore, the results of the multimeter were in agreement with the impedance analyzer (taken at the same potential).

This experiment provided compelling evidence against a direct correlation between gas sensitivity and impedance. Neither resistance nor impedance was a sufficient condition for differentiating sensitive devices. This testing, however, did provide a basic range for reasonable devices. From this chart, it is apparent that resistance was not a sufficient parameter for segregating gas sensitivity. It should be noted, however, that gas sensitive devices tended to range from 100 – 2000 ohms.

A specific incidence of poisoning of the device indicated that sensitivity and impedance parameters can become decoupled. Prior to exposure to acetone, sensor 3.2.4#1 had an impedance value of approximately 600 ohms with a baseline range from 500-1500 ohms during testing. When the device was exposed to acetone, the impedance increased to approximately 12 kilo-ohms. After approximately one week, the impedance

recovered to 700 ohms. Its gas sensitivity, however, was completely destroyed. Additionally this sensitivity could not be recovered with additional cleaning treatments (discussed in Chapter 5) even though these treatments resulted in lower impedance. As a result, the resistance parameter was shown to be completely independent of gas sensitivity. This factor alluded to the need for a rapid gas testing method for all devices.

2.3.2 I/V plots for contact assessment

The current voltage (I/V) plot is a common tool used to identify Schottky barrier height in a metal/semiconductor interface. During the characterization process for porous silicon, the I/V plot was used to evaluate the device for stable and ohmic contact. Contact stability was an issue with many devices. For an unstable device, the standard deviation of the measured current was greater than 50% of the average value.

Within the porous silicon formation process, two methods of contact were attempted. The first method of contact was direct deposition of gold with a CVC E-beam evaporator. Evaporation is characterized by a highly anisotropic coating on the surface of the pores. I/V plots for evaporated gold contacts are given in Figure 2-21. It should be noted that with this process, a high degree of variability was noted. The yield of wafers manufactured with this technique was typically around 5%. Sensors with a large gas sensitivity (relative to electroless metallization contact) were produced.

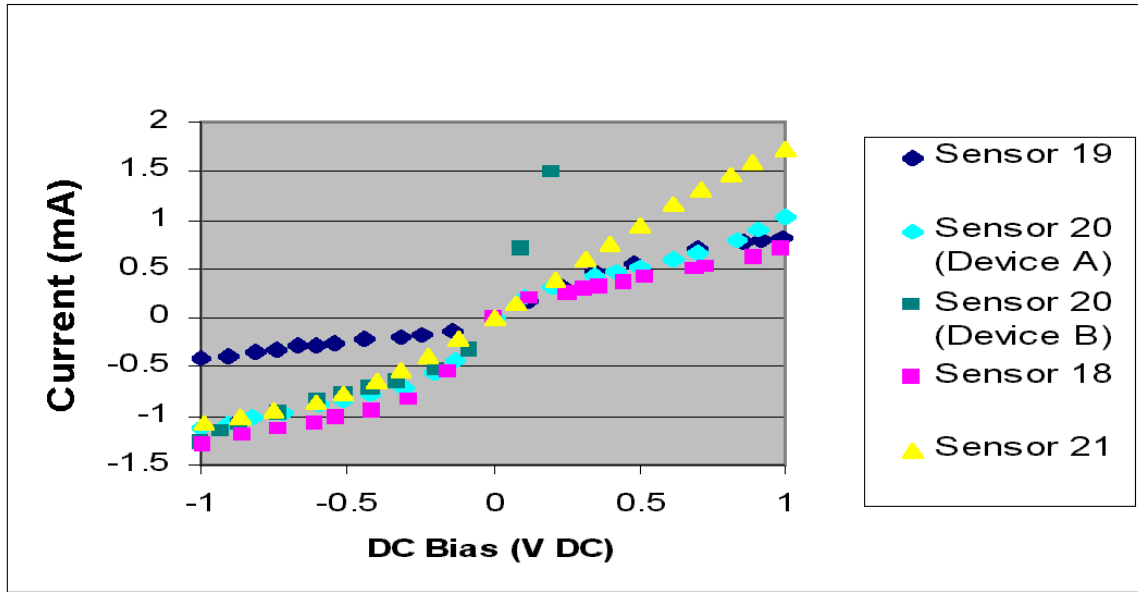


Figure 2-21: Variations in the I/V characteristics of gas sensors fabricated with an evaporated gold contact pad

An alternative method of contact was electroless metallization of porous silicon structure followed by an evaporated coating of gold. Depending upon the specific form of porous silicon that was fabricated, this method produced a highly ohmic contact. This lower contact resistance, however, was also correlated with a smaller impedance change when the device was exposed to gas. An I/V plot of an electroless metal contact is given in Figure 2-22.

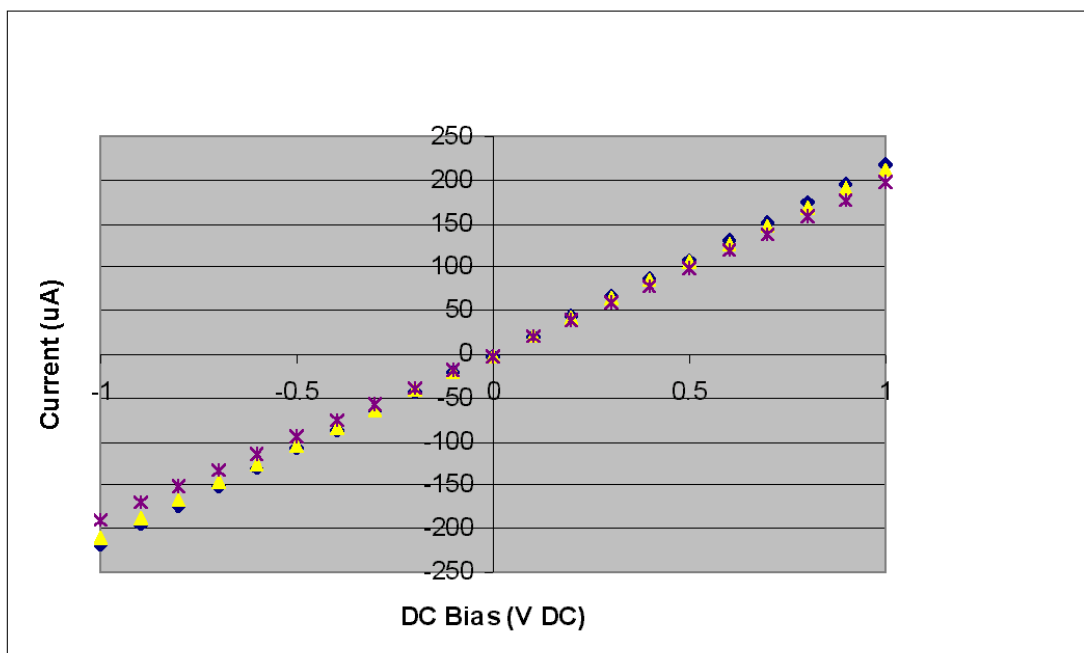


Figure 2-22: I/V plots of three devices formed with the electroless metallization method

While the former case indicated non-ohmic contact, it also periodically led to devices with a larger sensitivity for a short pulse of gas. This conclusion, however, must be weighted by the fact that over 80% of all fabrication runs were performed without electroless gold. Within the total manufacturing run of 25 wafers of porous silicon, only 3 wafers were formed with electroless metallization techniques. Since all improvements in fabrication were geared toward the results of the direct e-beam pads, little improvement in the sensitivity of electroless gold pads occurred. As a result, opportunities associated with optimization of a porous silicon structure with an electroless interface exist.

2.3.3 I/V plots assisting a manufacturing decision

The I/V plot was also an effective tool for evaluating the porous silicon manufacturing processes. In one example, the decision of intentional misalignment was refuted by simple electrical inspection of the device. The technique itself was an attempt to circumvent issues associated with wirebonding to a porous silicon / gold surface. In order to improve the ease of bonding to the surface, the gold pads of a given mask were often misaligned such that a fraction of the gold pad was in direct contact with silicon and not on the porous silicon surface (Figure 2-23). This small island of flat surface was used as a bonding location. An electrical investigation of this approach, however, revealed that the gold was not conformally coating the trench that separated the Au/silicon area from the Au/Porous silicon area. As a result, the conductivity over this area was highly non-ohmic. Results of this test are illustrated in Figure 2-24. One potential solution to this issue is to increase the total thickness of gold coated onto the pads of the porous silicon wafer. With this process, however, a new recipe for photolithography may be necessary.

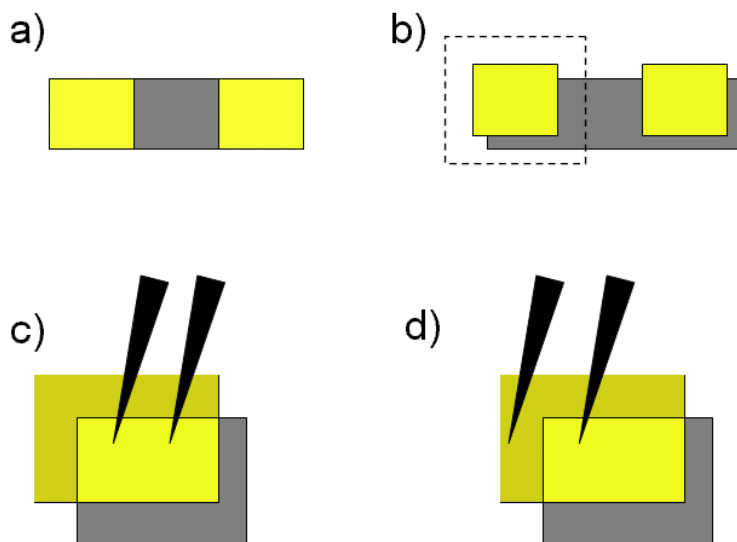


Figure 2-23: a) Normal porous silicon sensor b) porous silicon sensor with misalignment
 c) detail section of probe configuration for gold-gold I/V test
 d) detail section of probe configuration for gold-step I/V test

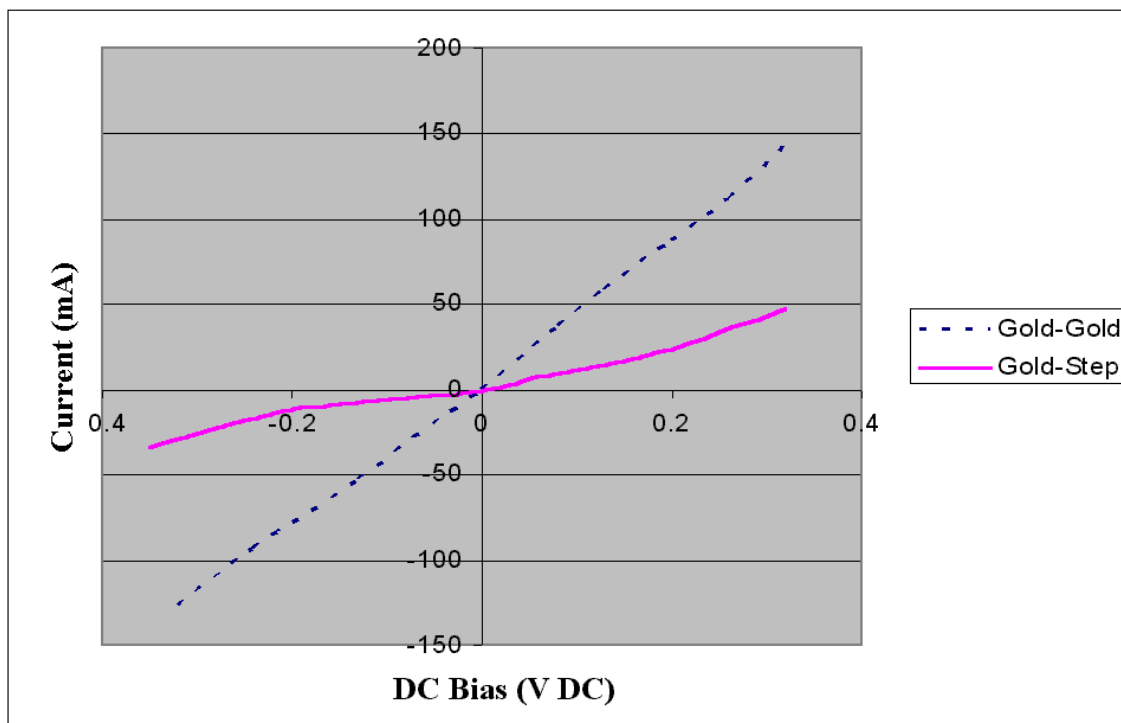


Figure 2-24: Detrimental effect of intentional misalignment

I/V analysis, in the end, was performed on almost all manufactured sensors. It served as an indicator for both ohmic device contact as well as a tool to assist manufacturing decisions. A highly ohmic contact, however, was not a sufficient criteria for evaluating porous silicon gas sensors (Figure 2-25). As a result, additional methods were sought.

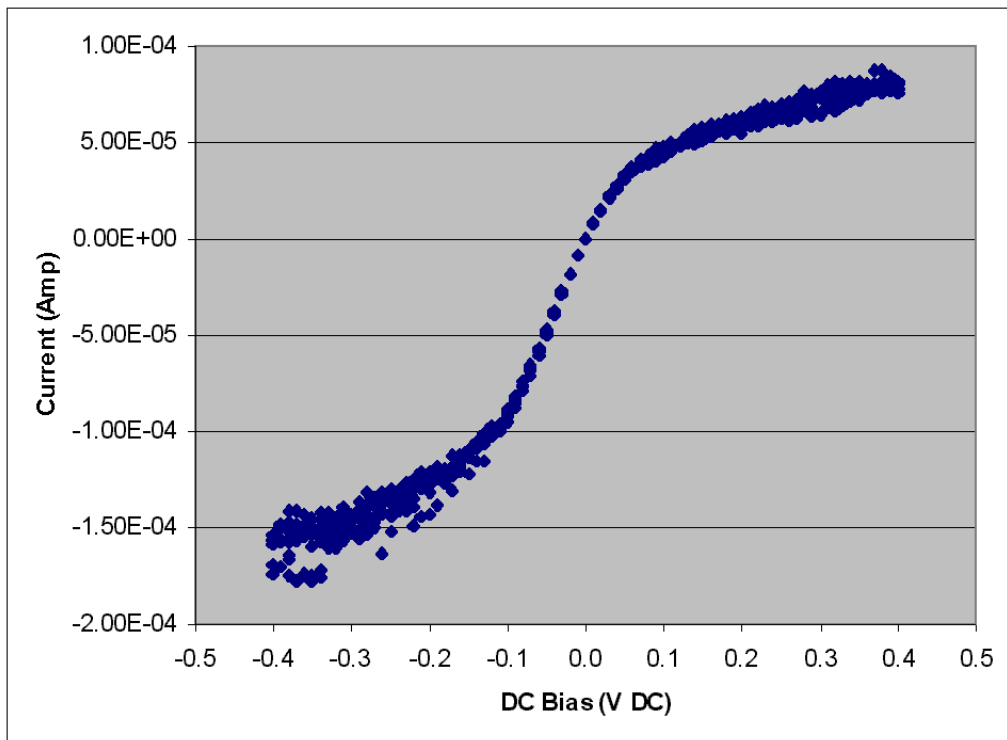


Figure 2-25: I/V plot of highly non-ohmic but gas sensitive device

2.3.4 I/V plots thru the device

In order to understand alternative current pathways and uncover any barriers, I/V analysis was conducted from the upper gold contacts through the bulk of the (100) silicon substrate (Figure 2-6b). The constant area for this probe configuration was 4 mm², hence the Schokley equation was adjusted from current density to current by the relationship:

$$j = \frac{i}{A}$$

[Equation 2-1]

In this equation, A is the area of constant current was assumed as the two pads on the upper surface of the device. The results are well matched to values predicted by the ideal diode law, the Schokley equationⁱⁱⁱ.

$$i_0 := i_s \mathbf{e}^{\left(\frac{nqV}{kT} - 1\right)}$$

[Equation 2-2]

In this equation i_0 is the observed current, i_s is the saturation current, n is the ideality factor, q is the charge of an electron, V is the supplied voltage, k is Boltzmann's constant, and T is the absolute temperature in the room. Assuming room temperature conditions q/kT is approximately 38.6. Fitting to the results from the I/V sweep through the device, one obtains that i_s is 0.03 mA and n is 0.1. A representative result is given in Figure 2-26.

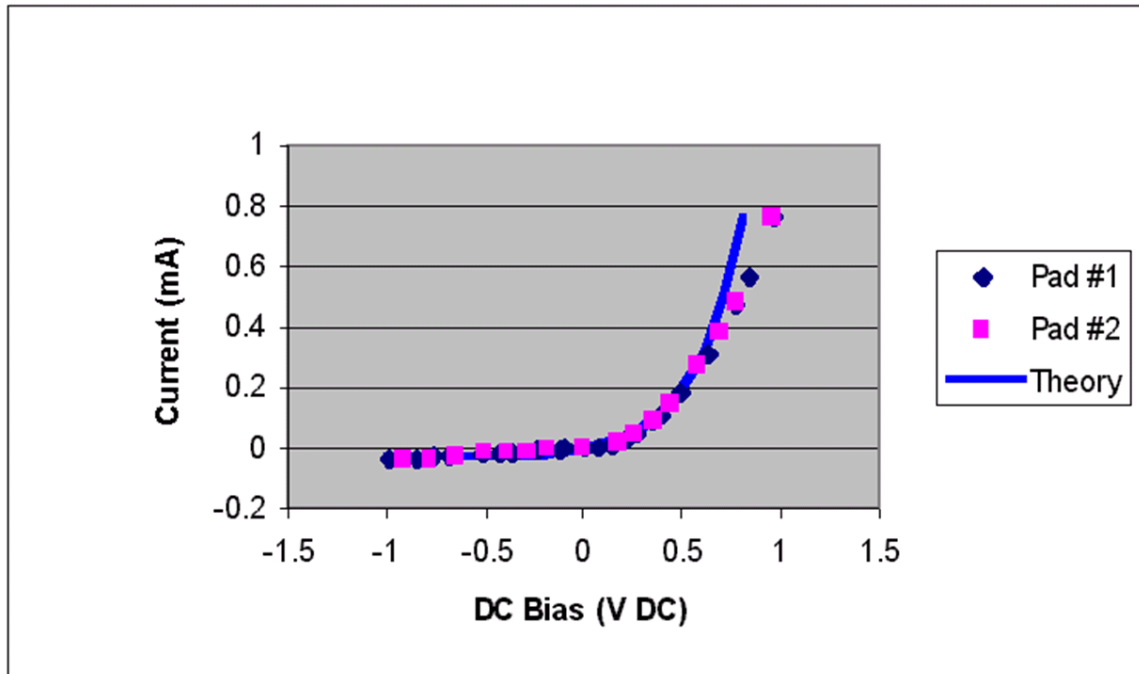


Figure 2-26: I/V plot of through-contact on a porous silicon gas sensor

2.3.5 Conduction in a second path

Given the relative length-scale of the device versus the thickness of the wafer and the relatively low doping level of the bulk silicon (1-20 ohm-cm), a secondary path for current was uncovered. This alternative pathway involved current traveling from the top contact through the wafer to the backside aluminum contact. Since a uniform aluminum coating with three ohms of resistance covered the backside of the device, the secondary pathway had an appreciable contribution to the measured parallel resistance. This problem could not be overcome through the removal of the aluminum, because it was an essential component for uniform etching of porous silicon. Removal of the aluminum layer would increase the uncertainty of the porous silicon etch process. Alternative solutions to this problem could include reducing the separation distance between the two contacts on the upper surface or selection of a silicon wafer with a higher resistivity. The

later solution, however, is highly problematic given that etch condition are typically based on low resistivity wafers.

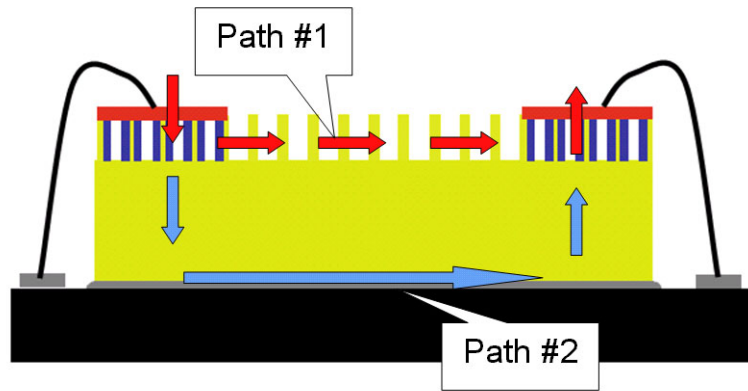


Figure 2-27: Schematic of 1) current path across porous silicon and 2) path through bulk of device and along backside aluminum contact

2.3.6 Gold adhesion

During the manufacturing process, the liftoff of the metallized gold layer was a process that had limited success. While liftoff was a source of considerable concern during fabrication, a residual aspect of this issue arose during sensor evaluation. Due to fabrication issues including the fundamental nature of etching porous silicon, the thickness of the silicon carbide layer, and the amount of deposited gold, a thin gold layer occasionally connected the two gold pads used for measurement. The thickness and uniformity of this gold layer were of a geometry such that the resistance between the pads was 20-50 ohms. Unfortunately these values were identical to the original target values for the manufacture of a low resistance porous silicon structure. The only means by which this error could be uniformly addressed was an analysis of the stability of the porous silicon structure under a nitrogen flow. If the gold runner was present, variation

during testing in the sensor was often less than 0.06 ohms. With this mechanism in place, sensors could be systematically screened for this error. Visual inspection served as a sufficient validation against gold adhesion issues (Figure 2-28).

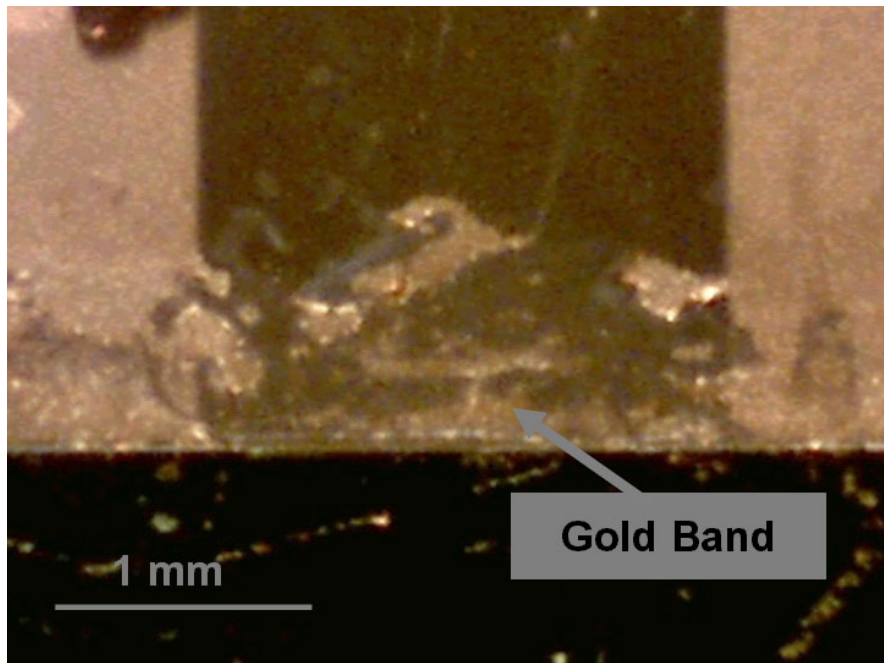


Figure 2-28: Picture of a porous silicon device with a large gold band that directly grounds the two gold connection together

2.4 Gas Response Measurement

The initial yield on the production of porous silicon gas sensors was less than five percent. The aforementioned environmental and electrical techniques for analyzing porous silicon gas sensors were essential due to the limited number of functioning devices that were achieved. In fact, from the original 21 wafer runs which produced a total of 252 devices, only 21 devices were of low ohmic resistance with a promising pore structure. Of these 21 devices, nine were successfully wire bonded for a period of three

or more hours. Of these nine devices, three produced a measurable gas response. In this section, the observed behavior and method of analysis for these three devices will be discussed.

2.4.1 Sensor #6

The first functional sensor, sensor #6, produced a detectable response to ammonia gas delivered at a concentration of 25-75 ppm at a rate of 20 SCCM. The device was evaluated under a carbon monoxide flow, but it did not demonstrate a response. The sampling waveform for all experiments was 100 mV AC at 1 kHz. Eight gas experiments were conducted on sensor #6, three of these resulted in a measurable response. In each case, recovery of the device took approximately 45 minutes after one 6 minute pulse of gas at a specified concentration.

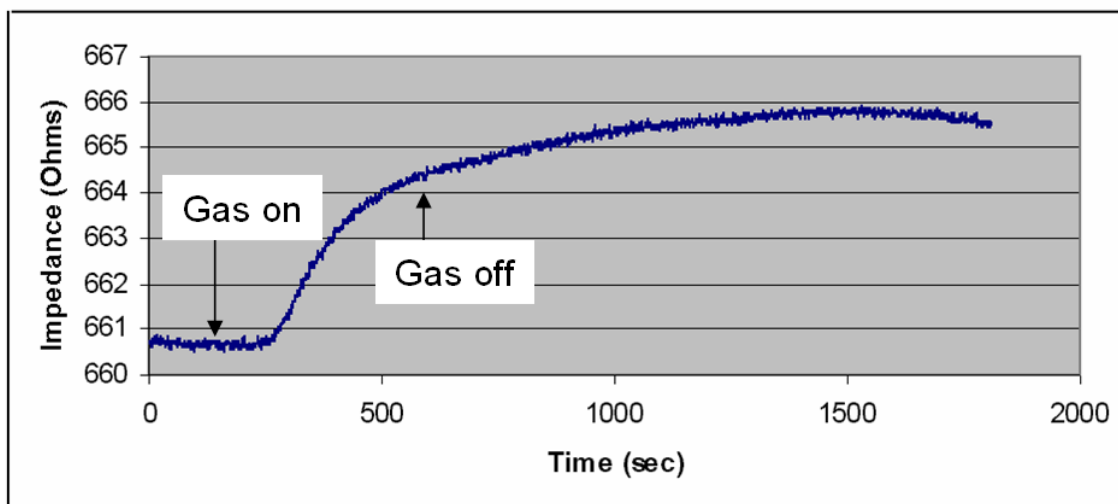


Figure 2-29: Response of sensor #6 to a six minute pulse of NH_3 at 50 ppm

2.4.2 Sensor #7

For the second sensor, sensor #7, the experiments were conducted at 20 SCCM and 120 SCCM with test gases of ammonia and NO_x. A total of approximately 60 tests were conducted on the device including temperature pulsing (Figure 2-13), gas evaluation (Figure 2-30), and variation of mass flow rate. In each case, sensor #7 was evaluated at a heightened temperature of 100 °C. Approximately 5 gas responses in total were observed during the course of testing. For each gas pulse the profile was 60 seconds of gas at a given concentration followed by 28 minutes of recovery.

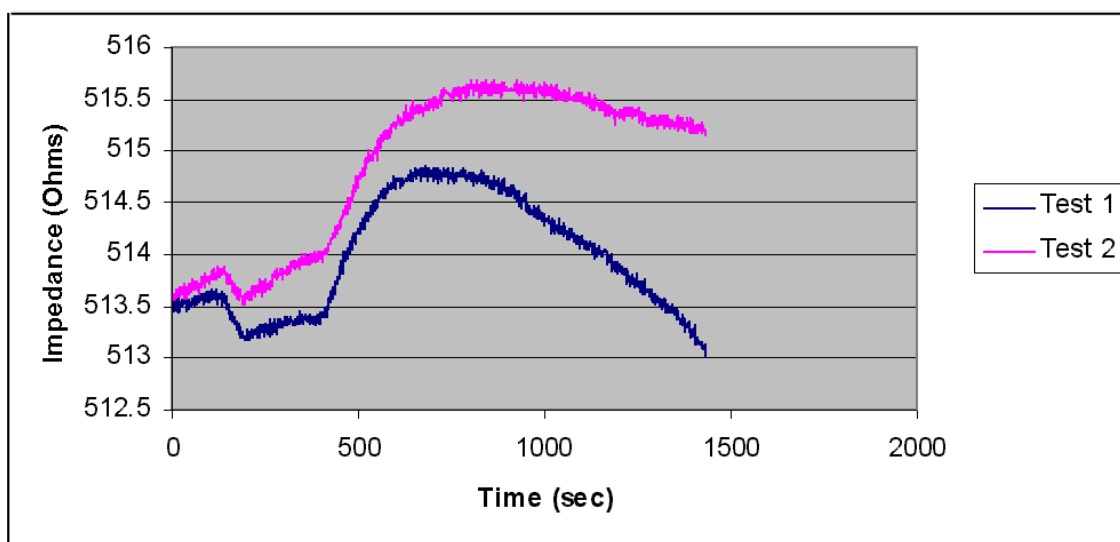


Figure 2-30: Two tests performed on sensor #7 at 7.5 ppm NO

The experimental testing for both sensors 6 & 7 was the flow through test setup with over 9 feet of tubing (Figure 2-1). Since the gas took approximately 9 minutes to reach the sensor and since the recovery time was 1/20th the rate of response, the experiment and recovery runs for these configurations lasted approximately 1 hour.

Within these experiments, several failures were noted during the attempt to repetitively test the device. Some known sources of error that contributed to the failure include the presence of a low frequency noise sources that confounded results, repeating of tests before full recovery of the device, and excessive duration of the gas pulse (led to saturation issues).

2.4.3 Sensor #17

Sensor 17 was evaluated under the experimental setup with approximately 1.5 feet of tubing (Figure 2-4). A combination of this configuration and the banding¹ of the porous silicon on the device led to unique and beneficial properties. The first beneficial property of the sensor was a rapid and reversible response. The only requirement for reversible purging of this device was a 3 minute pulse of high purity nitrogen at a flowrate of 20 SCCM. This corresponded to a recovery that occurred at approximately 1/3 the rate of response. Experiments were conducted on sensor 17 with gas concentrations from 3 ppm to 110 ppm with a fixed impulse of 60 seconds. An additional experiment conducted on sensor 17 was a variation on the impulse length for the test gas from 30 seconds up to 3 minutes.

¹ Banding refers to porous silicon structures with non-uniform pore growth across the surface of the device. These non-uniformities can lead to the presence of several forms of porous structure on one device.

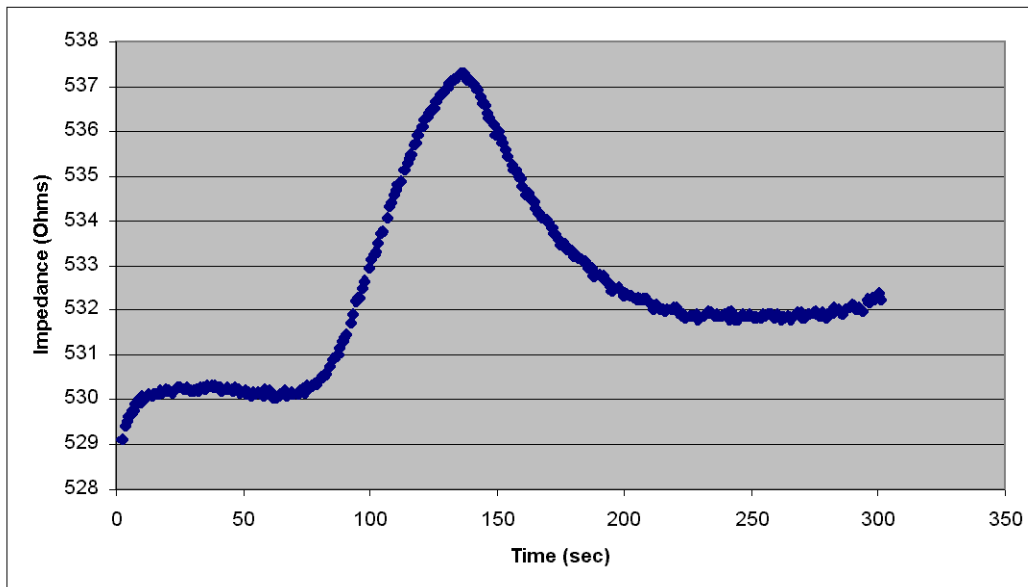


Figure 2-31: A response of sensor #17 with a shorter recovery time

2.4.4 Preliminary signal processing

Early signal processing techniques were unique to the specific batch of porous silicon under analysis. Processing on sensor #6 involved a two part system. After obtaining the initial gas response, the signal was compensated linearly according to the temperature of the experiment. Once that process was completed, the impedance value was measured by taking the average of the value of the signal before the gas exposure and subtracting this value from the 10 point average obtained exactly 6 minutes after the initial response. For sensor 6, which had an impedance level of 1.46 k Ω , a compensation rate of -16.3 $\Omega/^\circ\text{C}$ was determined (see Figure 2-21). This rate, although quite high, stabilized the baseline of the sensor's response and allowed for simple solution extraction. The results from the three experiments are given in Figures 2-32 through 2-34.

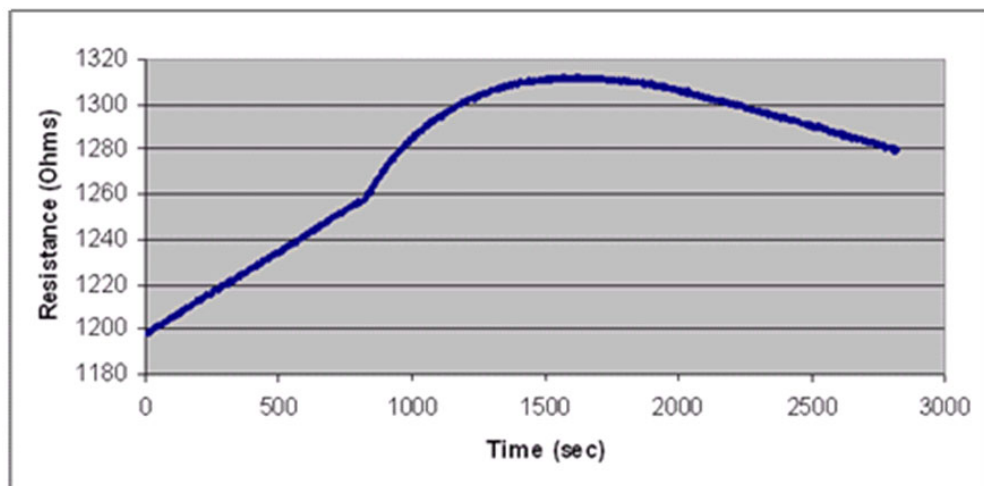


Figure 2-32: Raw sensor output of device 6 to 50 ppm NH_3 at 20 SCCM

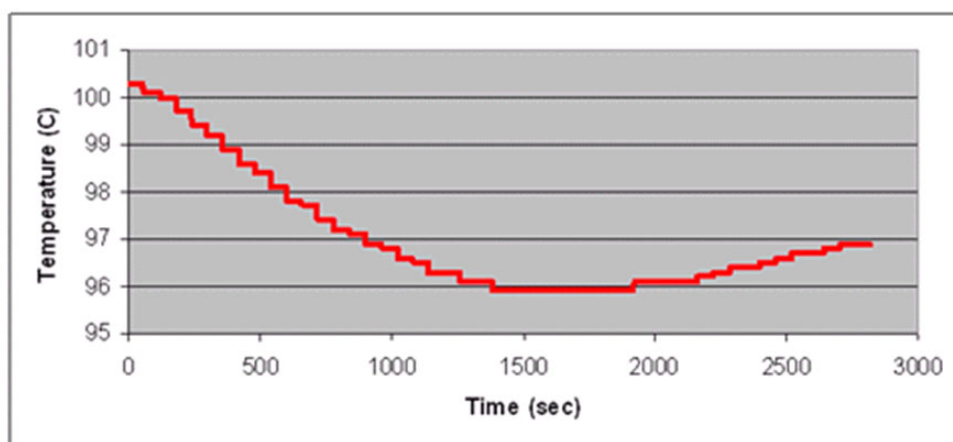


Figure 2-33: Temperature variations during experiment

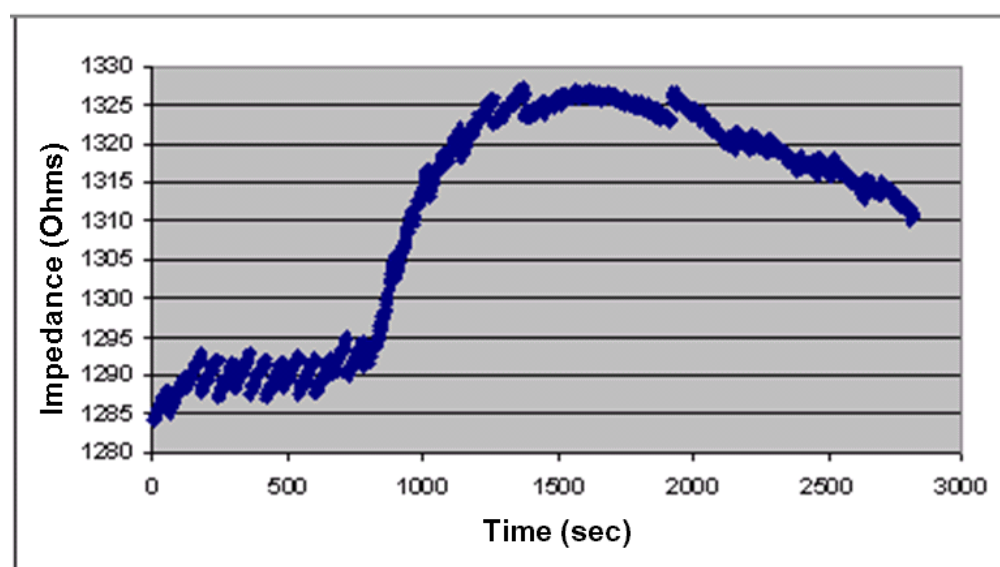


Figure 2-34: Sensor output after linear temperature compensation

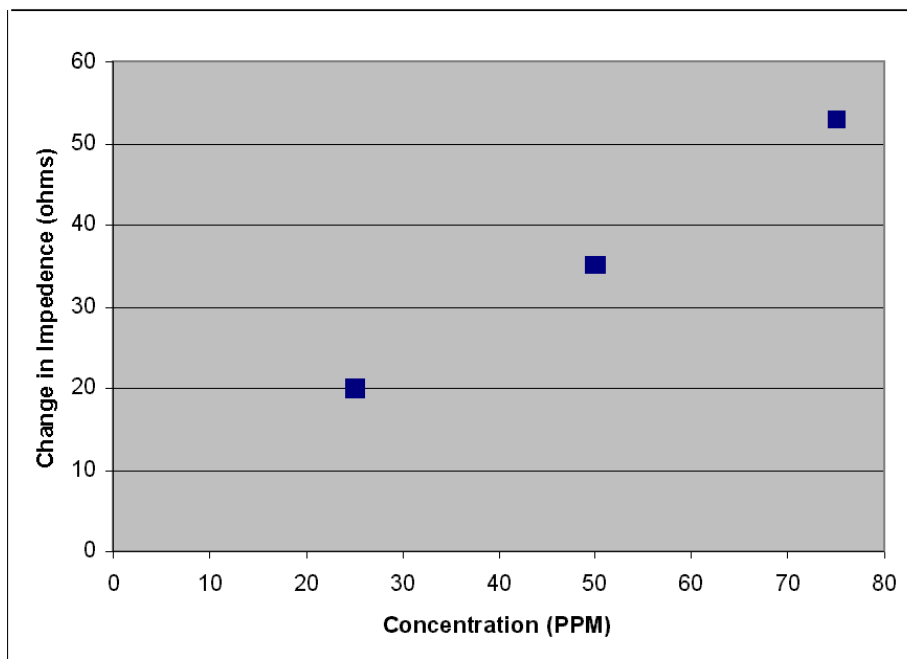


Figure 2-35: Results for sensor #6 after three different exposures

The routine for extracting data from sensors #7 and sensor #17 was similar to the method used for sensor #6. In both cases, only two data points were taken in order to ascertain the slope change associated with the gas response. The first data point was immediately prior to the inflection point that indicated a gas response. In both Figures 2-30 and 2-31, one can observe that this point is quite distinct. For sensor #7, some error was introduced by choosing these data points because a repeatable dip in impedance was observed prior to a gas response. This dip was uniform in shape for all ammonia exposures. For sensor #7, the second data point (the peak response) was taken at the local maxima within the given timescale. For sensor #17, since the pipe length was shorter and travel times were more stable, the maxima was selected as a data point exactly 60 seconds after the first data point. Figures 2-36 illustrates the selected points on the responses of sensor #7.

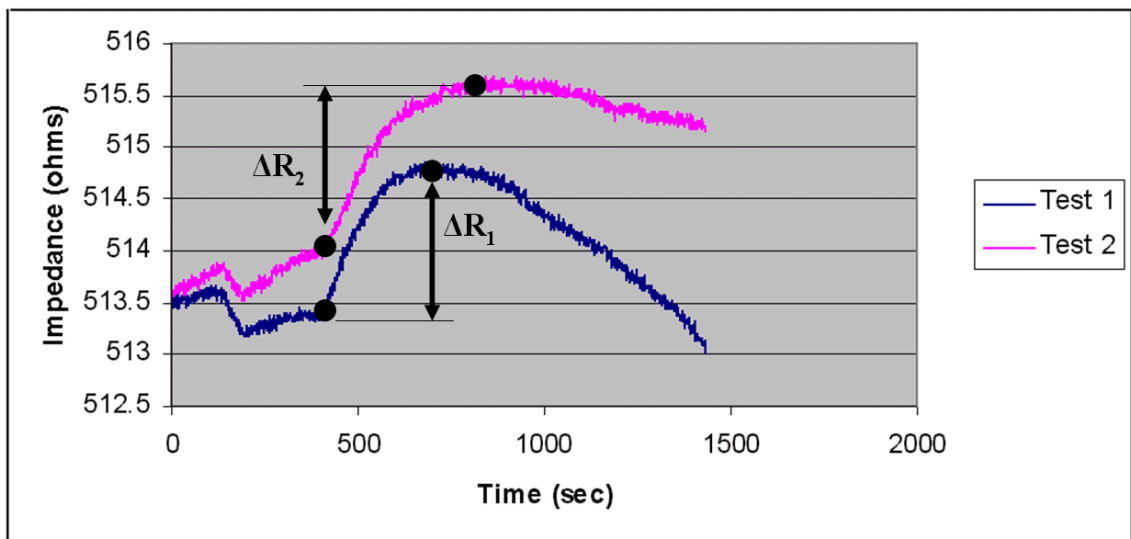


Figure 2-36: Indication of how data points were recorded for Sensors #7 & #17

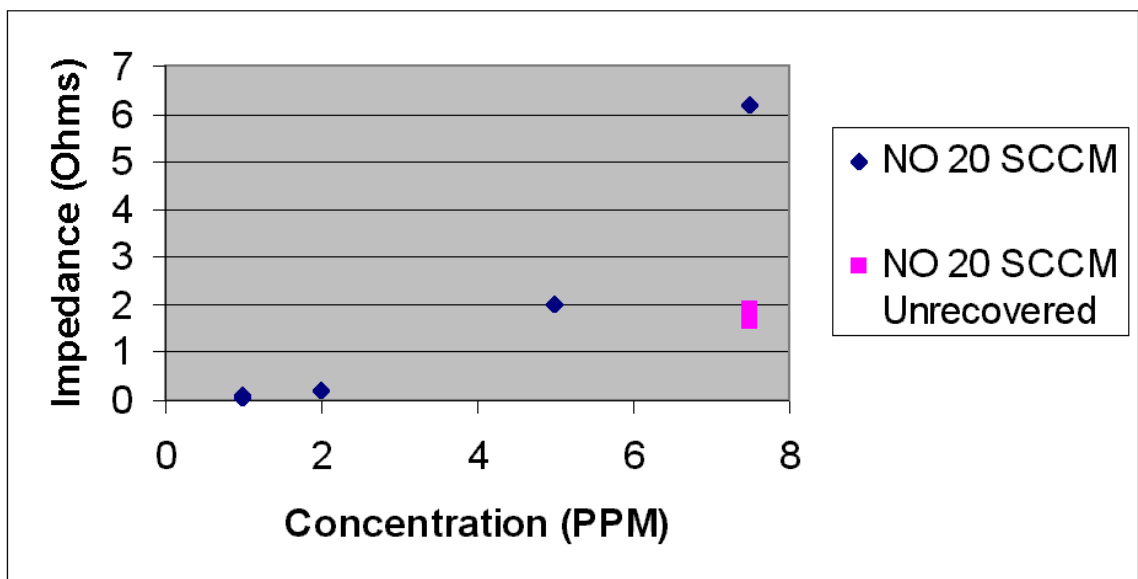


Figure 2-37: Processed gas responses for sensor #7

During the process of data extraction, several sources of error were noted. The first error was associated with drift of the device. If the sensor possessed substantial positive drift, the measured impedance change was artificially large. Similarly if the impedance change occurred during downward drift, the measured change was artificially small. To counter this effect, measurements on highly drifting baselines were rescaled by the average of the baseline over the experiment.

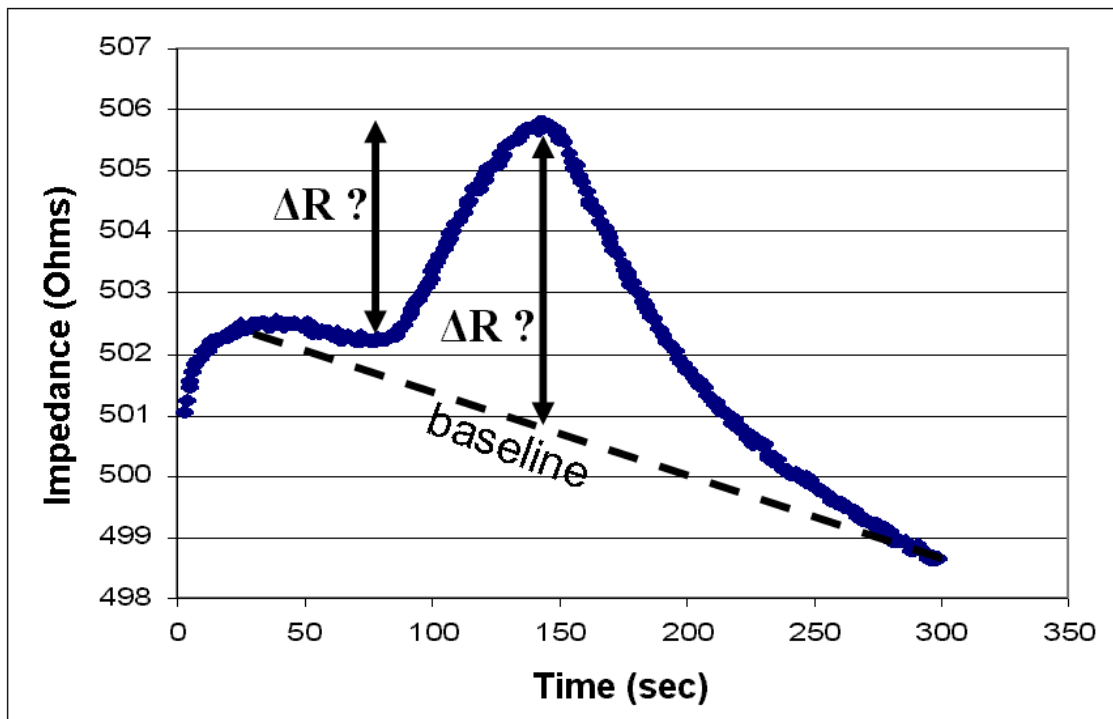


Figure 2-38: Illustration of difficulty in determining “actual” delta R on drifting baseline

A second distinct error was associated with the exact location of “initial” gas exposure for the first data point. The observed onset of gas exposure occurred slowly over a time three to seven second period. While the lower approximation represented the actual onset of gas, its specific location was more difficult to distinguish than that of the

upper bound for this onset region. To resolve this issue the upper bound and lower bound were approximated, and a data point 3 seconds after the lower bound was arbitrarily selected as the onset data point.

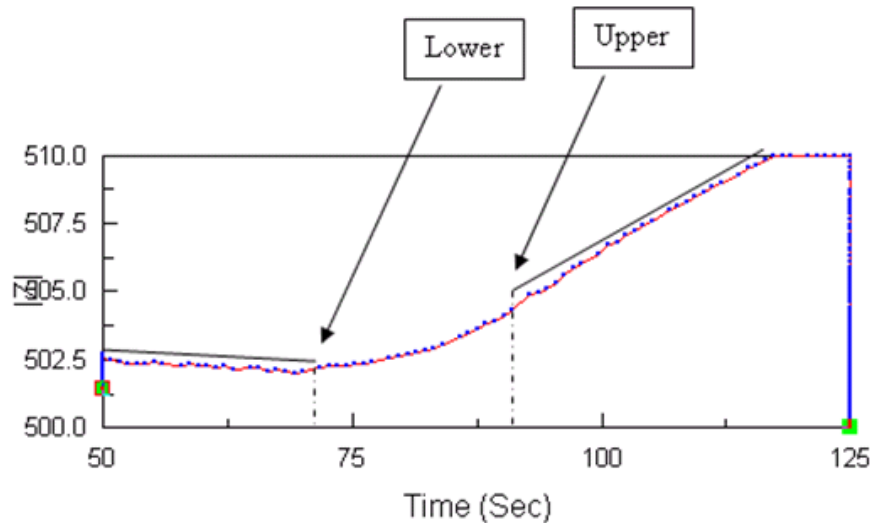


Figure 2-39: Gradual onset of gas response in sensor #17

2.5 Performance Characteristics for Sensor 17

2.5.1 Lower onset of detection to NO_x

Given a subset of 36 data points for the gas response of sensor 17 to NO at various concentrations, the lower onset of detection (LOD) could be computed. This limit was of particular interest in order to establish the limitations of the device and place its operation into a feasible real world context. In order to compute the lower exposure limit, the set of 36 data points was first fit to a linear regression scheme (Figure 2-40).

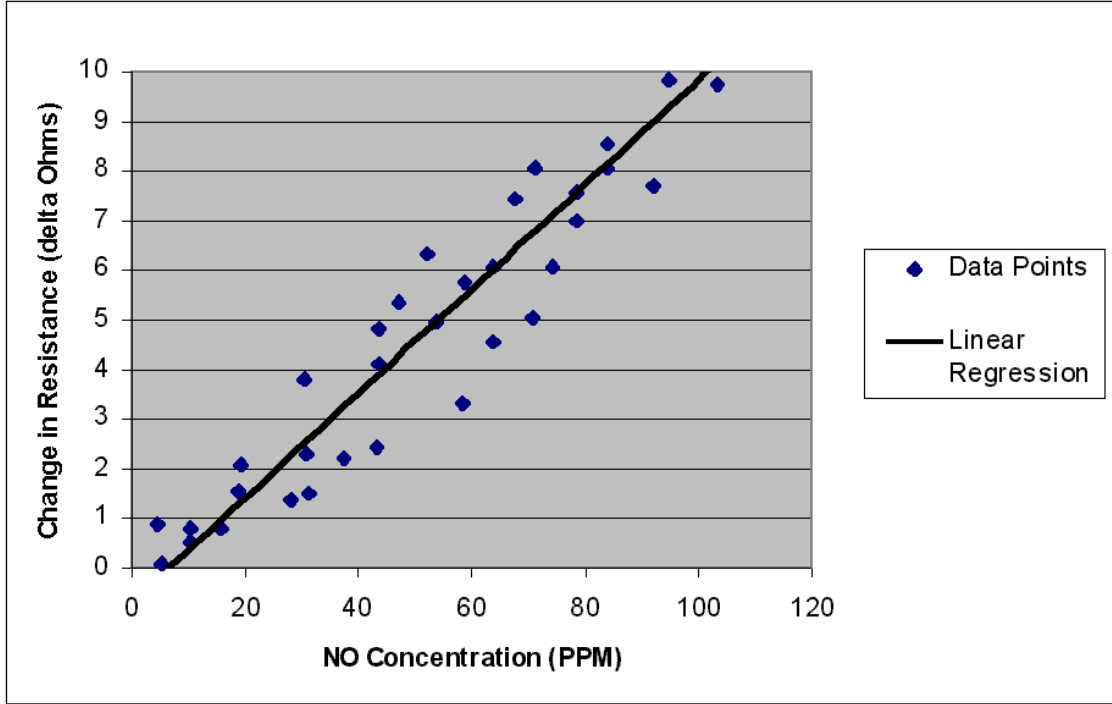


Figure 2-40: 36 data points with linear regression scheme for response of sensor #17

The equation for the linear fit for the 36 data points of NO_x response in a range of 2-100 ppm was:

$$\Omega(c) := .105 c - .6879$$

[Equation 2-3]

For this case $\Omega(c)$ was the resistance change observed in the device as a function of concentration and c was the instantaneous concentration in ppm. From this linear approximation, one notes that sensor 17 had a sensitivity of 0.105 ohms/ppm. Based upon this linear approximation, the variance of the response was computed as:

$$\sigma^2 = \sum_{n=1}^N \frac{(x_n(c) - \bar{x}(c))^2}{N - 1}$$

[Equation 2-4]

In equation 2-4, σ is the standard deviation of the actual data points from the linear approximation, N is the number of unique data points which are taken at a specific concentration, $x_n(c)$ is the value of the linear approximation evaluated at the specific concentration of “ N ”, and $x(c)$ is the actual data points at a specified concentration. It should be noted that since the data points are not taken at a single concentration, each data point is referenced to the linear approximation evaluated at the same concentration. Applying this equation to the results of sensor 17, one obtains a deviation from the linear approximation of 1.03 ohms. Based upon our previous definition (Chapter 1, Section 1.1.2), sensor 17’s LOD can be computed by doubling the deviation, plugging this value into equation 2-3, and solving for c . This yields a LOD for sensor 17 to NO_x of 26 ppm.

Several comments should be made based upon this result. The first critical factor is that this reported value is a conservative estimate to the limitation of analysis. No signal processing has been performed on the device in order to remove noise or reduce variability. In fact, the only signal analysis was a direct reading of the impedance change from the raw data file. The second factor that should be considered is the pulse duration for this analysis. The resistance change is based upon a 60 second exposure to NO_x . Through modifications in the pulsewidth of gas delivered to the device, the signal can be “boosted” to a higher magnitude at the cost of recovery time.

2.5.2 Transient analysis

The transient analysis of sensor #17 revealed a critical behavior of the device for the purpose of additional evaluation. In order to test transient response of the device, a gas sensor was pulsed with packets of gas of various widths. As one can see from Figure

2-41, increased pulse duration results in an increased impedance change of the device. For gas pulses of a duration of less than 60 seconds, the response has a linear derivative response with respect to time. Finally it should be noted that this response is well correlated with an error function approximation. This result is anticipated since the error function is a solution to Fick's law applied to a semi-infinite domain.

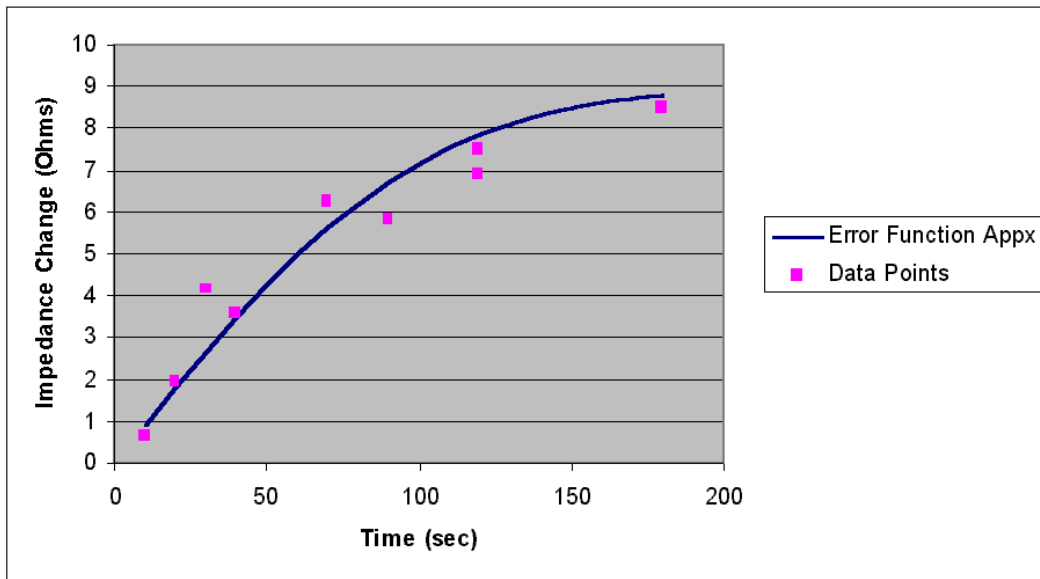


Figure 2-41: Sensor 17 reactivity at 70 ppm for various widths of NO at 20 SCCM

2.6 Motivation for a Novel Testing Technique

With a complete set of electrical, environmental, and gas pulsing experiments, the substantial variability in performance of porous silicon gas sensors has been demonstrated. While these techniques are not self-sustaining as a method for characterizing the porous silicon gas sensor, they do offer critical insight into issues that must be addressed. The relatively erratic device performance at this time can be attributed to both a learning curve on the manufacture of the device as well as a lag in learning from previous wafer runs. With devices bottlenecking at the wirebonding stage,

information on performance was not be rapidly transferred to improve the newest batch of devices. As a consequence, successive generations were manufactured with the same errors as earlier designs. In order to alleviate this issue, a new method of sensor analysis was essential. With this method testing would need to be faster and capable of acquiring statistically significant sets of small amplitude responses. Additionally, the analysis method needed to circumvent the wirebonding process such that more rapid design iterations could occur. A method that achieved these requirements will be discussed in the next chapter. With these changes in both the manufacturing and evaluation process, the yield rate for porous silicon gas sensors with any measurable gas sensitivity could be elevated above its original 1.2% average.

REFERENCES

- ⁱ L. Seals, The application of porous silicon surface and photo-catalysis – and electrochemical properties to sensor development, Physics Theses Georgia Institute of Technology (2002)
- ⁱⁱ L. Seals, J. Gole, A. Tse, P. Hesketh, Rapid, reversible, sensitive porous silicon sensor, Journal of Applied Physics, 91 (February 2002) 2519-2523
- ⁱⁱⁱ Sze, Physics of Semiconductor Devices, 2nd Edition, Wiley Interscience, New York, 1981.

CHAPTER THREE

GAS PULSING METHOD

3.0 Introduction

In this section, a novel parametric method of gas evaluation for a sensitive device in a room temperature environment will be detailed. A review of the experimental conditions utilized for characterization of the gas sensor will be given, and the noise sources inherent in this system will be described. From this discussion, the need for an alternative evaluation method will be presented. To meet this need, a Fourier Spectrum data analysis method based on periodic gas pulses will be described. In this method, the sensor's output will be transformed to the frequency domain, filtered to remove noise, and then transformed back to the time domain. This time domain signal will then be analyzed for 30 repeated cycles of gas. Post processing will provide the statistical distribution resulting from a gas sensor's exposure to a specific concentration of gas. Transient analysis of the device's signal as it tends toward an oscillatory equilibrium position will also be described. An example of the entire process will demonstrate the method's immediate applicability to gas sensor analysis. Finally the value of this system as related to the characterization of other sensors will be provided.

3.1 Experimental Conditions

3.1.1 Experimental setup

In order to describe enhancements to the evaluation method of the porous silicon gas sensor, a review of the current evaluation method is essential. The experimental

setup for the porous silicon gas sensor is illustrated in Figure 3-1. The objective of this configuration was to deliver a continuous flow of high purity carrier nitrogen (research grade, Airgas) that could be modulated rapidly with pulses of test gas. Calibrated cylinders of 1000 ppm NH_3 , CO , and NO_x (Airgas) were connected to calibrated mass flow controls (1179A, MKS Instruments) via $\frac{1}{4}$ inch stainless steel tubing. Gas was mixed at a $\frac{1}{8}$ " junction and driven onto the surface of the sensor at 100 SCCM. Thermocouples (Model 5TC K-type, Omega) positioned in the center of the gas traveling through the tubing and on the backside of the sensor package monitored the temperature variations throughout the tests. The sensor was connected to precision micromanipulator probes (DCM, Microtech) which were in turn connected to an impedance analyzer (Model 1260, Solatron). Impedance sweeps were performed with a generated 100 mV rms AC drive voltage at 1 kHz. The sampling rate was 1 Hz. Optional heating was performed with a 0-100 Watt resistive heater (Weber).

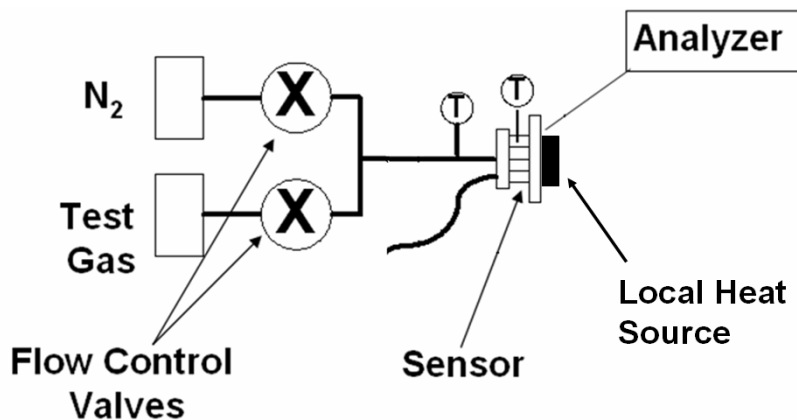


Figure 3-1: Configuration for all gas pulsing experiments

Based upon this design, the operating premise was to dilute a test gas into an inert carrier gas in order to produce a lower concentration of test gas. The cylinder of test gas was a 1000 ppm cylinder diluted and certified by AirGas. Dilution of this concentration can be described by:

$$[\text{Conc.}]_f = \frac{\dot{V}_{\text{test}}}{\dot{V}_{\text{test}} + \dot{V}_{\text{N}_2}} [\text{Conc.}]_{\text{cylinder}}$$

[Equation 3-1]

For this case \dot{V}_{test} represents the volumetric flow rate of the test gas, \dot{V}_{N_2} is the volumetric flow rate of the carrier gas, $[\text{Conc.}]_{\text{cylinder}}$ is the concentration of the cylinder of test gas, and $[\text{Conc.}]_f$ is the final concentration delivered to the sensor's surface. Kollⁱ highlights the advantages of such a system versus common alternatives in terms of simplicity of setup, relatively low cost, and compatibility with methane and CO measurement. Disadvantages of such a design include a limited operating range proportional to the sensitivity of the mass flow controllers (MFC) and incompatibility of mass flow controllers with certain volatile organic compounds. The alternatives to a mass flow controller system for variable concentration inspection include premixing of gas into cylinders with a Schlenk line, gas chromatography injection ports, and mixing bubblers.

Based upon the calibrated specifications provided by MKS Instruments, the stated sensitivity of the test gas mass flow controller was 2.0% of full scale. During operation, the N_2 carrier gas MFC was held at a fixed value of 100 standard cubic centimeters per minute (SCCM). The rated full scale drift of this controller was 1.0% of full scale. The 1000 ppm test gas cylinders supplied by AirGas had concentration ratings of 2% of full scale. By performing an uncertainty analysis on equation 1 with the aforementioned

independent deviations, the relationship between uncertainty and the volumetric flow rate of the test gas mass flow controller is:

$$\omega_4 := 20 \sqrt{\frac{2500 + 12500 V1^2 + V1^4 + 200 V1^3}{(V1 + 100)^4}}$$

[Equation 3-2]

In this case, ω_4 is the deviation in ppm of the overall system and $V1$ is the volumetric flow rate in SCCM for the test gas mass flow controller. Plotting over the area of operation for the experiments:

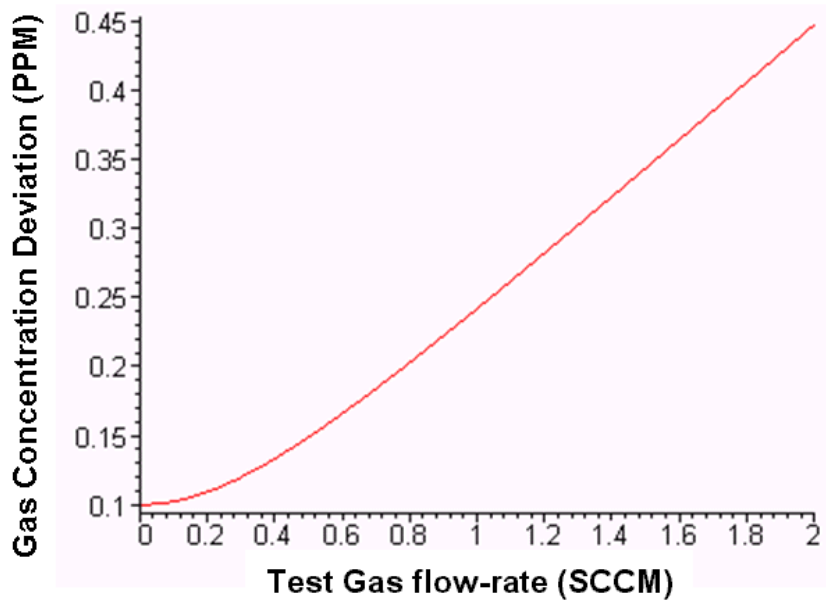


Figure 3-2: Uncertainty of experimental gas concentration for a test cylinder at a concentration 1000 ppm and a N_2 flow-rate of 100 SCCM

Noting that the test gas flow rate of 2 SCCM corresponds to approximately 19 ppm when all operating conditions are combined, one can observe that the systemic

variability was approximately +/- 0.45 ppm. The upper bound was limited to 2 SCCM, the full scale flow rate of the test gas MFC. Using equation 1 along with the maximum flow rates for the mass flow controllers, it can be shown that the maximum delivered gas concentration to the surface of the sensor is 2% of the cylinder's concentration or approximately 20 ppm. The lower boundary was the 0 SCCM case.

A final consideration of the experimental setup was the travel time for the gas to the sensor once the test valve was opened. An approximation of the average travel time (assuming incompressible, laminar flow through tubing of a constant diameter) at a prescribed flow rate is:

$$t_{pipe} = \frac{L A}{V_{test}}$$

[Equation 3-3]

For the flow through experiment, the length of the pipe (L) was approximately 30 cm (12 inches), the area of the pipe (A) was 0.02 cm², and the volumetric flow rate (V_{test}) was 2 SCCM. These parameters, applied to equation 3-3, yielded a travel time of approximately 19.5 seconds. Experimentally this value appeared to be closer to 23 seconds.

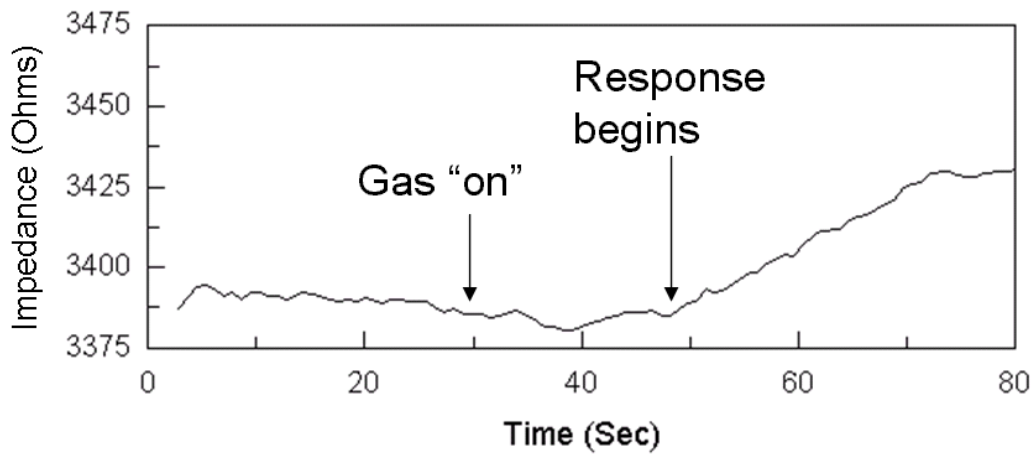


Figure 3-3: Experimental validation of delay in system

Verifying the uniform incompressible flow can be accomplished through an investigation of the Reynold's number for this system. The highest velocity occurs when the 100 SCCM flow passes through the 1/8" diameter stainless steel tubing. At this point the cross section area for the flow is 0.02 cm^2 . The corresponding average velocity for these conditions is 0.75 m/s. Interpolating with the assumption of nitrogen at room temperature from tabulated valuesⁱⁱ, one obtains a kinematic viscosity (ν) of $1.54\text{e-}4 \text{ m}^2/\text{s}$. Defining the hydraulic diameter (D), which is equal to the cross sectional diameter for flow through a pipe, the Reynolds number for the flow is then:

$$RE := \frac{\nu_{avg} D}{\nu} = 4.09$$

[Equation 3-4]

Since the transition region for a flow occurs at a Reynolds number of approximately 2300, this flow is highly laminar. Therefore disparities between the

computed travel time and the observed travel time must be associated with instability in the flow as the valve is opened.

3.1.2 Environmental factors

The porous silicon gas sensor was highly sensitive to environmental factors. In Chapter 2, the values for environmental sensitivity were tabulated. Although these results demonstrated that environmental sensitivity was high, complete control of temperature, pressure, humidity, light, and other environmental variations was not obtained during experimentation. Several of these variations were the result of testing in an open air environment, an attribute of the experimentation that was related to wirebonding of the devices. Given the highly sensitive nature of the device, environmental parameters had a measurable influence on the output of the device.

In order to properly and consistently characterize devices, a mechanism for extracting or minimizing the effect was necessary. Prior to minimization, however, an empirical understanding of the problematic noise sources will be provided.

The predominant factor that led to an enhanced presence of noise was the presence of local pressure drifts in the experimental environment. The resulting pressure pulses observed in the gas response were a combination of two factors. The first factor was an inability to bond and subsequently package the devices into a sealed environment. Since no wire bonds could be placed on the surface, all testing and probes had to be mounted over the surface of a bare wafer. A second factor of variability was the sensor's placement in a fume hood. The fume hood controller appeared to oscillate in a highly periodic manner with a frequency dependent upon specific conditions in the laboratory.

The combination of these parameters had a significant influence on the device. Pressure variation on the surface of the device resulted in an impedance change ranging from 10-500 ohms across a time span of 500 to 1000 seconds. This periodicity was well documented throughout experimentation and appeared with a frequency of range from 1.4 to 3.5 mHz.

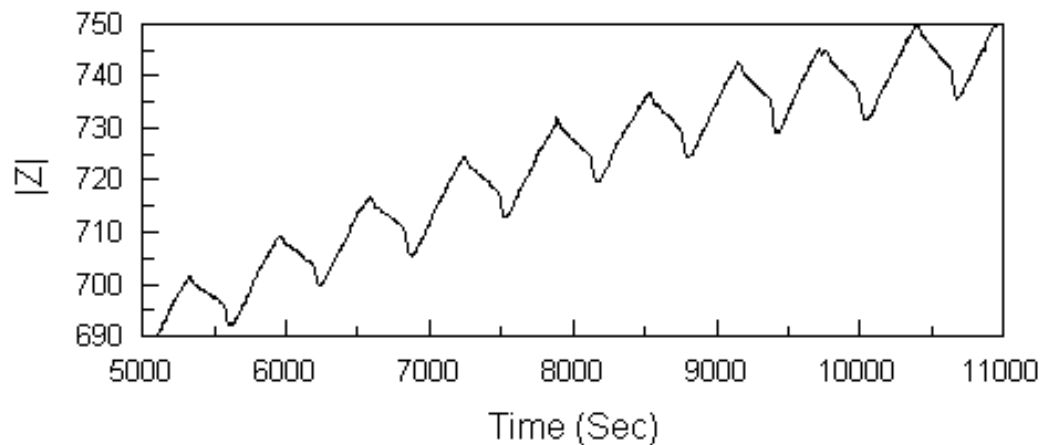


Figure 3-4: Picture of periodic pressure waves (frequency of 1.50 mHz)

Temperature was another significant source of noise during experimentation. Unlike pressure, however, this parameter could be effectively characterized in the open air testing environment. With sensitivities ranging from 5 – 100 $\Omega/^{\circ}\text{C}$, localized variations of a room temperature environment could result in baseline drifts an order of magnitude greater than the gas response. The room environment itself tended to periodically fluctuate in temperature at frequencies between 3.2 mHz to 5.5 mHz.

Two final noise sources to be considered during the experimentation were humidity and laboratory noise. For the porous silicon devices in this setup, however, the

gases under study were maintained in a dry state. Additionally moisture was limited on the surface due to a continuous exposure to 100 SCCM dry research grade N₂. Furthermore, no distinction was observed between sensors that were recently placed into the test chamber and exposed to gas versus those devices that had been entrained under a dry nitrogen flow for days. For these reasons, no additional measures were placed on the control of moisture during experimentation.

The second issue, laboratory activity, was problematic, infrequent, and distinct. In the case of specific pore morphologies of porous silicon, external vibration of vacuum pumps and other machinery increased noise levels in the sensor's baseline. Venting of the Paralene deposition machine, a device located in close proximity, occasionally resulted in a fixed shift of the device's impedance. No recovery was observed in the two hours following the perturbation.

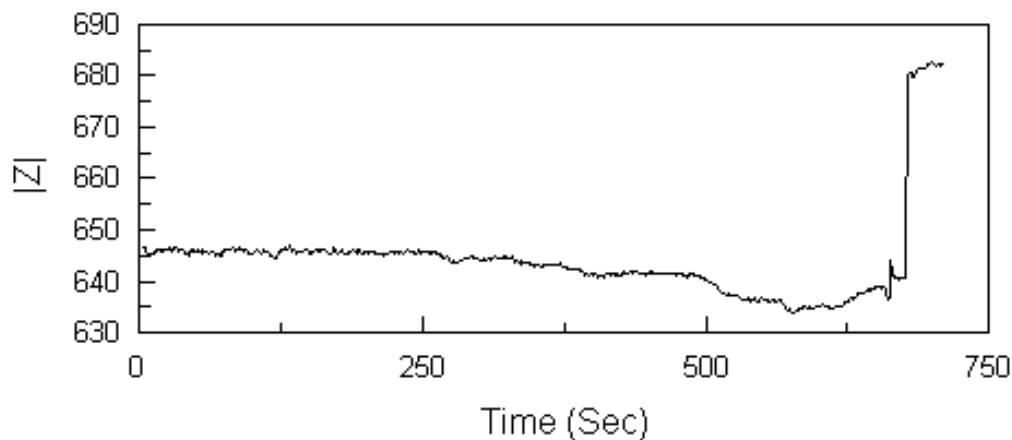


Figure 3-5: Impedance spike due to external laboratory disturbance

3.1.3 Review of discrete analysis

In the prior discussion of empirical noise sources (3.1.2), a Fast Fourier Transform (FFT) of a porous silicon gas sensor response was used to isolate the noise

sources. This method confirmed that the thermal and pressure noise in the fume hood were highly periodic in a narrow band and capable of isolation. In order to generate this frequency transform and apply it in a more generalized manner, specific attributes of the relationship between a discrete time domain and a discrete frequency domain signal were investigated.

Several relationships can be directly drawn for a signal that is transformed from the time to the frequency domain. For example, a signal sampled at a given rate has a resolution in the frequency domain given by: ⁱⁱⁱ

$$df = \frac{1}{(N - 1) dt}$$

[Equation 3-5]

$$T = (N - 1) dt$$

[Equation 3-6]

For equation 3-5, df is the resolution (in Hz) in the frequency domain, N is the total number of samples, and dt is the period between samples (in seconds). As one can see, the resolution is not only dependant upon the rate of sampling, but also on the total time span (T) over which the signal is sampled. In order to maximize resolution of a plot in the frequency domain for a fixed sampling rate, one requires a large number samples. Also, the total band is limited by the sampling rate of the discrete signals. This relationship is defined as:

$$f_{band} = \frac{1}{2 dt}$$

[Equation 3-7]

In this equation, f_{band} is the total frequency band over which FFT analysis is valid. Outside this band, frequencies are aliased with one another and are not discernable. This equation, which is based upon the physical implications of a transform to the frequency domain, implies that resolution in the frequency domain is inversely related to the time between discrete samples. For the case of the Solartron 1260 Impedance analyzer, the maximum sampling rate ($1/dt$) is limited to 1 Hz. Since the periodic noise sources for the gas sensor operating in a laboratory environment occur at 1.8 mHz, 3.1 mHz, and 4.8 mHz, the selected frequency must be outside this band. Furthermore the selected frequency for gas pulsing should, at minimum, be separated from the noise by a distance related to the resolution of the system.

3.1.4 Selection of operating frequency

The factors that dictated the appropriate operating frequency for the gas pulsing method were related to the device under study, the experimental apparatus, and previously discussed noise sources. Consideration of these factors was a critical step in demonstrating the value of the gas pulsing method.

The first consideration when selecting the operating frequency was related to the control valves in the experimental apparatus. Delay in the control valves placed a constraint on the maximum rate at which the gas system could be pulsed. Because the valves took approximately three seconds to open and close, the total pulsing frequency was set at 41 mHz. At this frequency a three second opening time would occur, the gas would be fully flowing for six seconds and then a three second closing time would occur.

Experiments at this frequency, however, were not repeatable. Experimental testing of different pulse widths revealed that the open and close error was greatly reduced if the frequency was kept below 33 mHz.

The second delay was the response of the device. In sections 2.5.1, a representative response for a porous silicon gas sensor with various pulse widths was outlined. In this response, it was observed that a delaying period of 6-7 seconds existed followed by a linear derivative response for 30-50 seconds. This observed behavior placed two constraints on the operating range. If the device was pulsed at a frequency greater than 83 mHz (1/12 Hz), no response would be observed. This limitation was a compounded constraint based on both the device and the experimental setup. On the other hand, the response of the device itself became nonlinear if the gas pulse was longer than 50 seconds. As one approached this value, increased irreversibility in the device was observed. Therefore, in order to obtain a stable reversible response, a lower limit for the pulsing frequency was placed at 12.5 mHz.

Based upon all of these factors, the operating frequency for the gas pulsing method on the porous silicon gas sensors was selected at 16.7 mHz with a 50% duty cycle. This value represented a balance between the upper and lower bound constraints. Figure 3-6 provides the range limitations observed and the resulting selection point for the gas pulsing method.

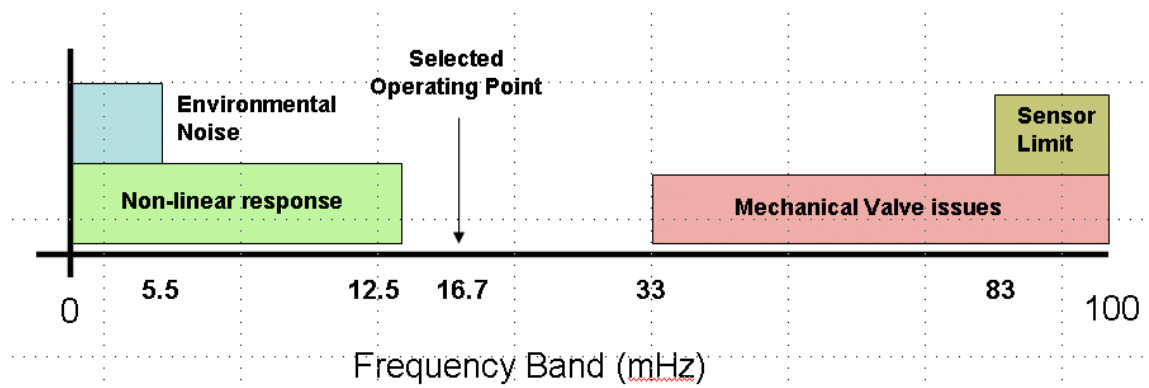


Figure 3-6: The available spectrum for gas pulsing

3.2 The Gas Pulsing Method

3.2.1 How gas pulsing works

The gas pulsing method design was based upon the observed operating behavior of the porous silicon gas sensor. For pulses of gas far below the time constant of the device, a linear, derivative response was observed. Additionally, for small doses of test gas, the sensor behaves reversibly with a hysteresis of less than 1/3 of the original response. The rate of change of the device was highly correlated to the particular concentration of gas to which the sensor was exposed. These factors, however, still left two fundamental questions unanswered in terms of the output of the porous silicon gas sensor. Is the observed output a gas response, or simply a random fluctuation of the baseline? Secondly, how should one manage the variability of the baseline and the presence of noise during testing? For the case of the porous silicon gas sensor, a feasible answer to these questions was periodic pulsing.

The noise factors described, in general, have repeatable trends in the frequency domain. Therefore, if one carefully selects a pulsing frequency that is not associated with the frequency of the noise, the clarity of the signal is considerably improved. To

accomplish this task, the mass flow controller on the test gas was pulsed in a periodic manner with cycles consisting of 30 seconds on and 30 seconds off. Due to the capabilities of the MFC and the need for custom external triggering, this method was manually implemented. The gas was subsequently delivered in a square wave periodic manner onto the surface of the device. Devices with a gas response, in turn, generated gas responses with the same periodicity (Figure 3-7).

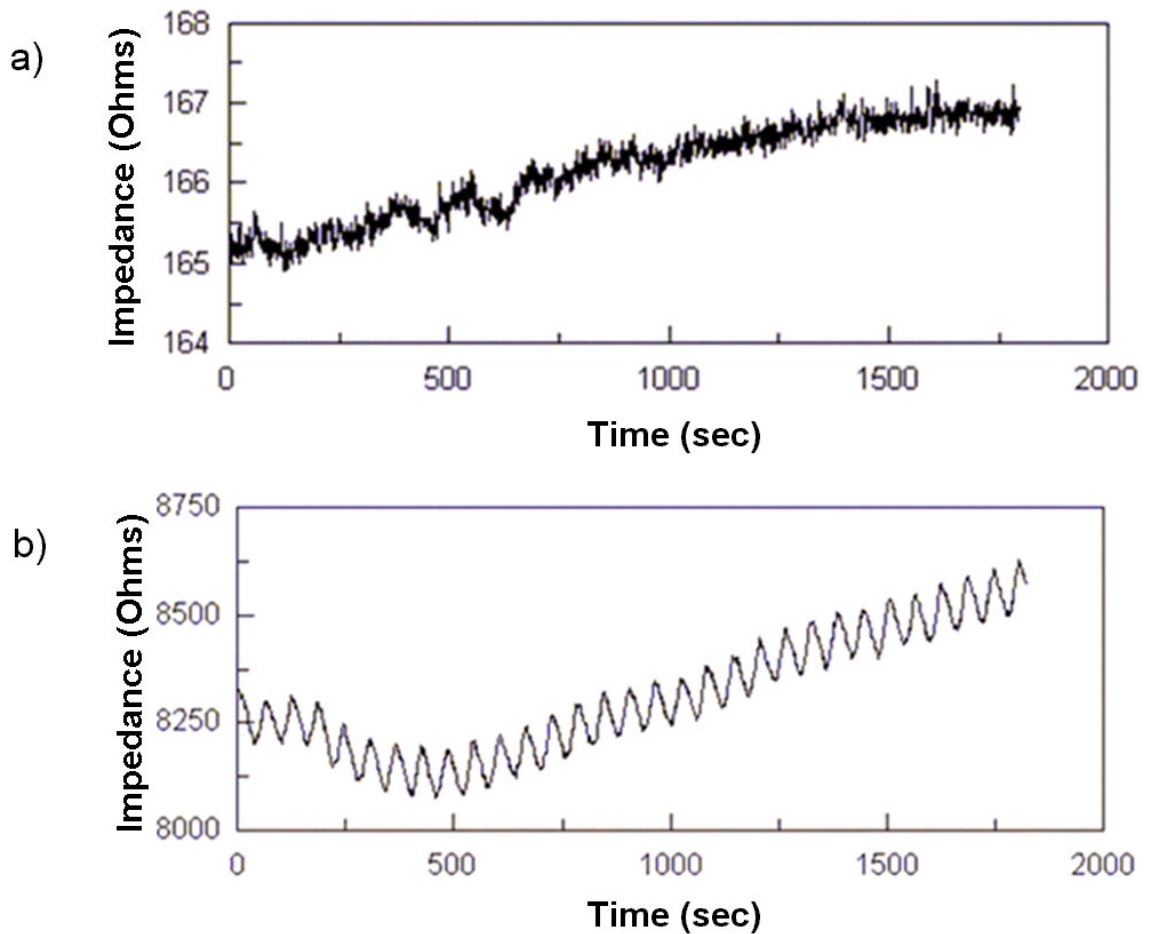


Figure 3-7: The output signal of a) a non-responsive device and b) a functioning gas sensor

A set of systematic criteria were established to screen and reject the gas pulsing experiments performed on the porous silicon gas sensor. This process was critical due to the highly sensitive nature of the device and the inherent errors associated with manual pulsing of the gas. The first rejection criteria a gas pulsing experiment was based upon a recurring error with the test system. Often the first experiment of each day showed a gradual improvement in response as time elapsed. This gradual onset of improvement would last for the first 15 to 20 pulses (15-20 minutes) with continuously observed improvement. This behavior did not occur if a new sensor was placed in the experiment in the middle of the day. It was therefore concluded that this error was directly associated with the testing apparatus. With additional experimentation, it was discovered that this error was associated with a dilution of the gas when the regulator was activated for the first time each day. To remedy this error, every morning the gas line was bled for 5 minutes through an exhaust line before the actual experiments were conducted. The existing set of experiments that were subject to this error were identified and rejected from further analysis. Figure 3-8 illustrates an example of this error and its appearance.

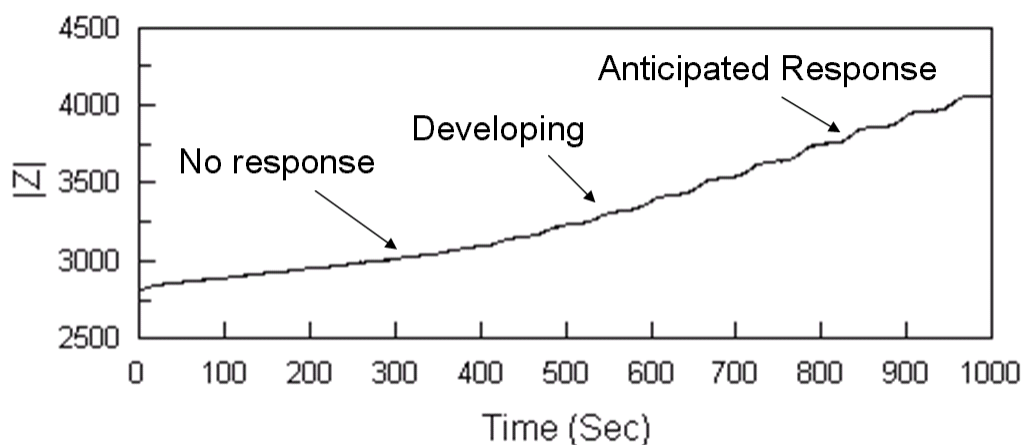


Figure 3-8: Example of a developing gas response (system error)

The second set of rejection criteria for experiments was associated with the timing of the pulses within the experiment. In order to make a pertinent comparison of over 200 devices, specific constraints were placed on the “maximum” allowable timing error due to the experimentalist. If the experimentalist timed the gas pulses incorrectly, the entire experiment was cancelled. The criteria for restarting an experiment were dependant upon the nature of the error. The experiment was restarted if any single pulse was more than 5 seconds from its intended point. For smaller errors, the rejection criteria was less quantitative but considered both the magnitude and frequency of the incorrect timings. The general rule stated that if the cumulative errors summed to 5 or more seconds of error, the experiment was withdrawn. External errors due to activity within the laboratory resulted in the resetting the experiment if the magnitude of the affliction was proportional to or greater than the gas modulations. As a result of these criteria, a total of 30 experiments were withdrawn due to excessive timing error.

3.2.2 Refuting the alternatives

It has been established that a single pulse response will not suffice as a testing method for the porous silicon gas sensor, and the gas pulsing method has been proposed as an effective means to generate a periodic gas signal. Alternatives to gas pulsing are temperature pulsing and pressure pulsing.

Temperature pulsing is effective for sensing films where a high amplitude linear response occurs over a limited temperature band. M. Roth describes a method of temperature pulsing for organically coated gas-sensors^{iv} that triggers a “periodic absorption and desorption process within the sensitive coating.” By triggering at a rapid

rate, CO measurements are distinguished from noise. Similarly, Ortega^v implemented an FFT measurement method for dynamic waveforms based upon temperature pulsing of a tin oxide gas sensor. This method was successfully combined a spectral heating pulse with transient analysis to perform a clustering of data. In the case of the porous silicon gas sensor, however, temperature modulation has a disruptive effect on the sensitivity of the device. Also with thermal sensitivities of 10-20 $\Omega/^{\circ}\text{C}$, small thermal cycles would impose large changes upon the sensor's baseline. In order to properly account for these effects, non-linear data processing techniques are commonly applied. Due to the non-linear relationship, the training time to program for the non-linear effect would add significant cost to each unit. Since the porous silicon sensor has been designed for low-cost, portable, and simple operation, temperature pulsing is not ideal and an alternative method is sought.

The second alternative, pressure pulsing, is a common method for purging a test line after a gas exposure. The device's pressure sensitivity was sufficiently high to detect variations in the fume hood. From the vacuum evacuations of Chapter 2, the device has demonstrated poor reversibility to large pressure changes with a time constant greater than 20 minutes. Additionally, modulation of partial pressure requires the ability to encapsulate the structure in a vacuum tight system with a control valve on the inlet and outlet side. Such configurations are in general both expensive and infrequently implemented in portable systems. For these reasons, a pressure modulated environment does not improve the ability to detect gas species in this case.

In addition to the individual temperature and pressure modulation methods, other periodic pulsing applications are centered on the modulation of multiple parameters to

achieve a single data point. Jatson and Davies^{vi} report that for a low-level CO monitor based upon a tin oxide film, a combination of electrical, thermal, and data sampling timescales are necessary. In this device, the surface is purged for 60 seconds with a resistive heating of the surface. Next the sensor is immersed in the test gas without heating for a “working period” of 90 seconds. Finally for 1 second, a sampling period occurs where the actual gas response is recorded and compared to a pre-calibrated point. Since the film itself is sensitive to temperature, a matched thermistor is provided to minimize the non-linear effects. Additional examples of combined methods include Cavicchi’s work on micro-hot plate gas sensors^{vii} and McAvoy’s work on Finite thermal impulse^{viii} with least squared modeling. While these methods were effective at solving their respective problems, a simpler solutions technique was sought.

3.3 Signal Processing for the Gas Pulsing Method

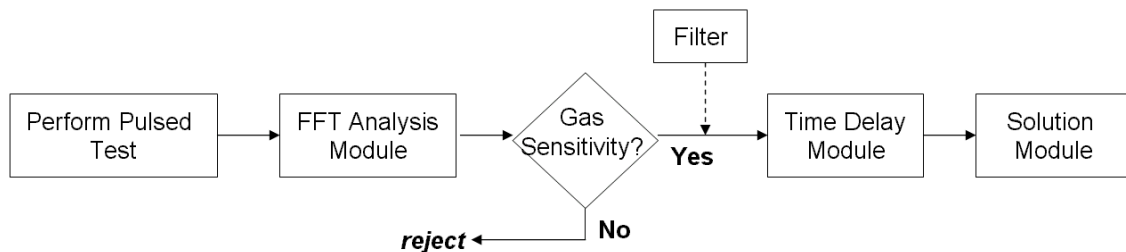


Figure 3-9: Flow chart for gas pulsing method

Given discrete values for the sampling rate, total test time, linearity of response, and gas pulsing frequency, one can develop a systematic routine to extract the impedance change associated with a given gas for a given duration of exposure. The process of data

analysis for quantification of a gas response can be divided into three functional modules: FFT analysis, determination of the time delay, and solution extraction. In the FFT analysis module, the signal was transformed from the time domain to the frequency domain. The data was optionally filtered in a band-pass manner such that only the frequencies of interest were analyzed. This phase also functioned as a pass-gate which only allowed devices with a reasonable frequency response to be further analyzed. The second module, determination of the time delay, involved a numeric sweeping of the gas response data in order to determine the exact moments when the sensor switched “on” and “off”. Finally in the solution extraction module, the average response, the distribution of the response, and the dynamic trends of the response were computed and plotted.

3.3.1 FFT Analysis Module

The first module, FFT analysis, performed three distinct functions. The first function was to input the sensor’s signal and transform it to the frequency domain. The second task was a basic filtering of the data and a recalculation of the frequency transform. The final component, plotting of the respective transforms, was a relatively trivial matter. The role of these preprocessing techniques was to prepare the data for a solution extraction. (For a discussion of common preprocessing techniques, see section 2)

In order to accomplish the transformation to the frequency domain, one must both define the attributes of the inbound signal and minimize the DC drift. For the case of the Solartron 1260 Impedance analyzer, the maximum sampling rate (dt) was limited to 1 Hz. Given this factor and other issues associated with noise sources, rate of gas response, and

the desired number of samples, the total test time equaled 1800 seconds. Since the sampling rate is 1 data point per second, the total number of samples (N) is also equal to 1800. These values, reapplied to equations 3-5 and 3-6, indicated that the total band that could be inspected in the system was from 0 to 0.5 Hz.

With the necessary attributes defined, the time based gas signal was transformed with Matlab to the frequency domain. After transformation, two functions were performed. The first function was validation of a gas response. For the porous silicon gas sensor, background noise associated with nitrogen pulsing around a 16mHz band was quite low. To validate this factor, gas pulsing experiments with a wide variety of porous silicon structures were performed. From these experiments, it was found that if a device had sensitivity to a given gas with a rapid response rate, the response was clearly detectable in the frequency domain.

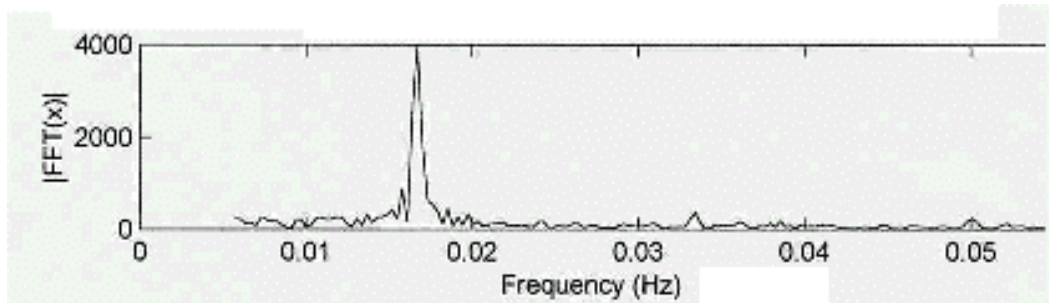


Figure 3-10: Example of a strong gas response with low noise

Upon validation of the gas response, a plot of the FFT spectrum for a gas exposed sensor offers a simple means for selection of devices. While the experiment itself does not quantify all performance attributes, it was an effective means of establishing minimum performance parameters. For example, by fixing the period of the gas pulsing

at 60 seconds, devices with initial response times much greater than 30 seconds were automatically excluded. The criteria for a functioning device can be altered through the modification of additional parameters including the duty cycle, concentration, and operating temperature.

The second function performed in this module was filtering of the noise sources. The choice to filter the signal must be carefully considered. Filtering does offer an opportunity to remove or reduce the effects of periodic noise sources within the room such as pressure fluctuations in the fume hood and random low frequency temperature effects. Unfortunately all numeric filters introduce some artificial components into the signal. These effects are problematic for the case of convergence analysis.

Given the necessity to balance between sufficient noise rejection and signal fidelity, a 3rd order Butterworth filter was implemented. This filter offered excellent noise rejection for the signal response after 10-12 pulses. Like all real filters, the Butterworth filter not ideal. To investigate where filtering becomes problematic, one should investigate the boundaries of the filter. The slope of the boundary of the filter is measured in dB/octave. By modifying the order of the filter, the dB/octave slope could be increased. This steep slope of the 3rd order filter led to a heightened ability to block frequencies that were close to one another. With increased order however, the unfiltered signal was also progressively destabilized. Figure 14 illustrates this artificial effect that can be introduced with higher order filters.

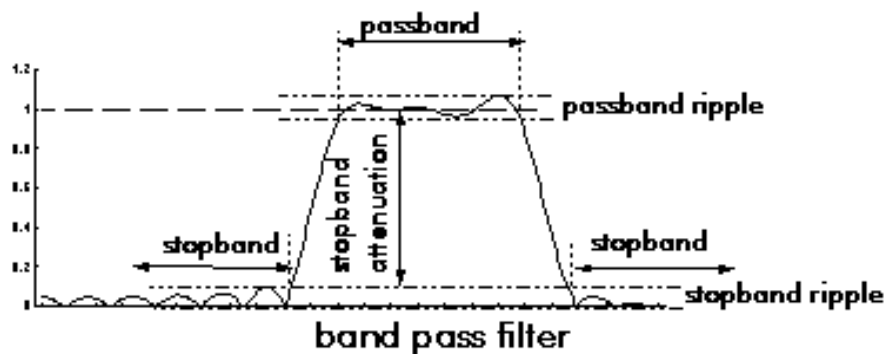


Figure 3-11: Example of non-linear effects on signal^{ix}

With the completion of the three tasks in the FFT module, the results of the gas pulsing method were ready for analysis in the time delay module. Figure 3-12 illustrates the difference in the output of a gas sensor before and after filtering. In these examples the absolute impedance of the device has been shifted downward. This trick acts as an additional filter against noise at zero hertz.

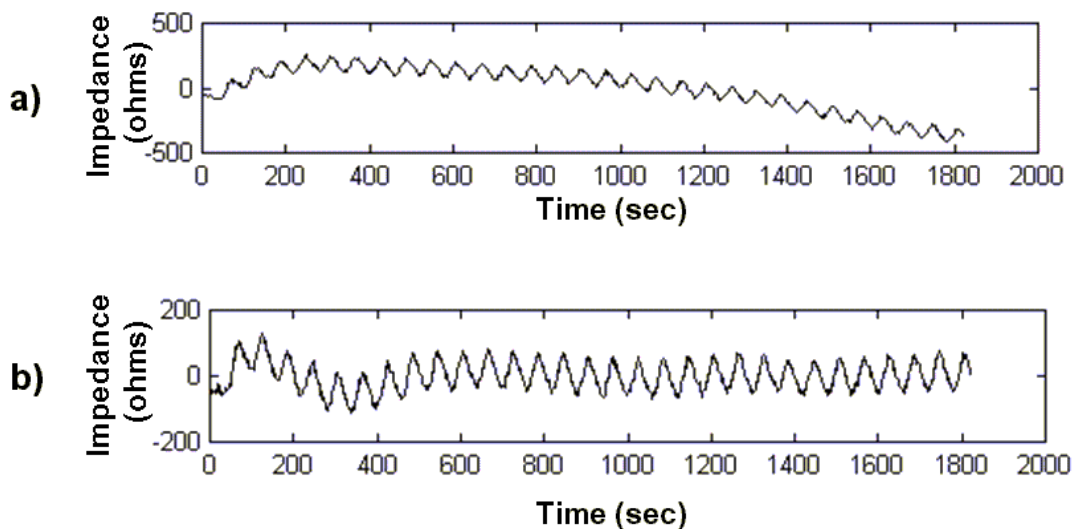


Figure 3-12: a) plot of raw data file and b) filtered data with artificial oscillation in the early response

3.3.2 Time Delay Module

The time delay module was designed as a method of preparing the data for signal analysis. To accomplish this task, the time delay module needed to ascertain the time at which each gas pulse began and ended. The beginning and endings appeared at corners, or locations where the slope of the signal rapidly switched directions. In order to automate the process, the corners needed to be referenced against a known point. Derivative or integral methods were unsuccessful due to localized noise errors. Since the gas pulsing was periodic (and verified with FFT analysis), all corners occurred in integer increments of 30 seconds after the first corner (i.e. 30, 60, 90...). Using this fact one only needed to discover the first “starting” point for the series. This value was dependant upon the individual sensor, the gas, and the experimentalist.

To visualize how the initial value was obtained, the gas response can be compared to a basic periodic wave. In a sinusoid, the time necessary to match the phase of a signal is often referred to as the time delay (Φ). By picturing the 30 gas response as a sinusoid, an approximate equation to represent the gas response is:

$$Y = A_0 \sin(\omega (t + \Phi))$$

[Equation 3-8]

In this equation, Y is the output of the device, A_0 is the amplitude of the gas pulses, ω is the natural frequency of the gas pulses, t is the time, and Φ is the time delay. For a narrow band surrounding the natural frequency ω , this equation is an accurate approximation. Even for the case where the output equation is not a sinusoid, the

principle of a time delay for an oscillatory signal is pertinent. With this analogy, a full understanding of the end objective was obtained.

The value of the time delay was dependant upon two parameters: the response time of the sensor and the synchronization error. The response time was effectively constant for a given device at a given concentration. The synchronization error, however, was associated with the relationship among the impedance versus time record in the computer, the stopwatch time, and the operator of the test gas controller. These three parameters resulted in a random error distribution during testing. Small variations between gas pulsing at 59.5, 60, and 60.5 seconds resulted in a slight shift in the average of all 30 responses. Additionally, when the operator originally synchronizes the stop watch to the impedance file, any error in the process linearly correlated to a change in the time delay. A maximum error during experimentation for this parameter was one second.

Given these sources of error, a need for the time delay module was established. The framework for the time delay module attempted to build off of the attributes from the previous module. In order to understand how the module operated, it is important to review why one was performing all of these modules. At the end of the signal processing, the objective was to obtain an impedance change, $Z_2 - Z_1$, at 30 locations on the plot. By setting up strict rejection criteria in the FFT module, two specific attributes were already known about all signals that were being analyzed in the time delay module. First, the gas peaks were exactly 30 seconds apart. Secondly, the gas peaks were the only data that was correlated on the 30 second increments. With this information known, obtaining the time delay was simply a matter of iterating through a range of possibilities.

To find the solution for the time delay, the algorithm initially assumed a known value for the time delay. Next the algorithm subtracted this point from a point 30 seconds later in time. This computation represented a single impedance change, $Z_2 - Z_1$, for the given time delay. Next the algorithm skipped over a 30 second block, and the process was repeated. The 30 second block was skipped because this was the recovery portion of the pulse. The process of measuring and skipping was repeated for 28 additional iterations. Once completed, the results of the first 29 pulses were averaged. This value represented the average response for the initially assumed time delay. The assumed time delay was incremented by 1 second and the whole process was repeated. This loop continued until all possible time delays had a corresponding solution average impedance change.

After obtaining the average for all possible delays, a plot was generated of the average ΔR versus time delay. For the case of a signal with a strong periodicity associated with the gas pulsing, this plot appeared sinusoidal in form. This behavior was anticipated from all of the analyzed signals because all plots that indicated a poor gas response have already been removed. The maximum peak of the sinusoid was the actual time delay of the experiment. Similarly the minimum valley of the sinusoid is a point that tracks the average recovery of the device over the 30 pulses. Small variations from individual pulses were averaged out and the response appeared quite smooth. At times ± 15 seconds from the maximum time delay, two values around zero exist. These values correspond to the average of the baseline for the experiment.

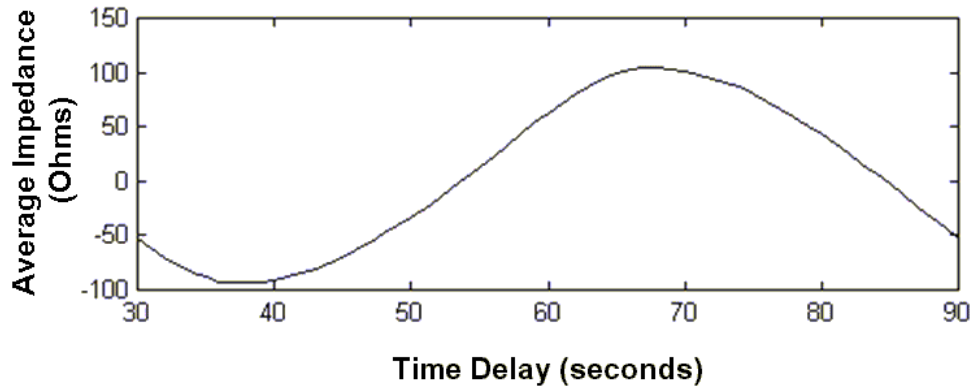


Figure 3-13: Time delay illustrating strong response and zero drift

Figure 16 illustrates an example of the time delay module. Notice that the maximum occurs at a time of 66 seconds, the signal is highly sinusoidal, and there is no vertical bias. Once a plot of this form was obtained, the time delay was evaluated and this information was passed to the solution extraction module.

3.3.3 Solution Extraction Module

Given the information from the FFT and Time Delay modules, the Solution Extraction Module was a straightforward implementation. In this module, the 30 point data set of gas distributions is extracted from the original gas response. To accomplish this task, the algorithm repeated the method outlined in the time delay module at only the point of the actual time delay. Additionally, the negative delta R, or recovery signal, was extracted. The recovery signal was useful because it was a measure of hysteresis in the system. In the final routine of the solution extraction module, both the positive delta R and negative delta R were plotted as a measure of stability. The interpretation of this plot will be provided with an example in section 3.3.4.

A final comment should be made on saturation with the pulsing method. Figure 3-14 illustrates a gas response with the pulsing method that has reached equilibrium between the gas response and recovery. If this equilibrium value was at the saturation point for the sensor, signal suppression would be apparent and the recovery would not be linear. With this method, however, equilibrium has occurred below the saturation point. This behavior demonstrates how the gas pulsing method, like other pulsing techniques, was a valuable safeguard against irreversibility issues. The ability to perform without irreversible saturation is an essential attribute for portable, low cost gas sensing.

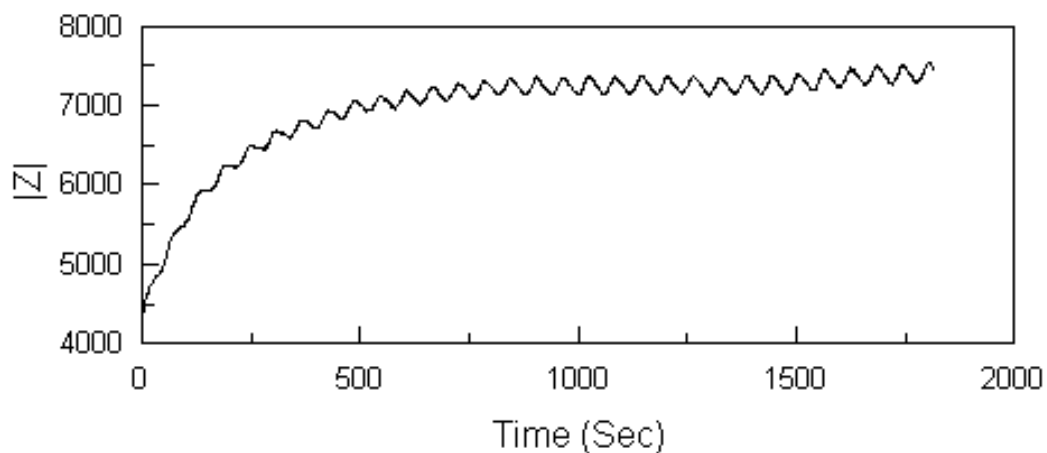


Figure 3-14: Example of raw data that illustrates rapid convergence between positive and negative delta R

3.3.4 An example

The functionality of the gas pulsing method is best indicated with an example. For this case, a porous silicon sensor was treated in HCl for four hours and dipped in electroless gold for 30 seconds. After these post processing treatments were complete, the

sensor was dried in an open-air cleanroom environment for two days and then exposed to 30 bursts of 20 ppm NH_3 . Additional conditions for this experiment were an operating temperature of 20 °C, a drive voltage of 200 mV AC, and no DC biasing.

This particular experiment has been selected for its ability to demonstrate an extreme case of experimental error. Since these errors are somewhat exaggeration, their propagation through the system was easily tracked. Examples of higher purity signals are detailed in Chapter 5.

In this case, the gas pulsing had three operational errors (poor switching of the gas) of approximately 2.5 seconds each during the 30 minute experiment. The raw and filtered output (centered about zero ohms) for the device with these operating conditions is given in Figure 3-15.

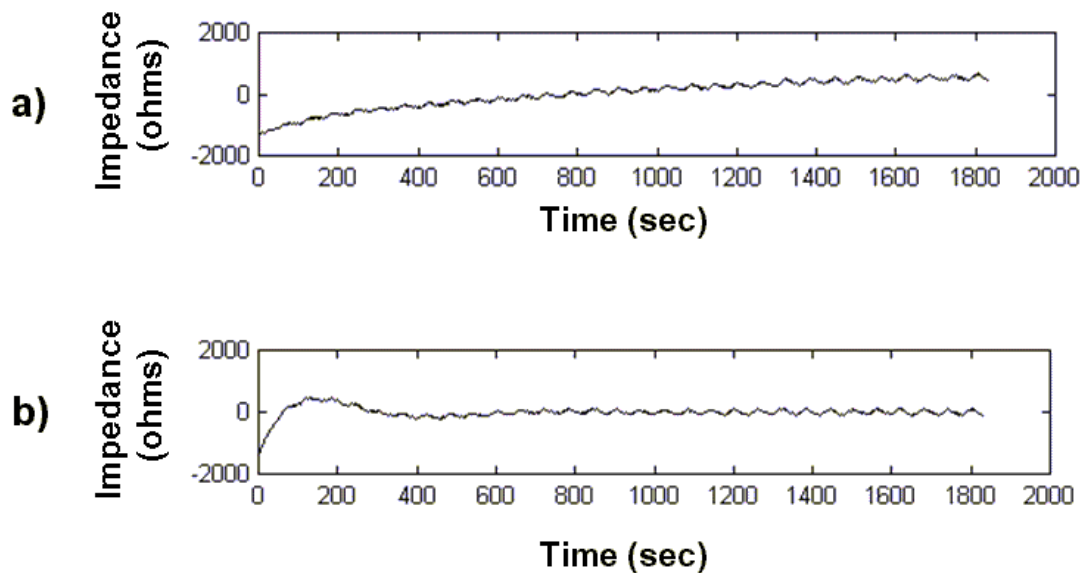


Figure 3-15: a) Raw impedance response and b) filtered impedance response

After conducting the experiment, the data was processed in the FFT module.

After transformation to the frequency domain, the experimental error was apparent, but the overall signal strength versus background frequencies was quite high (Figure 3-16).

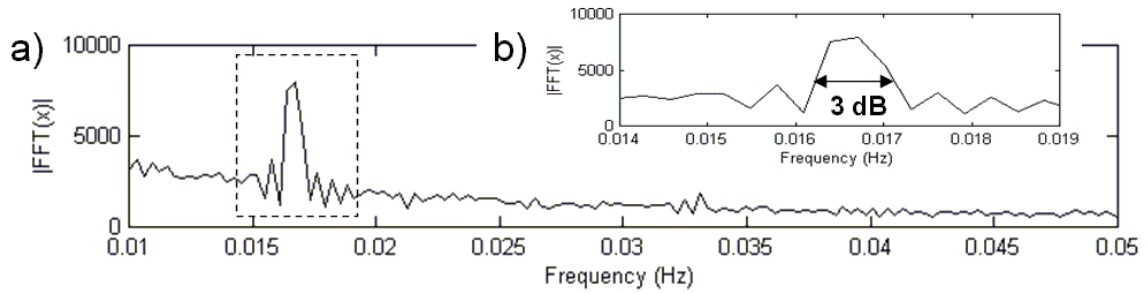


Figure 3-16: a) FFT of sensor response b) detail of “spread” of gas pulse

From this plot, several attributes should be noted. First the primary response has a 3 dB width spanning from 16.1 mHz to 17.2 mHz. These frequencies correspond to periods of 58.5 seconds and 61.7 seconds. This width correlates well with the documented error for the experiment.

After FFT analysis, the data was processed in the time delay module. From this module, three parameters of the gas response were uncovered. The first parameter was the fidelity of the gas response. If the gas response had been a false positive in the FFT domain, this module would have demonstrated more than one peak. This parameter was potentially invaluable for data validation and offers a technique to combat false-positive situations. The time delay output for this response is given in Figure 3-17. For this time delay module, the output appears with a sinusoidal shape.

The other two parameters of interest from this plot are the time delay for maximum signal (Φ_{\max}) and the time delay for minimum signal (Φ_{\min}). For this case,

Φ_{\max} was 66 seconds and Φ_{\min} was 36 seconds. As anticipated, these responses are exactly 30 seconds out of phase. Finally it should be noted that the average value of these two delays was not zero. This solution was anticipated because the original raw data file possessed a nearly monotonic drift during the course of the experiment.

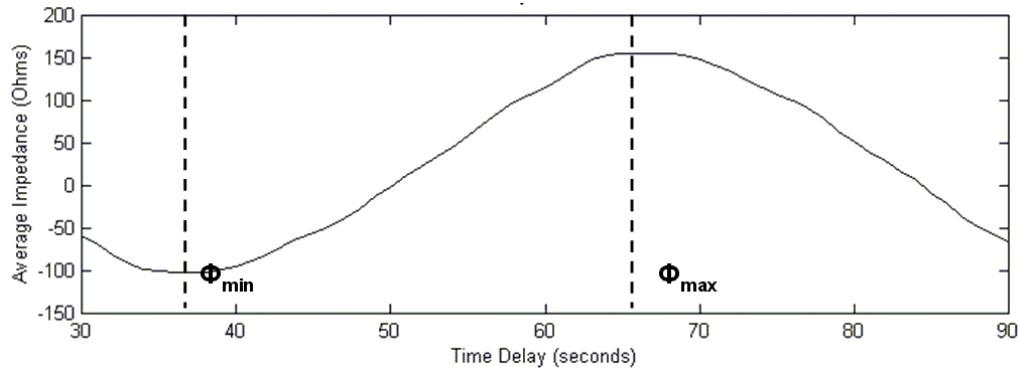


Figure 3-17: Time delay module for the example signal

The final data analysis module is the solution extraction. For this case the value for time delay that was passed into this module was 66 seconds. With the time delay and gas signal, this module computed and plotted the device response for each pulse of gas. Additionally the statistical behavior of this response was given. For this case, the average gas response of the device to 20 ppm on NH_3 was 162 ohms with a deviation of 24 ohms. The dynamic plots shown in Figure 3-18 illustrate a critical parameter that was observed in most gas responses. Positive delta-R or the gas response of the device was instantaneous from the first gas pulse and was repeatable throughout the 30 pulses (Figure 3-18). This was the data from which the average and deviation were computed. The negative delta R plot illustrates the convergent behavior of the system. Due to the pulsing method, the surface of the device always had a 30 second period to desorb some

of the previously absorbed species. Initially this gradient was small and hysteresis resulted. As the sensor accumulated gas, however, the reverse gradient increased, and the sensor desorbed a greater quantity of ammonia. This equilibrium below the device's saturation level was critical for the feasibility of the device in monitoring applications.

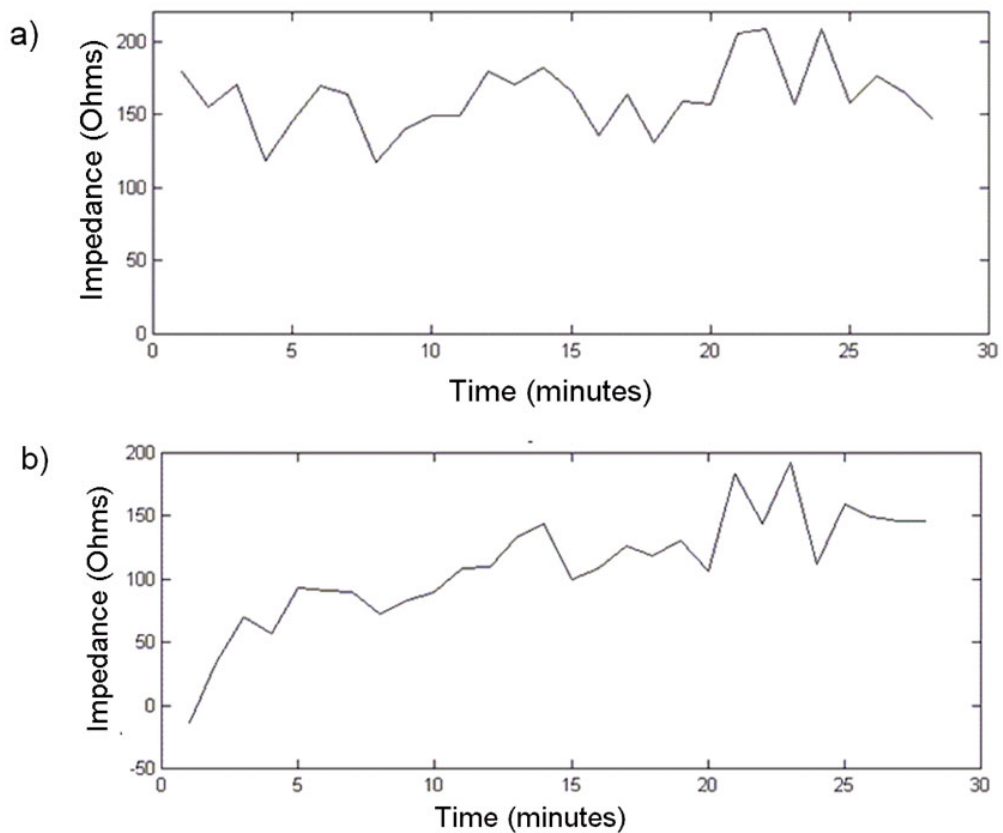


Figure 3-18: a) Positive delta R gas response b) Negative delta R or recovery of gas response

3.4 Issues Associated with the Gas Pulsing Method

3.4.1 Windowing

A critical issue associated with frequency domain analysis of a sampled signal in the time domain (T) is the effect of windowing on the signal. Windowing is a phenomenon associated with transforming a time domain signal that exists for only a discrete time. If one does not sample for a sufficient duration, the effects of windowing can become quite appreciable and adds considerable resolution error to a frequency domain analysis. Error associated with windowing is commonly referred to as leakage. As a simple illustration of windowing, one should consider the impulse function:

$$w(t) := \begin{cases} 1 & |t| < \frac{1}{2} T \\ 0 & \text{otherwise} \end{cases}$$

[Equation 3-9]

By carrying out the Fourier transform of this function, one obtains:

$$w(\omega) = 2 \frac{\sin\left(\frac{1}{2} \omega\right)}{\omega}$$

[Equation 3-10]

$$\omega = 2 \pi f$$

[Equation 3-11]

From this representation, several important characteristics should be noted. In the limit as omega tends to infinity, this function converges toward the delta function.

However, for discrete values of the window, the following shape develops.

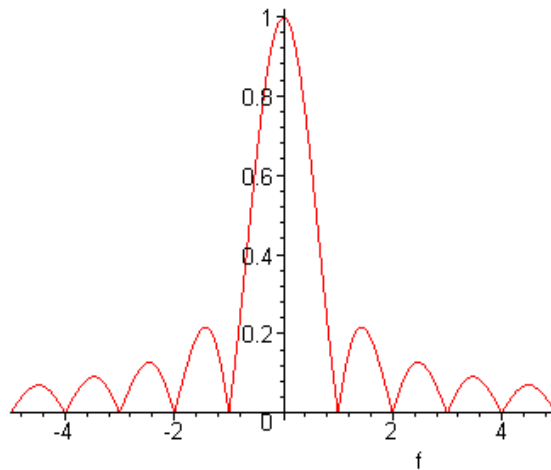


Figure 3-19: Discrete transform of the impulse function with side lobes

Classically, the effects of a window on a digital signal are classified according to two primary criteria. The first criteria, the 3 dB bandwidth, refers to the distance from the center of the impulse where the power of the signal is $\frac{1}{2}$ of the peak value. By understanding the 3 dB bandwidth, one can gain a substantive appreciation for the magnitude of the artificial leakage of the signal.

The second classification for different windowing options is the dB drop of the first side lobe. While the first measure described the spreading of the signal, the later parameter describes the contribution of artificial side lobes that have been generated (Figure 3-19). Unlike the band spreading contribution, however, this parameter can be shown to be a discrete value of 13dB. By comparison, some artificial filters are capable of achieving dB drops of around 30-40 dB for the side lobes. Often these filters, however, improve the dB drop of the side lobes but increase the widening of the main lobe.

For the case of digital sampling of the porous silicon gas sensor, the actual signal obtained can be interpreted as the combination of an infinite gas signal multiplied by the defined square window. The value T represents the total time duration of testing. Based upon the given analysis of the square window, the 3dB bandwidth for the experiment is defined as:

$$3dB = \frac{.85}{T} = 0.47 \text{ mHz}$$

[Equation 3-12]

It should be noted that this widening is an artificial widening. The actual signal itself is still prone to a width based upon the variance of the signal. To further reduce this effect, one can sample for a longer period of time.

3.4.2 The effect of manual switching

As previously stated, the mass-flow controllers that drive the mixing of a gas to an appropriate concentration are actuated with an analog switch. The timing of the switch is entirely dependant upon the user and prone to error for the 60 events that occur during the course of any one experiment. These errors are manifest in the gas response in several forms.

The first effect of erroneous switching is a proportional, one-time change to the gas response. This error is caused by one timing error during the course of the experiment. Since the gas sensor responds proportionately to the pulse duration for timescales less than 45 seconds, this error is directly proportional to the user's deviation in time from the correct trigger point. If we apply the case of a 1 second error for a

device with a 10 ohm/second response rate, the effect on the overall average of the sensor during the experiment is 0.22%. Therefore as long as the errors are constrained to a minimal amplitude and frequency, there effect can be trivialized by the averaging of the 30 gas responses.

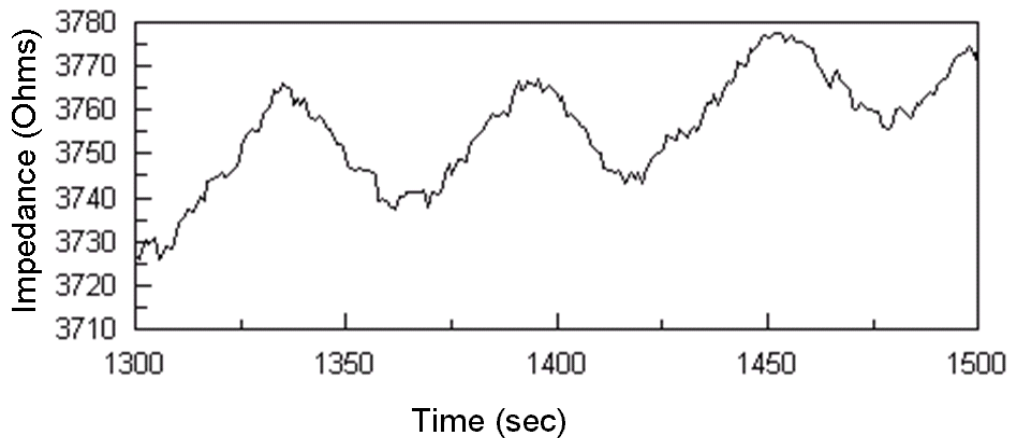


Figure 3-20: Reduced amplitude of middle pulse due to operator error

The second form of error is variability between two or more experimentalists and their given techniques. For the case of the manual gas pulsing system, four different operators were used. If an operator is improperly trained, they could introduce additional errors through subconscious decisions on when to trigger the gas. More specifically, if a user does not use a uniform method for determining when to turn the gas on and off, then the duty cycle of the gas pulsing would be influenced. Hypothetically this error would be repeated throughout the course of the test and would subsequently have a directly proportional influence on the final signal. In practice, this error was minimized through proper training and evaluation of an individual's method for consistency between operators.

The third concern with the manual system was synchronization of the gas signal to the stopwatch used for the manual pulsing. While it has already been shown that the “time delay” module could effectively resynchronize the two signals, several implications of this method should be discussed. The time delay itself is an aggregate measure of the cumulative effects of the sensor’s response time, the variability in the mass flow controllers, and the operator’s synchronization error. Since it is an aggregate measure, the time delay was composed of several artificial factors that limit its use for any functional engineering measures. As a direct consequence, the time delay of a gas pulsing system is not solely related to the sensor under interest and any attempt at correlation would be subject to error of a magnitude proportional to the measure.

3.5 Applications of the Method

3.5.1 Benefits and costs of method

The gas pulsing method is an interesting alternative for sensor analysis that allows for quantification of a device in an open air environment. The subsequent chapter will discuss how this method can be applied to porous silicon gas sensors in order to evaluate different pore morphologies, metal coatings, and electrical conditions. In all cases the fundamental benefit is that the gas pulsing method establishes a benchmark such that performance attributes between two or more devices can be directly compared. For prudence, however, it is important to highlight both the advantages and disadvantages of this system.

The benefits of the gas pulsing method are closely aligned with the advantages of porous silicon versus other sensors. The technique is low cost, rapid, and enhances

reversibility of the system on which it is performed. Additional benefits include the ability to benchmark devices that are otherwise not comparable, an ability to detect gas signals when environmental signals are dominant, and a general ease of automation. From a speed of evaluation standpoint, the gas pulsing method expedited testing from 1 data point every 6-8 hrs to almost 60 data points per hour.

The gas pulsing method does possess several distinct disadvantages versus the single pulse method. The primary disadvantage is that transient information is distorted by the pulsing. Since the time domain signal is now a result of periodic pulses, transient analysis will be a measure of both the system's transient performance and the sensor's transient behavior. While the actual time to evaluate a device has decreased, the theoretical limit has effectively increased. Finally the maximum signal for a given concentration is not achieved. If one were to pulse the device to saturation, a larger change in impedance would result. In gas pulsing some of the impedance rise has been traded away in order to increase the reversibility of the reaction.

The combination of these advantages and disadvantages suggest two important opportunities for the gas pulsing method. First, gas pulsing is an effective method for analysis of gas sensors that are susceptible to base-line drift. While one always desires a large gas signal, the ability to detect the presence of a small gas response helps the experimentalist improve the gas sensor and its operating conditions. Less guessing is required because a statistically significant set of data has been pooled in a reasonable timescale. The second opportunity associated with gas pulsing is an application in a reduced scale of the same system. If the size of the system was reduced to a MEMS scale, and if the valve actuation and gas delivery were more rapid, the time between

pulses could be scaled downward approximately 10 fold. Subsequently, the time to detection would be less than three minutes. Through improvements in the device's sensitivity, the required time for a pulse could be even further reduced. With this property, the market potential of porous silicon gas sensors would be dramatically increased.

3.5.2 Additional Applications

Since one of the primary benefits of gas pulsing is analysis for gas sensors that have a small amplitude response and are in an early development phase, it is important to describe the attributes of a “developing” gas sensor (for this application). Obviously sensors with a millisecond response do not require this method because mechanical oscillations of the valves and gas delivery system would be slower than the response of the device. Devices with responses on the order of minutes or hours, however, are prime candidates. This is because the time to measure a response will be reduced from the hours necessary to obtain steady state to a timescale of approximately 30 pulses. Additionally, this method is effective for devices where baseline drift and noise are an issue. If the device is not subject to drift or noise, then it is better to provide one large pulse of gas and obtain the maximum signal. Most sensors, however, are highly suspect to noise and baseline drift. Finally, it is important that a device possess either a logarithmic or linear gas response with time. If a majority of the impedance change occurs during the final 30% of the response (highly non-linear behavior), then this method will be inefficient and sensitivity will be poor.

The first logical application of this method beyond the porous silicon gas sensor is other sensors based upon a porous silicon framework. Within this application, several published reports on porous silicon demonstrate issues that are potentially resolved with the gas pulsing method. L. Pancheri's^x description of a "very sensitive porous silicon NO₂ sensor," includes such attributes as a baseline drift that was not recovered within 30 minutes of relaxation as well as a recovery time of around 10 minutes. The gas response in this application was measured as a relative change of impedance versus a known baseline. Furthermore, the overall dynamics of the response were logarithmic in nature. S. Zangooie's vapor sensitivity analysis of thin porous silicon layers^{xi} revealed a time to reach 90% of the final value to be around 20 seconds but a recovery rate on the "minutes" scale if the device was fully saturated. Finally Guoliang Wang's ellipsometric gas sensing by copper deposition on porous silicon^{xii} also revealed a device with a linear onset lasting several minutes and a drifting baseline. In all of these examples, the gas pulsing method could effectively determine the response with higher fidelity and resolution.

Devices comprised of materials other than porous silicon are also afflicted by slow, semi-reversible equilibrium positions, high sensitivity to noise, and a drifting baseline. X.C. Zhou's quartz crystal microbalance gas sensor^{xiii} has a response time of 5-7 minutes, a recovery with 20-40% hysteresis, heightened reversibility for smaller doses, and drifting. Initial response data appears highly linear. In another example, Ilona Koronvzi investigated the Kamina[®] for medical diagnosis. They discovered that if the chip was flushed with clean humid air and stepwise exposed, performance was more uniform. By implemented the pulsed gas method, however, they could gain additional

information through a more systematic treatment of the pulses and data processing based upon parametric logic. Finally P. Althainz's tuning of a gas-sensor microsystem^{xiv} for water, methane, propane, benzene, and toluene had a response time of 250 seconds with a linear onset. Additionally this team showed that thicker coatings increased the response time from 20 to 250 seconds in order to enhance selectivity above noise factors. Through pulsed gas methods, the thinner films with shorter response times could be utilized.

3.6 Conclusions

A novel parametric method for the analysis of gas response in porous silicon gas sensors has been developed. This method utilizes preprocessing of the information in the frequency spectrum as well as parametric knowledge relating to the nature and frequency of the response. Within the method are three modules that serve a role in reducing noise, locking onto the gas signal, and extracting the pertinent measure. Currently thermal and pressure noise have been minimized with this method. Finally this process is robust with potential applications in porous silicon sensors, thin-metal oxide sensing, and micro-resonating systems.

REFERENCES

- ⁱ CMOS Capacitive Chemical Microsystems for Volatile Organic Compounds, A thesis of Andreas Koll, Swiss Federal Institute of Technology Zurich, 1999 DISS ETH No. 13460
- ⁱⁱ Y. Cengel, Fundamentals of Thermal-Fluid Sciences, First Edition, McGraw-Hill, (2001) Table A-18
- ⁱⁱⁱ R. Priemer, Introductory Signal Processing, Advanced Series in Electrical and Computer Engineering – Vol. 6, World Scientific 1991, pg. 129-161
- ^{iv} M. Roth, R. Hartinger, R. Faul, H. Endres, Drift reduction of organic coated gas-sensors by temperature modulation, Sensors and Actuators B 36 (1996) 358-362
- ^v A. Ortega, S. Marco, A. Perera, T. Sundic, A. Pardo, J. Samitier, An intelligent detector based on temperature modulation of a gas sensor with a digital signal processor, Sensors and Actuators B, 78 (2001) 32-39
- ^{vi} J Watson and G. Davies, A low level carbon Monoxide monitor, Sensors and Actuators B 2 (1990) 219-222
- ^{vii} R. Cavicchi, J. Suehle, K. Kreider, M. Gaitan, P. Chaparala, Optimized temperature pulse sequences for the enhancement of chemically-specific response patterns from micro-hotplate gas sensors, 8th International Conference on Solid-State Sensors and Actuators and Eurosensors IX (1995) 823-826
- ^{viii} T. McAvoy, Engineering Technology in a Sustainable World, 3 (1996) 9-10
- ^{ix} J. Bores, Introduction to DSP, Bores Signal Processing (February 2003)
http://www.bores.com/courses/intro/filters/4_spec.htm
- ^x L Pancheri, C. Oton, Z. Gaburro, G. Soncini, L. Pavesi, Very sensitive porous silicon NO₂ sensor, Sensors and Actuators B, 6974 (2003) 1-3
- ^{xi} S. Zangoie, R. Bjorklund, H. Arwin, Vapor Sensitivity of thin porous silicon layers, Sensors and Actuators B 43 (1997) 168-174
- ^{xii} G. Wang, Modification of vapor sensitivity in ellipsometric gas sensing by copper deposition in Porous Silicon, Sensors and Actuators B, 4263 (2002) 1-9
- ^{xiii} X. Zhou, S. Ng, H. Chan, S. Li, Detection of organic amines in liquid with chemically coated quartz crystal microbalance devices, Sensors and Actuators B 42 (1997), 137-144

^{xiv} P. Althainz, A. Dahlke, M. Frietsch-Klarhof, J. Goschnick, H. Ache, Reception tuning of gas-sensor microsystems by selective coatings, *Sensors and Actuators B*, 25 (1995) 366-369

CHAPTER FOUR

APPLICATIONS OF THE GAS PULSING METHOD

4.0 Introduction

Quantification of performance is an essential component to new product and process development. It has previously been shown that variability in signal output was a predominant error associated with the analysis of porous silicon. It was also shown that porous silicon gas sensors possessed a high degree of output uncertainty. This uncertainty was poorly correlated to factors such as device resistance with a 10mV supply, thermal sensitivity from 20-110 °C, and photoluminescence under ultraviolet illumination. Also, distinction between gas response and noise was quite poor. Electrically, a high degree of variation in the resistance and current-voltage profile existed. The combination of these factors suggested that an alternative testing method was necessary.

In the previously discussed gas pulsing method (Chapter 3), a technique was developed that did not require stability in the baseline resistance or low thermal sensitivity. As a result, a motivation for applying the gas pulsing technique to porous silicon gas sensors has been developed. With this method, thermal noise, random fluctuation, and long settling times were mitigated through the use of the gas pulsing method. As an addition benefit, testing times were diminished. Finally the uniformity of the metric has been used to correlate results from the set of gas pulsing experiments.

The gas pulsing method was applied to three distinct aspects of the porous silicon development process. In the first application, gas pulsing has been utilized to discern

responsive devices from non-responsive devices. The ramifications of this approach were critical to the design process. By measuring small, poor gas responses, one could benchmark the current performance of a device and determine the steps necessary for incremental improvements.

The second application was gas pulsing of cleaned and metallized porous silicon structures. Based upon the affinity of various pore configurations to a given treatment, manufacturing techniques for improving the sensitivity and selectivity were performed. In the final application, the gas pulsing method was used for evaluation of porous silicon for performance parameters. This study confirmed the accuracy of the procedure and highlighted the simplicity of the technique for characterization studies.

Finally it should be noted that the collective application of the gas pulsing method is somewhat unique. Certainly the concept of pulsing gas on a surface in order to control saturation is not novel. What is significant in this study is the integration of gas pulsing, signal analysis, and specific criteria of the gas sensor for the purpose of measuring small amplitude signals. With these collective attributes, a technique for uniform characterization of a device can be presented.

4.1 Rapid / Reliable Method for Gas Sensitivity Screening

The greatest confounding factor during the analysis of preliminary results was the presence of fictitious gas signals. This erroneous data was difficult to discern qualitatively due to its similar shape and appearance to that of a gas response. Quantitatively, the methods presented for preliminary data analysis did not offer consistent mechanisms for sensitivity and selectivity discernment. These errors were

apparent because the baseline drifted with a high magnitude that appeared qualitatively similar to that of a gas response. Figure 4-1 illustrates a gas response and a high magnitude drift in the baseline. In the case of the drift in Figure 4-1, the mass flow rate was fixed at 20 SCCM of nitrogen with no test gas delivered during the entire experiment. As one can see, these errors ruled out the possibility of directly correlating the absolute impedance value to the presence of a gas. In order to quantify and bring value to the observed data, screening and signal processing were necessary. To meet this need, the gas pulsing method was applied as a screening method. In the following section, the unique benefit of this technique will be demonstrated.

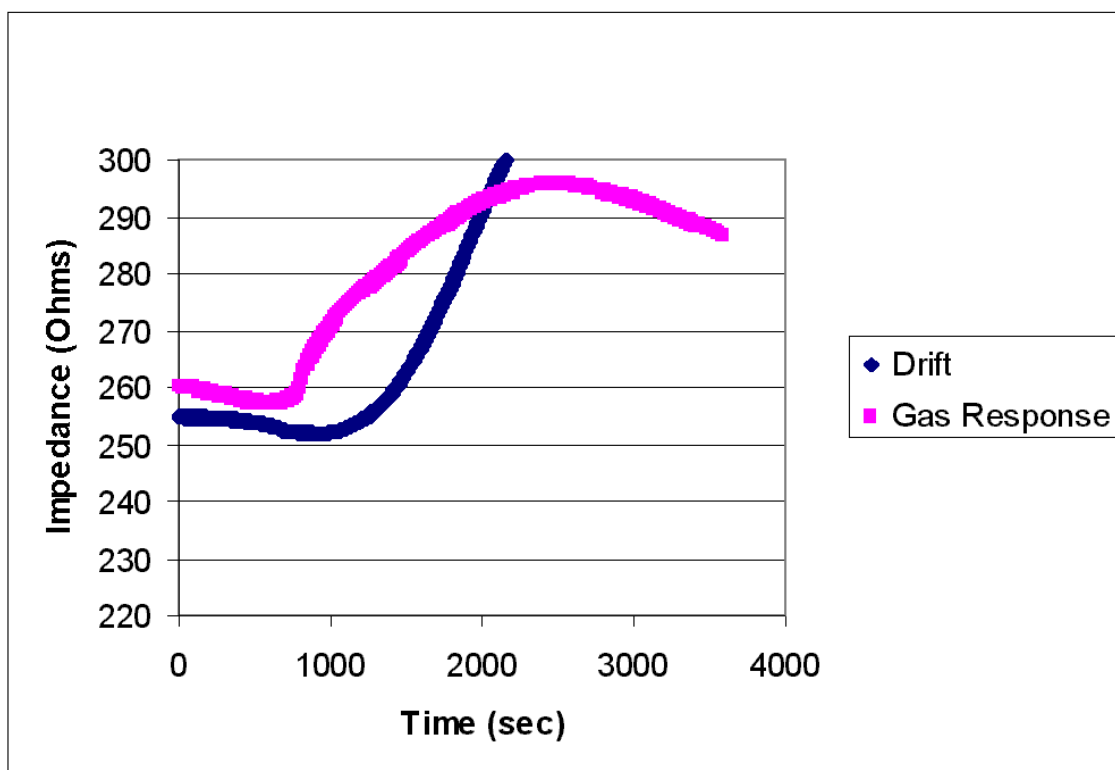


Figure 4-1: Illustration of a false signal (drift) under only a nitrogen flow and a gas signal under preliminary results for exposure to 50 ppm NH_3

4.1.1 Alternative screening techniques

Several alternative methods for the screening of gas sensitivity exist. Before discussing alternative screening techniques, however, the definition of screening for this application will be outlined. The screening process refers to the ability to uniformly and distinctly separate a gas sensitive device from an insensitive device. In general the process of screening is qualitative and rapid when responsive devices possess a substantial sensitivity relative to noise factors. In the case of the porous silicon gas sensor subject to part-per-million levels of CO, NO, and NH₃ over a 30-60 second window, the gas response was quite small. Many of the responses were on the order of 0.5-10 ohms. Since the magnitude of the gas response was often proportional to the noise level, many simple screening methods were ineffective. Examples of alternative screening techniques include repeat trials, time scale analysis, and correlated parameter analysis.

Repeat trial analysis is a fundamental aspect of experimental procedure. In the case of the porous silicon gas sensor, this process could not be blindly applied. The repetition of experiments was limited by the presence of a highly unstable baseline, a slow gas response, and the functional life of the device. Also the testing apparatus for the analysis of the gas sensor were unable to fully restrict thermal and atmospheric noise. For example, a sensor with a 10 ohm response would often possess a temperature sensitivity of 20 $\Omega/^{\circ}\text{C}$. With temperature fluctuations on the order of $\pm 0.3^{\circ}\text{C}$, discernment of the signal was not consistently achieved. With settling times on the order of hours, the extraction of ten data points could require several days of testing. Often the device would fail prior to the extraction of a complete set of data. In the end, the inability

to hold a precise sampling point for timescales greater than a few hours prevented the use of this method.

A second method for the screening of functional gas sensors is a time scale analysis of the result. With such a method, one provides a known gas concentration or similar stimulus to the system. As a logical consequence, an output signal should appear. Based upon the material under study, an approximation on the rate of the response should be known. Devices that fall outside the bound of this simple logical sequence are rejected.

Time scale analysis loses effectiveness when the transient response of the device is unknown or if the testing conditions are changing. In the case of the gas sensor, both of these detrimental parameters exist. The time constant for the porous silicon device was highly dependant upon the specific pore structure developed and the gas under test. At one end of the published range for the transient response, Wangⁱ and Zangooieⁱⁱ independently reported response times on the order of 20 seconds. At the other extreme, L. Pachini'sⁱⁱⁱ NO₂ sensor was reported with a response time of approximately 10 minutes. In the characterization process for the porous silicon gas sensor, the structure of porous silicon that was manufactured varied between experiments. We observed that porous silicon can be manufactured with a range of transient response. Figure 4-2 illustrates the approximated time constant (90% of full scale) for two sensors from different manufacturing runs. These results confirmed that steady state time scale analysis for single incidence gas pulsing was an unreliable screening approach.

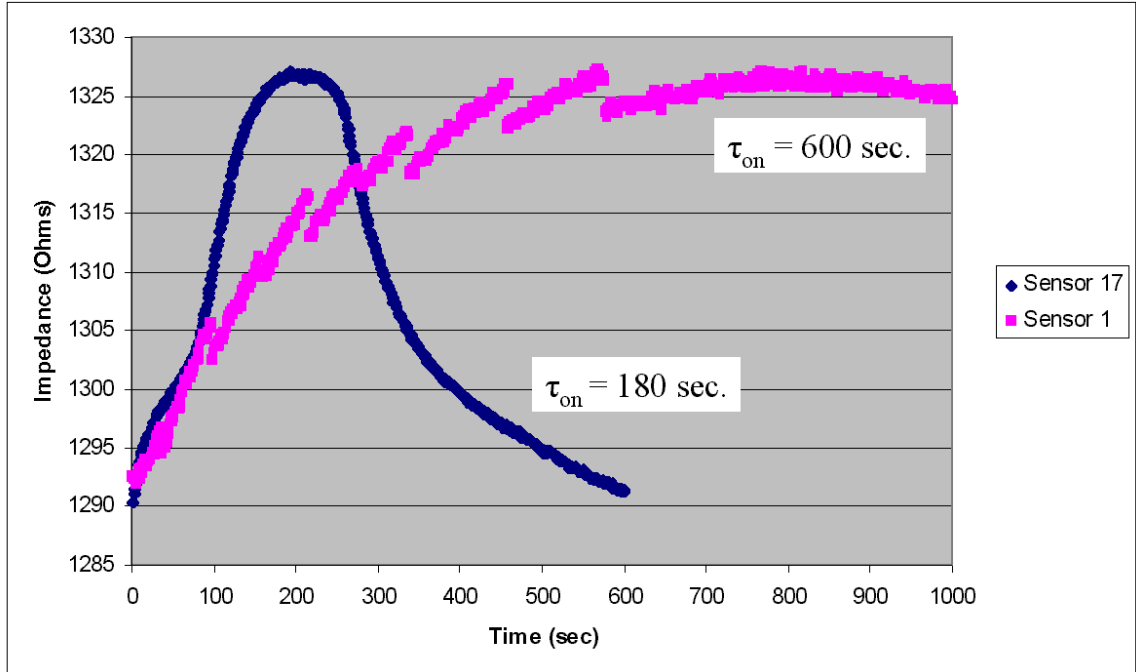


Figure 4-2: Time constant for two devices turned on until saturation

A third method for screening was correlated parameter analysis. In this method, one seeks any attribute of the device under test that strongly correlates with the actual parameter of interest. For example, if the porous silicon gas sensor's sensitivity was entirely dependant upon nano-porous formation, one could test all devices for their photoluminescent properties. Since photoluminescence is an effect of nano-scale porous silicon, this parameter could be used as a screen for devices. For this study, correlation was attempted between gas sensitivity and resistance, I/V sweeps, frequency sweeps, visual inspection, noise amplitude, photoluminescence, and thermal sensitivity. Unfortunately, no correlation could be found between one of these parameters and gas sensitivity.

4.1.2 Screening attributes within the gas pulsing method

The gas pulsing method offered an effective screening method for differentiating random noise from gas response. In the screening process, a frequency domain relationship was sought. If a sensor's responded to gas repeatedly in a short timescale, then the process of uniformly pulsing the gas over the surface would produce a specific frequency (Figure 4-3). Conversely, if the device does not have gas sensitivity, then the gas pulsing frequency will not be present in the device's output. By repeating the gas sampling process on a set of sensors, one can differentiate responsive devices and effectively screen the set of devices.

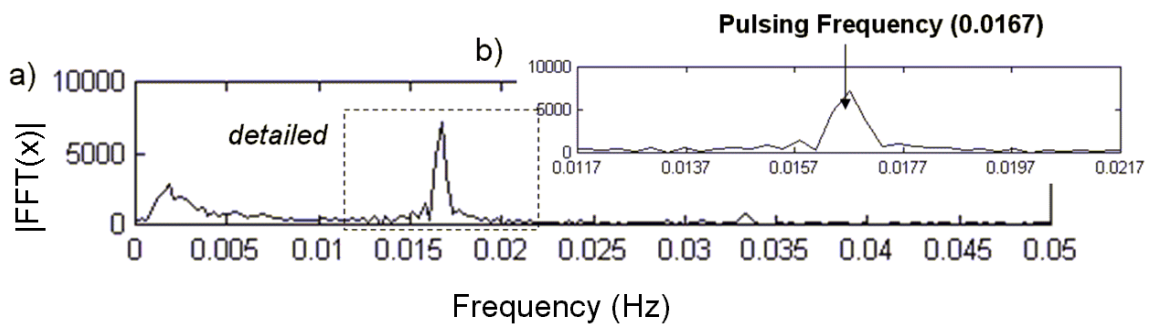


Figure 4-3: a) FFT of a highly responsive device and b) a detail in the area of interest

The fidelity of this method was based upon several significant requirements associated with the device, the testing method, and the nature of the response. The first requirement for this method was that the sensor's output should not generate a high amplitude response at the gas pulsing frequency when gas was not present. Since this parameter was not known unless tested, all devices required analysis under a nitrogen

flow in order to rule out this error. Figure 4-4 illustrates one example of nitrogen testing of a device to ensure that the pulsing frequency was not present in the FFT result.

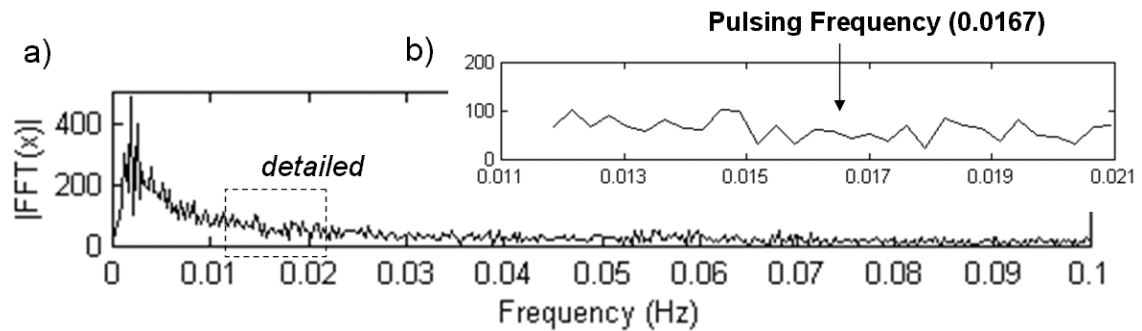

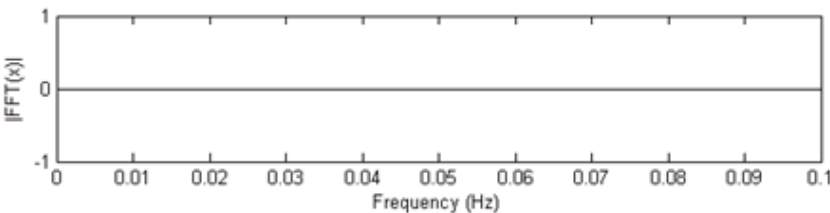
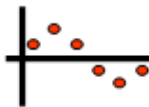
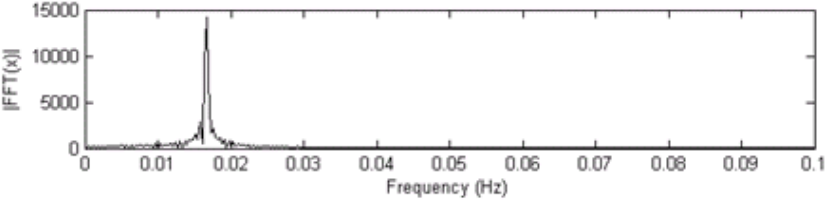
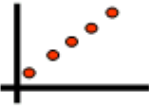
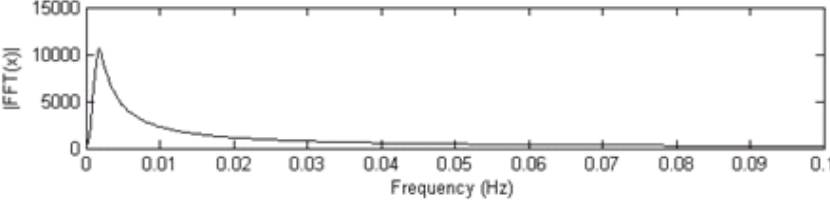
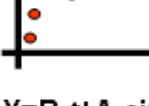
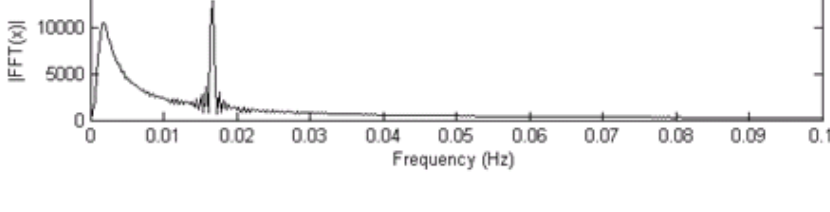


Figure 4-4: a) FFT of nitrogen only pulsing of a device and b) a detail of the FFT in the area of interest

The second requirement for a gas pulsing screening technique was related to the signal processing of the result. This requirement stated that the process of signal analysis should not generate the frequency of interest artificially. The possibility of such an error was refuted by both an analysis of the frequency program with test conditions as well as the result from non-responsive devices. Test conditions performed on the gas pulsing method included a zero-slope positive amplitude test signal, a linear slope test signal, and a sinusoidal signal. The results of these tests are shown in Table 4-1.

Table 4-1: Results from test signals

 <p>$Y=A_0$</p>	
 <p>$Y=A_0\sin(\omega t)$</p>	
 <p>$Y=B_0t$</p>	
 <p>$Y=B_0t+A_0\sin(\omega t)$ $A_0=100B_0$</p>	

A secondary indication that the algorithm was functioning properly were the result of non-responsive devices. While this knowledge was *post hoc*, it further demonstrated that the algorithm would not “artificially create” the frequency of interest. Over 50 experiments with gas pulsing at 0.0167 Hz and signal conditioning demonstrated no signal at the gas pulsing frequency. The only exception to this rule was the presence of a few spurious pulses over the 30 minutes window. These artifacts did not produce a distinct response in the frequency domain. Figure 4-5 illustrates an example of a non-responsive sensor that was “screened-out” by the gas pulsing method.

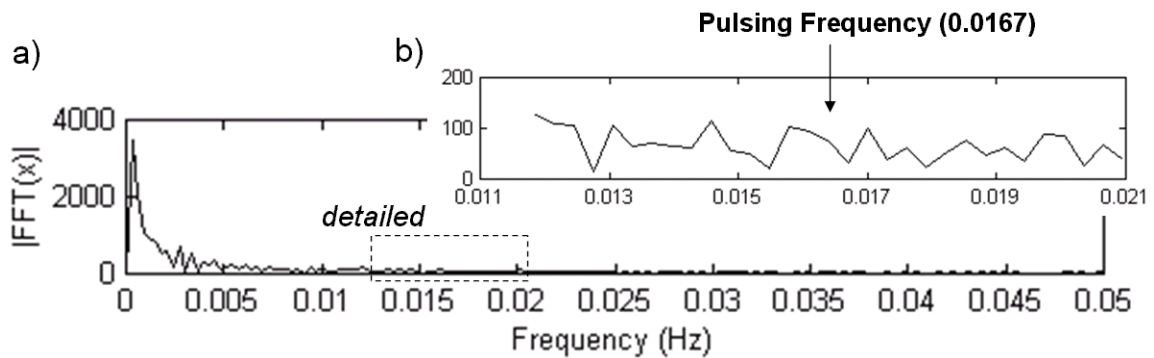


Figure 4-5: a) Non-responsive device output in the frequency domain and b) detail of area of interest

The final requirement considered in the screening process was the contingent possibility that pressure, temperature, or mass flow rate could generate an artificial signal. For the first two factors, the process itself minimized the contingent risk. Since the entire configuration was operating in the “open air” environment, and since the mass flow controllers restrict the flow, pressure variation was based upon changes in the room and not the gas line. Temperature uncertainty in the room, as discussed in Chapter 2, did influence the sensor’s response. The gas pulsing system was designed to remove random

noise that was not correlated to the pulsing frequency of the system. Of greater concern, however, was the possibility that the gas flow delivered to the surface of the device was varying in temperature and consequently artificially producing or diminishing a gas response. To test this possibility, the outbound stream was monitored for temperature fluctuation. No periodicity consistent with the gas pulsing was uncovered. This result can also be explained by the attributes of the experiment. Temperature effects associated with the difference in temperature between the test gas cylinder and the nitrogen cylinder were minimized because one mass flow controller was outputting gas at a rate of 1/100 that of the 2nd controller. The two gas lines were always within 2 °C of one another and the temperature sensitivity of the devices was on the order of 1-20 $\Omega/^{\circ}\text{C}$. Also the temperature of the gas delivered to the sensor was sufficiently thermostated. Based upon these factors, a measurable temperature modulation was not present.

Mass flow rate, as a potential confounding sources, had to be treated differently then pressure and temperature. Logically, there was a high probability that some fluctuation in the mass flow rate was occurring when the controller was switched between the test gas and the nitrogen line. To test this parameter, the flow rate of the nitrogen flow was modulated in a periodic manner, and the impedance was tracked. Figure 4-6 provides the results from a representative analysis. In this study the mass flow rate was varied from 100.4 SCCM N₂ to 80.0 SCCM N₂ at a frequency of 16.7 mHz. As one can see, variations of mass flow rate had no influence on the impedance of the device and conversely did not generate a response at the pulsing frequency (Figure 4-6).

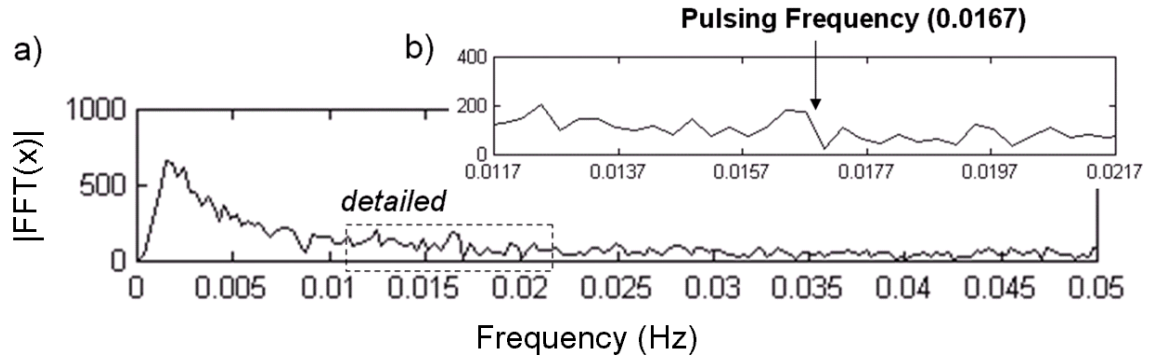


Figure 4-6: Mass flowrate study with rate variation from 80 to 100.4 SCCM N₂

With the completion of the mass flow rate test, a sufficient case had been generated for the use of the pulsing method in a “screening” application. As a logical extension of this effort, the gas pulsing method was applied to a random set of 30 porous silicon gas sensors. The results of this investigation are subsequently discussed.

4.1.3 Sample matrix and gas pulsing

With a sufficient evidence that the gas pulsing method could be used for differentiation of sensitive and non-sensitive devices, the method was applied to a matrix of sensors, test gases, and operating conditions. The sensors themselves were comprised of manufacturing iterations ranging over a 6 month time period. The features manufactured over this time had drastic variations in the type of porous silicon formed, the presence of contaminants on the surface, and type of metallization contact used on both the front and backside of the device. The total matrix was comprised of a total of 30 devices from 8 different manufacturing runs. By applying a diverse set to the analysis, the objective was to uncover a dominant design for formation process of porous silicon.

Since the uncertainty of the performance of any one unit was high, and the variability in the manufacturing technique was large, the samples were initially randomized into 6 groups of 5. This randomization would minimize the probability of drawing conclusions from an isolated trend in the devices. The opportunity cost of this decision was a further reduced probability of repeatable results. After dividing the sensors into an initially randomized group, a feature analysis was conducted. This analysis was conducted in order to determine 1) the possibility of correlations between gas sensing and some physical parameter and 2) to increase the probability that a gas response trend could be correlated to a specific input or test. The features analyzed included impedance, I/V sweep, frequency dependence, visual attributes, and photoluminescence.

The procedure for each of analysis was quite rapid. Resistance sweeps were initially conducted with the multimeter measured from pad to pad in both directions. This technique was used because it was a basic metric that could be compared to earlier analysis performed in the same manner. Once the resistance was taken in both directions for the small amplitude direct current, the device was loaded into the impedance analyzer and an I/V sweep was performed with a 10mV AC, 1 kHz source signal with biasing from -1.0 to 1.0 volt. Once completed, a frequency sweep was performed on the device with a 10mV AC wave with a varied frequency from 10 Hz to 10 kHz.

For the photoluminescence study, a qualitative analysis with the set of sensors was performed in a darkened room. With this analysis, ultraviolet light was shone onto the surface of devices which were photoluminescent in the orange-red spectrum. The intensity of the light was visibly distinct among the devices. As a result, the devices were

grouped into a qualitative range from 0 (no photoluminescence of any form) to 0.5 (weak photoluminescence / photoluminescence only in partial regions) to 1.0 (brilliant photoluminescence). While admittedly this technique was highly qualitative, the distinction between ranges was quite apparent and multiple samples were distinctly catalogued into each group.

Once a complete set of parameters were characterized, the results of the characterization were analyzed with the purpose of separation according to distinct trends. Resistance and I/V sweep characteristics appeared highly randomized with no linear pattern associated with a given manufacturing run or location on a wafer. In general the measured resistance ranged from 150 ohms to over 50,000 ohms. As previously stated, the photoluminescence results were highly differentiated. Visual inspection under optical magnification of the pore structure had failed to produce distinct trends. As a result of these characteristics, the sensors were divided first according to their resistance levels, then according to their photoluminescence parameter. Finally the sensor groups were balanced to separate devices from the same manufacturing run that had ended in the same group. This effort functioned as a tertiary division criteria. With this information, the testing sets were appropriately balanced and prepared for testing.

With the sensors fully separated, the testing sequence was initiated. For each set, a specific gas was targeted for analysis. Gases within this study included NO_x, CO, and NH₃. A test sequence for a particular gas sensor within a given set involved a nitrogen pulsing, a frequency sweep, an I/V sweep, and a test gas pulsing. Optional support experiments involved mass flow rate sensitivity studies and elevated temperature testing. The nitrogen pulsing tests involved replacing the test gas line with research grade

nitrogen. This test ensured that the line was clean and that the device was not responsive to external criteria. The results of this analysis also served as a comparative baseline response. The I/V and frequency sweeps were performed with the same operating criteria as the analysis of the gas sensor. These operating criteria included the AC sampling voltage on the impedance analyzer, the temperature of the test, and the mass flow rate of the nitrogen during the experiment.

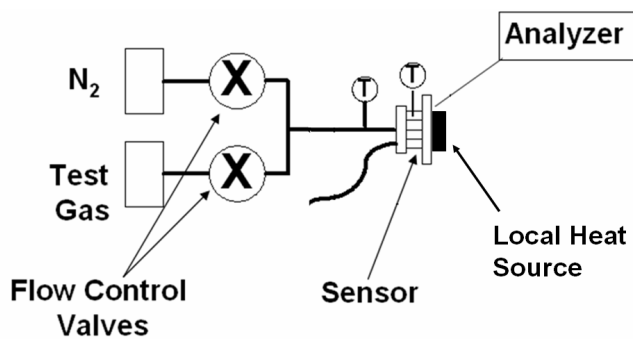


Figure 4-7: The experimental setup

The test gas pulsing and nitrogen pulsing experiments followed the experimental method for gas pulsing as discussed in Chapters 2 and 3 (Figure 4-7). With this method, a gas pulse was driven across the surface of the test device in a periodic manner. Impedance and temperature information was simultaneously recorded. These results were analyzed with the *signal processing for gas pulsing method* as outlined in Chapter 4. In this method, the results of the experiment were transformed into the frequency domain, filtered, analyzed for signal strength at a frequency of interest. This method offered a clear distinction between responsive and non-responsive sensors. In addition, since the objective of this application was to differentiate responsive sensors, a

quantitative metric was added to the process. Quantifiably, the magnitude of the FFT at the frequency of interest must be two times the magnitude of all frequencies in a band of +/- 5 mHz (referred to as the “noise band”) surrounding the center frequencies of 16.7 +/- 1 mHz (referred to as the “signal band”). The ratio of these parameters was given as:

$$\eta = \frac{signal_band_{max}}{noise_band_{max}}$$

[Equation 4-1]

By specifying the band in this method, the standard variations associated with the timing of the valves will not cause the device to fail the screening process. Also frequencies attributed with pressure and thermal noise in the room (which occur at frequencies more than 10 mHz away from the test frequency) will not dictate the screening process (Figure 4-8).

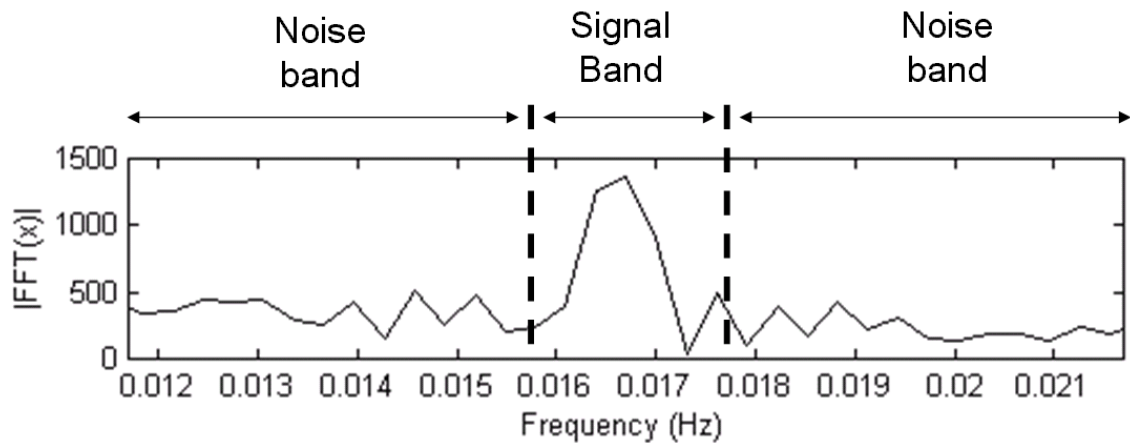


Figure 4-8: Illustration of the signal and noise band regions for a device that passes the screening process

4.1.4 Results

The aforementioned screening method was applied to a CO and NH₃ sensitivity analysis of the 30 sensors that comprised the test matrix. The first distinct result was the instability of three devices within the matrix. With baselines in the mega-Ohm range and variability in the 10kΩ range, the devices were considered unusable and were discarded. For the 27 remaining devices, each device was tested with CO, NH₃, or both. It should be noted that none of the ten sensors tested under a 20 ppm flow of CO were responsive. Of the 23 tests for NH₃ sensitivity, two devices resulted in a positive response, two devices produced a weak gas response that failed the test criteria, and 19 devices were non-responsive. Table 4-2 illustrates the results of this analysis.

Table 4-2: Results from untreated sensor testing (bold indicates a strong response)

Sensor	Gas	Response	Sensor	Gas	Response
3.2.1 D	CO	No	3.2.1 B	NH3	Yes
3.2.1 E	CO	No	3.2.1 # C	NH3	No
3.2.3 # 11	CO	No	3.2.1 F	NH3	No
J 3.2.4 #7	CO	No	3.2.1 # I	NH3	No
J 3.2.4 #9	CO	No	3.2.3 #4	NH3	No
3.2.3 #5	CO	No	Wafer 13 #2	NH3	No
PL #1	CO	No	3.2.1 #A	NH3	No
3.2.3 #8	CO	No	J 3.2.4 #4	NH3	Yes
3.2.3 #7	NH3	Yes	J3.2.4 #6	NH3	Yes
3.2.1 G	NH3	No	3.2.3 #2	NH3	Yes
3.2.3 #6	NH3	No	Wafer 13 #1	NH3	No
3.2.3 #1	NH3	No	J3.2.4 #1	NH3	No
3.2.3 #10	NH3	No	3.2.3 #9	NH3	No
3.2.1 H	NH3	Yes	J 3.2.4 #8	NH3	No

This testing indicated a strong sensitivity to ammonia in approximately 7% of all tested devices, a yield similar to that observed from earlier generations. The primary benefit of this approach, however, was the reduction in testing time and the improvement

in the metric for analysis (small amplitude responses were detected). During the discussion of preliminary results, approximately 18 sensors were analyzed over a 3-1/2 month period. On average preliminary testing of each sensor involved approximately 5-10 gas pulses. With the gas pulsing method, 33 sensors were evaluated with a minimum of 30 gas pulses each in less than one month. Additionally, the FFT served as a benchmark metric with which to classify the devices in a comparative manner.

An investigation of select results in combination with the method from section 4-1-3 illustrates the effectiveness of the method. With the signal/surrounding ratio set at 2.0, the false positive frequency (probability that no gas produces a gas signal) was zero incidents in 33 devices. In general, however, one must note that this parameter is describing a false positive incidence rate for the sensitivity of the device (and not the false positive according to gas selectivity). For the objective of screening out non-responsive sensors, the selected criteria were quite effective.

Similarly this method was effective at isolated two sensors with a positive response to ammonia at 20 ppm pulsed with a period of 60 seconds. In both positive situations, one can observe multiple noise sources that could have served as interference for the one pulse testing scheme. Figure 4-9 provides an example of a device with a signal/surrounding ratio of 3.01.

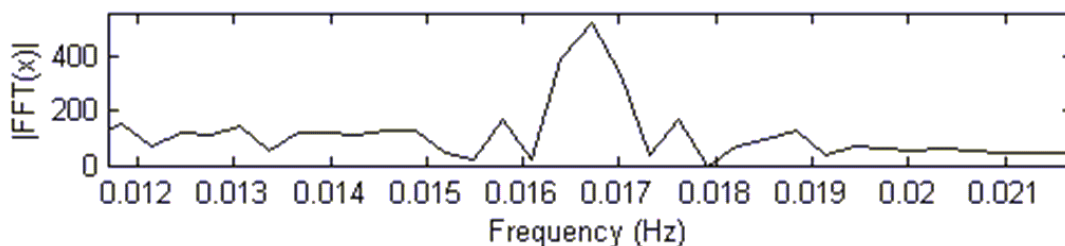


Figure 4-9: Response of device to 10 ppm NH_3 at 100 SCCM

While the results of this metric were successful for excluding non-responsive devices and uncovering positive responses, this criterion was restrictive to weakly responding devices. Figure 4-10 illustrates an example of a noisy signal with a small amplitude response and its corresponding FFT in the frequency range of interest. This signal, when processed, resulted in a signal/surrounding ratio of 1.8, a non-responsive classification.

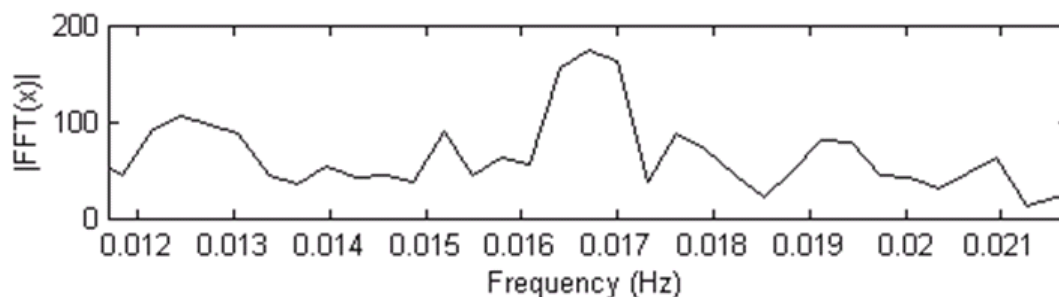


Figure 4-10: a) The case of a weak response ratio of 1.6. (2.0 is the cutoff standard)

Monotonic drift was an additional area of concern with this screening method. In general, such drift had no influence on the screening procedure. In extreme cases of monotonic drift, however, it appeared that the gas response was suppressed in the

frequency domain and subsequently a gas sensitive device would fail the screening method. To quantify the effect of monotonic drift on this technique, an experimental signal was processed with the FFT algorithm and screening method. The form of the test signal was:

$$y = A_1 t + A_2 \sin(\omega t)$$

[Equation 4-2]

In this test equation, $A_1 t$ term generated a monotonic drift. The sine component simulated a gas response at a frequency of 16.7 mHz. Based upon this analysis, it was determined that a total drift 44 times the amplitude of the gas response would result in failure according to the algorithm. Figure 4-11 illustrates the results from applying the test signal with various magnitudes of drift amplitude (A_1). The parameter η (equation 1) is the corresponding output of the FFT algorithm based upon the test signal.

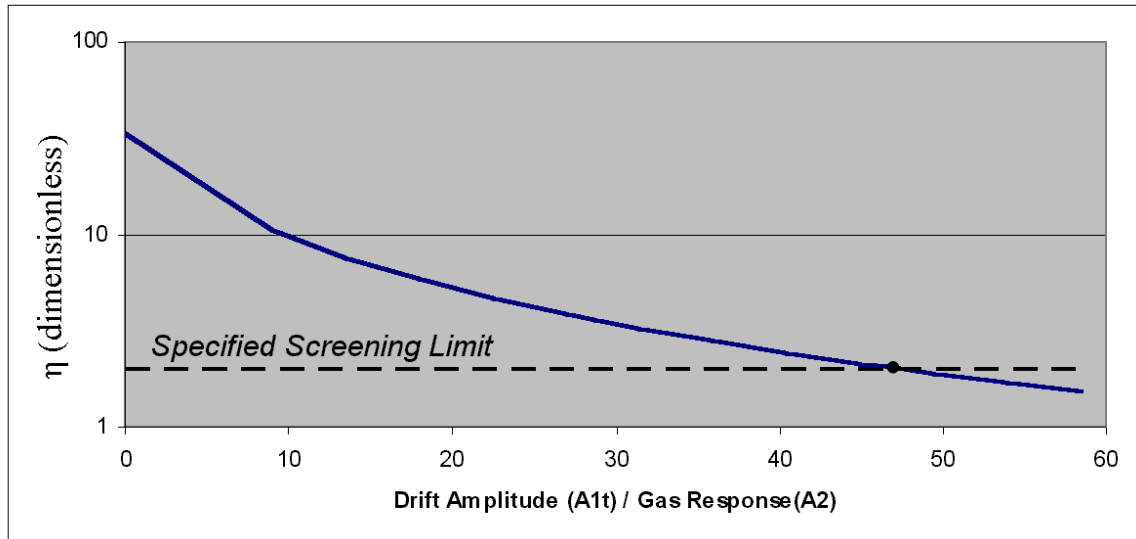


Figure 4-11: Results from applying the test signal to the signal processing algorithm

In an attempt to mitigate these issues several solutions were attempted. The first effort was to fit a linear approximation to a system with high drift. While this attempt was quite successful for highly linear signals, the algorithm became highly unpredictable for situations where the drift was slightly non-linear. In a second attempt at signal resolution, a $1/f$ algorithm was fit to the case of monotonic drift. Again, in the case of slightly non-linear response, the algorithm became highly unreliable. Of greatest concern were inflection points of nonlinearity. At these points the algorithm was high discontinuous. To mitigate these failed signal processing attempts, sensor experiments that indicated a drift of 40 or more times the gas signal were re-evaluated.

While the system did possess inherent weaknesses associated with monotonic drift, the overall process was quite successful at screening devices. Monotonic drift of the same order as discussed above occurred only three times during the entire evaluation process for the untreated sensors. For all other incidents, the method rapidly separated the devices according to their gas performance. This allowed for a focus on gas sensitive devices rather than the entire set of sensors on the wafer.

4.2 Cleaning and Metallization of Porous Silicon

After establishing a technique for screening, the gas pulsing method was investigated as a method to assess “improvement” to porous silicon gas sensors. The need for improvement was quite clear. The lowest concentration detected from early results was around 15 ppm of NH_3 and 22 ppm of NO_x . These levels were underperforming for a porous silicon gas sensor relative to the work by L. Pancheriⁱⁱⁱ who has obtained ppb detection levels for NO. Although the porous silicon gas sensor operated at a lower

power level than these devices, the sensitivity still required improvement in order to consider field applications.

4.2.1 Historical impetus for method

The historical background for electroless treatment is centered upon improvements to related to photoluminescence and reduction in impedance. Gole^{iv} and Prokes^v, *et. al.* describe a cleaning process for porous silicon in which treatment with HCl was found to produce the most efficient enhancement of the photoluminescence signal. Furthermore stable photoluminescence occurs for HCl concentrations in the range of 0.2-3 molar dilute in H₂O. Appropriate immersion times for the cleaning process ranged from 3-5 hours.

The benefit of cleaning porous silicon before electroless treatment for optical benefits was described by Gole^{vi}. In this discussion, electroless copper and silver were coated onto the surface of porous silicon through either a HeNe laser or with UV lamp exposure. In order to improve the deposition process, sensors were initially cleaned with an anhydrous concentrated hydrazine to remove fluorine from the surface. A 6 M HCl/MeOH solution was also used to enhance photoluminescence on the surface. It was also suggested that photoluminescence was a critical parameter for deposition of electroless metals into a porous silicon surface. Finally surface heating was shown as a trivial parameter in the electroless metal coating process into porous silicon.

In a direct application to porous silicon gas sensing, Seals^{vii} demonstrated the use of electroless metal to effectively lower the contact resistance at the porous silicon / gold interface. This work also described the use of photocatalysis for the electroless

deposition of gold. This technique replaced the traditional Pd metal catalyst approach. With this process, measurements of 100 ppm of HCl, NH₃ and NO were obtained.

4.2.2 Equipment and procedure

The testing procedure for electroless metal deposited sensors was identical to the screening methodology. The process of evaluating a cleaned and treated sensor required a resting period of approximately 12 hours before the testing with gas. If the sensor was not sufficiently dry, the impedance of the baseline would be highly unstable and erratic. The I/V sweep of a wet device revealed a dramatic unidirectional impedance increase (Figure 4-12). In consequence this analysis was useful for determining when a device was dry and ready for testing.

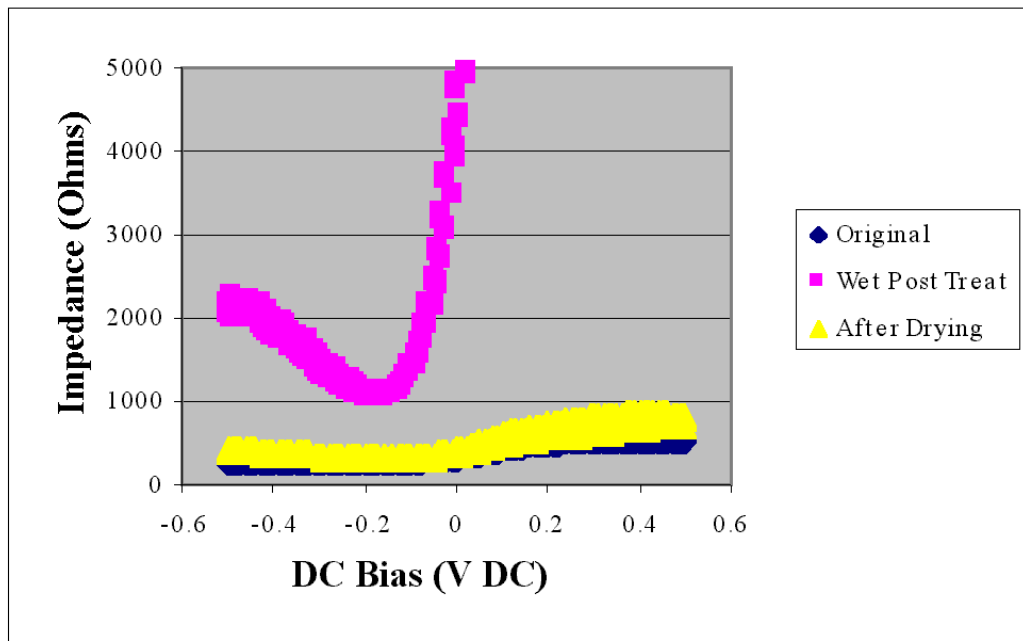


Figure 4-12: I/V sweep of a device before and after drying

The equipment for metallization was comprised of porous silicon gas sensors, dilute aqueous 1M HCl, and an electroless metal of interest. The two investigated electroless metals that met with success were gold and tin. The wafers treated in HCl and electroless metal spanned seven generations of gas sensor manufacturing. The age of the sensors that were treated ranged from less than two weeks to five months old.

The cleaning process for the gas sensor involved one of two common techniques. In the first technique, a four hour soaking in 1:5 44% HCl dilute in methanol. Following the treatment, the device was placed in methanol for approximately 3 minutes and then allowed to sit in air until dried. This cleaning recipe was similar to those described by Gole^{viii}, *et. al* for the enhancement of photoluminescence of porous silicon films. The second cleaning technique was a 3-1/2 hour soak in 3M CH₂Cl₂ dilute in deionized water. Following the CH₂Cl₂ soak, device was similarly immersed in methanol and then air dried. By performing the cleaning process, it was shown that the propensity for electroless metal deposition was enhanced. Furthermore, in this procedure, the electroless metal deposition had occurred under room lighting and temperature.

After cleaning of the surface, the porous silicon gas sensors were treated with select electroless metals. The two electroless metals selected for this investigation were gold and tin. The gold electroless solution was *Transene Bright Electroless Gold-Type 1*. This commercially available solution possesses approximately 1/2 tr. oz of gold per gallon of solution. The solution itself has a pH of around nine, and it was advertised as a compound for the uniform deposition of 24 karat gold onto various metallic surfaces. The electroless tin solution was formed from 5g Tin Chloride, 7.7g NaOH, 9.7g

Sodium Citrate in 100mL water. Table 4-4 outlines exact recipes that resulted in successful improvements to porous silicon gas sensors.

In order to deposit the electroless gold onto the surface, the published recipe recommended a heating of the solution to 50-90 °C. In order to deposit a sub-monolayer of gold in a controllable timetable, the operating temperature was instead chosen at 22 °C. For 30 seconds the cleaned sensor was suspended in a 3 mL pool of electroless gold solution without agitation. After treating one batch (3-5) of sensors the solution was discarded. After suspension in the electroless gold, the sensors were sprayed with deionized water for approximately 15 seconds. Finally the sensor was sprayed with methanol for around 30 seconds and allowed to air-dry for 12 hours.

For the electroless tin deposition, a similar recipe was followed. The freshly cleaned devices were immersed in 1-2 mL of electroless tin solution for a specified time between 10-30 seconds at room temperature. After immersion the devices were washed with deionized water for approximately 10 seconds and then sprayed with methanol for approximately 10 seconds. A drying time of approximately 12 hours was allocated.

Table 4-3: Outline of common cleaning recipes

Cleaning #	Solution (Concentration)	Immersion Time	Post Rinse
T1	HCl dilute in CH ₄ (4 M)	30 seconds	methanol immersion (3 min)
T3	HCL dilute in CH ₄ (1 M)	3.6 hrs	methanol immersion (3 min)
T4	CH ₂ CL ₂ dilute in H ₂ O (3 M)	4.0 hrs	methanol immersion (3 min)
T5 (2 parts)	HCL dilute in CH ₄ (1.6 M)	3.5 hrs	n/a
	CH ₂ CL ₂ dilute in H ₂ O (3 M)	4 hrs	methanol immersion (3 min)
T6	HCL dilute in CH ₄ (1.2 M)	5.5 hrs	methanol immersion (3 min)

Table 4-4: Recipes for common electroless metal deposition

EL Test	Solution	Immersion Time	Rinse
EL #1	Transene EL Gold Solution (not diluted)	30 sec (no agitation)	120 sec H ₂ O, 30 sec CH ₄
EL #3	Transene EL Gold Solution (not diluted)	30 sec (stirring)	15 sec H ₂ O, 30 sec CH ₄
TinEL #1	5g Tin Chloride, 7.7g NaOH, 9.7g Sodium Citrate in 100mL water	13 sec (no agitation)	10 sec H ₂ O, 10 sec CH ₄
TinEL #2	5g Tin Chloride, 7.7g NaOH, 9.7g Sodium Citrate in 100mL water	32 sec (no agitation)	5 sec H ₂ O, 10 sec CH ₄

Table 4-5 A sample table of gas sensors that were metallized

Sensor #	Cleaning #	Metal	EL Test	Gas	Concentration
3.2.1 H	T3			NH ₃	20 PPM
3.2.1 H	T3	Au	EL #1	NH ₃	20 PPM
3.2.1 I	T5			NH ₃	20 PPM
3.2.3 #1	T6	Sn	TinEL #1	NH ₃	20 PPM
3.2.3 #1	T6	Sn	TinEL #1	CO	20 PPM
3.2.3 #2	T6			NH ₃	20 PPM
3.2.3 #6	n/a	Au	EL #3	NH ₃	20 PPM
3.2.3 #7	T5			NH ₃	20 PPM
3.2.3 #7	T5			NH ₃	10 PPM
3.2.4 #1	T6			NH ₃	20 PPM
3.2.4 #1	T6	Sn	TinEL #2	CO	20 PPM
3.2.4 #1	T6	Sn	TinEL #2	NO	20 PPM
3.2.4 #4	T1, T4			NH ₃	20 PPM
3.2.4 #4	T1, T4			NH ₃	15 PPM
3.2.4 #4	T1, T4			NH ₃	10 PPM

4.2.3 Results

Consistent with metallization results in other sensing applications, the deposition of electroless gold and tin resulted in improved sensitivity and selectivity to specific chemical species. Additionally electroless tin deposition demonstrated sensitivity to CO, a gas that was previously undetected by the porous silicon gas sensor. By comparing the impedance output of gas sensors with various metallizations, the selectivity between species at a given concentration was demonstrated. It is important to note that these results are based upon a flow of the given gas species without an interfering gas. Through the use of the gas pulsing method, the results of various experiments could be compared in a uniform manner with the same metric.

In order to evaluate the performance of the coated devices, the gas pulsing method was utilized. For this application, the entire gas pulsing procedure as described in Chapter 3 was utilized. In this process the gas was pulsed across the surface of the device over a 30 minute period. Once the pulsing was completed, the sensor's output was transformed to the frequency domain and analyzed in a range centered on 16.7 mHz. If sufficient signal strength was detected, the signal was processed in the time delay module. This module locked onto the periodic oscillations of the signal. Finally in the solution extraction module, the average and standard deviation for all 30 pulses taken across the surface a given device were reported.

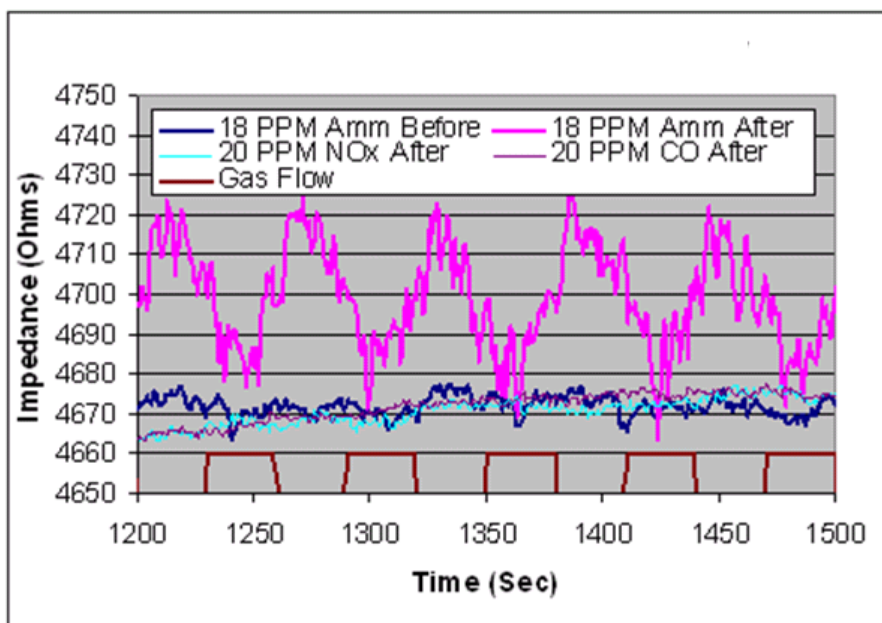


Figure 4-13: Response plots for an electroless gold treated device

Figure 4-13 provides the raw data plots for a sensor before and after electroless gold treatment. The most distinct result from this process was a 10x magnification of the NH_3 sensitivity of the device. From this Figure, several other trends should be noted. For this device, a small response to NH_3 before treatment was noted. This behavior was commonly present in gas sensors that were successfully enhanced with electroless gold. Secondly, CO was not detected before (not indicated) or after electroless gold treatment. This trend held universally for all electrolessly gold coated devices. Finally it should be noted that the ammonia before and CO after signals have been vertically adjusted for ease of comparison between baselines. The actual range of baseline responses for the devices was from 900-4000 ohms.

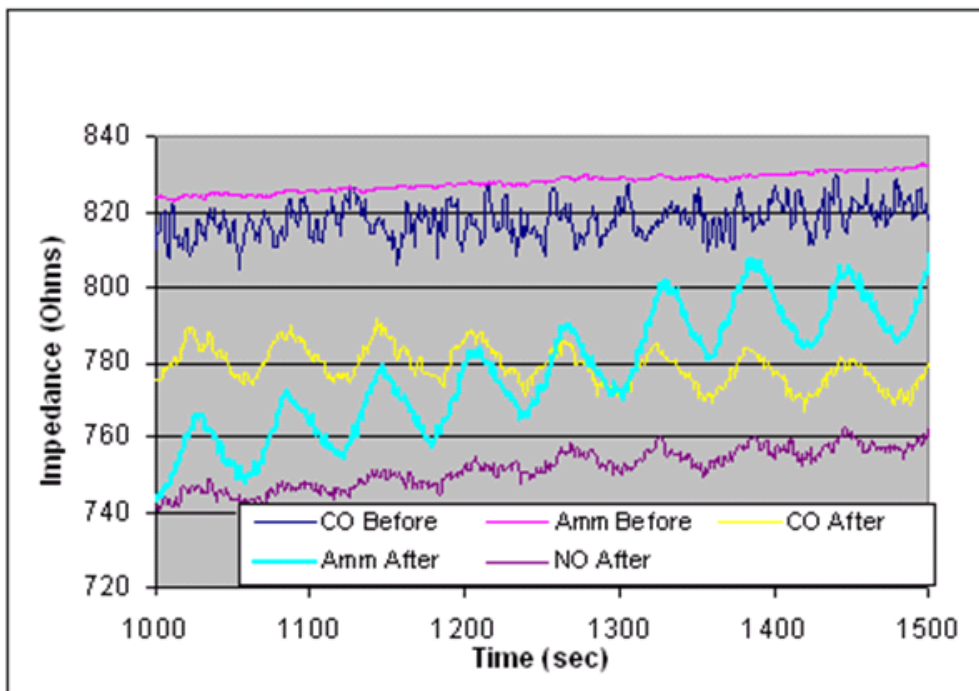


Figure 4-14: Response plots for an electroless tin coated device

Figure 4-14 illustrates the effects of tin coating on the performance of a device. From this figure, several unique differences from gold coating should be noted. First the tin coated device demonstrated sensitivity to CO. This sensitivity was entirely not present prior to the coating of the device. Similarly ammonia sensitivity of the device was not apparent prior to treatment, but was apparent after treatment. Since the device appeared to respond to several gases, a set of environmental tests were run on the tin coated devices. These tests indicated that the gas responses were not caused by temperature, mass flow rate, or gas line contamination.

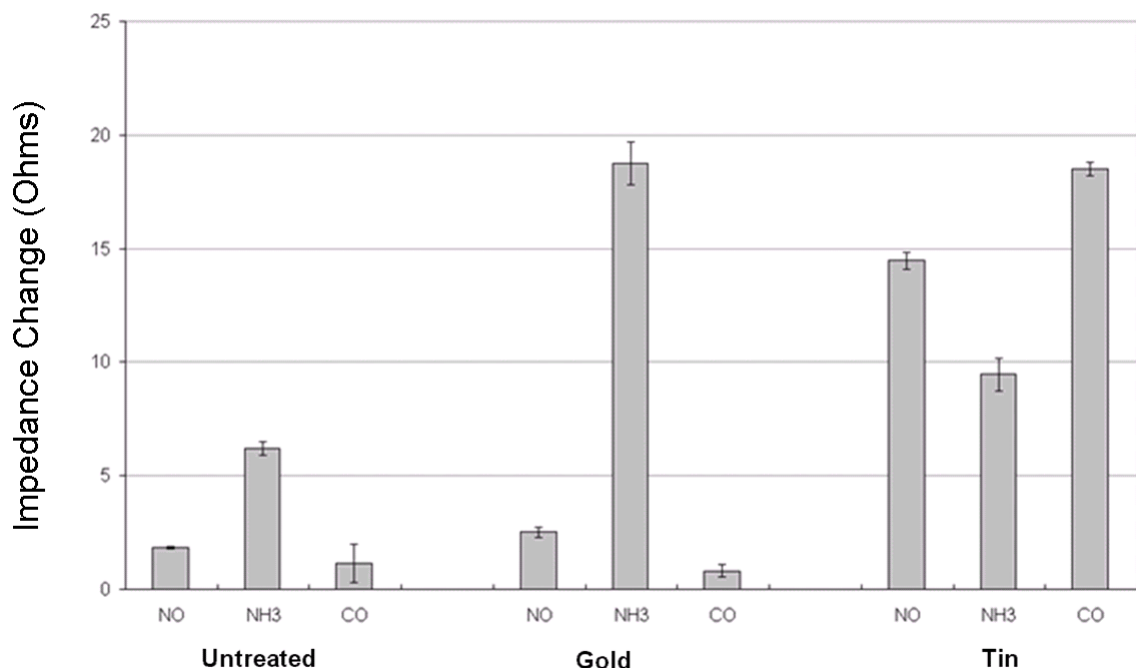


Figure 4-15: Comparison of impedance response to 20 ppm of test gas at 100 SCCM

Figure 4-15 outlines the cumulative results of the metallization process when combined with the gas pulsing method. As one can see, the gas pulsing method enabled a tangible metric for comparison among a range of devices and gas species. It should also be noticed that these impedance changes of the range of 5-20 ohms were successfully extracted from baseline values that ranged from 450-4500 ohms. Appendix E provides the exact sensors where electroless coating was successful.

4.3 Device Characterization

In congruence with the original objective of this paper, the gas pulsing technique was applied in multiple characterization applications. Two specific applications subsequently discussed include a lower onset of detection and signal discernment in a thermally

fluctuating field. In these cases, the gas pulsing method demonstrated an ability to analyze data rapidly with a high degree of flexibility.

4.3.1 Lower onset of detection

In order to evaluate the lower onset of detection, the gas pulsing method required one adjustment. Traditionally all gas pulses had occurred at 20 ppm. In order to determine the lower onset curve, however, the concentration had to be stepped in a range from 0 ppm to 19 ppm. For this analysis, various concentrations of ammonia at room temperature were pulsed onto an electroless gold coated porous silicon device. The electrical operating conditions for this experiment were a 100 mV AC wave at 1kHz with no DC biasing. The gas pulsing period was one minute with a 50% duty cycle.

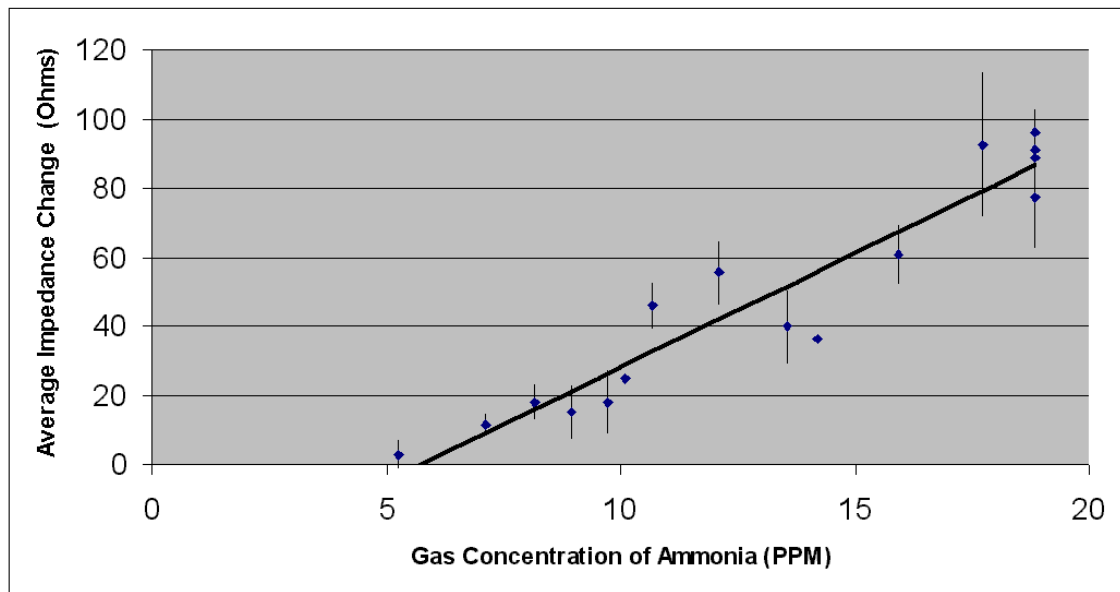


Figure 4-16: Lower onset of detection for an electroless gold coated gas sensor

The results from 16 groups of 30 gas pulses are given in Figure 4-16. Vertical bars are the standard deviation of the individual gas responses during the entire run. The entire run sequence was taken over a five day period with retrials at 19 ppm taken at the start of each day. The screening criterion outlined throughout this chapter has been performed on these results. All experiments below 5 ppm failed this benchmark and were subsequently not included (6 trials in total). A linear regression curve fit has also been correlated to the data. The equation for this linear approximation is:

$$y = 6.6058 x - 37.889$$

[Equation 4-3]

From this equation, one can observe that the sensitivity for this device to ammonia is 6.606 Ω /ppm. By repeating the LOD analysis as outlined in Chapter 3, a standard deviation of 9.60 Ω was obtained for the 480 gas pulses referenced to the linear average. Once this deviation was obtained, one simply doubles the value, substitutes the solution back into equation 4-3 for y, and solves for concentration level “x.” For this case, the lower onset of detection for this device under ammonia flow was 8.60 ppm.

As one can see, the gas pulsing mechanisms can be simply applied with variations in concentration to determine the lower onset of detection. Similar to other applications of the gas pulsing method, the number of tests performed over a given period of time has been dramatically increased. Also baseline drift issues have been systematically screened, and responses below the zero crossing are more easily identified and removed. It must be noted, however, that this lower onset of detection is interwoven into the selected method. This measurement is actually the ability to measure a response of 30

seconds of gas followed by 30 seconds of nitrogen for this particular device. If the lower onset of detection were instead references to the saturated response of the device, a fundamental lower value for the LOD would be obtained. In order to acquire such a metric, however, fundamental improvements in the reversible response of the device would be required.

4.3.2 Thermal and gas fluctuation

Give the relative sensitivity of porous silicon gas sensors to temperature variation, several experiments were conducted to determine the correct operating temperature for the device. Based upon results from the Figaro gas sensor^{ix} and other devices previously described, improved response kinetics were anticipated with increased temperature. To verify this possibility, the gas sensor was mounted on top of resistive heater (refer Figure 2-9). With the gas pulsing technique, experiments were performed from 22 °C to 100 °C. The elevated temperature experiments demonstrated a marked decrease in the sensitivity of the device. Table 4-5 outlines the results from this inspection. As one can see, the gas response (ΔR) of the device was reduced from 31 Ω for the room temperature case to less than 5 Ω for the case of the 100 °C tests. At the same time, 100 °C tests revealed no hysteresis between response and recovery. Additionally, the baseline during the measurements was flat relative to the low temperature experiments. This indicated a rapid response from the device at elevated temperatures. Finally, in a manner characteristic of silicon, the baseline resistance of the sensor was inversely correlated to the device's temperature.

Table 4-5: Results from elevated temperature testing of a porous silicon gas sensor

Temperature	Measured Gas Response	Average Impedance (baseline)	Steady after 30 Pulses
105.4 °C	4.88 +/- 2.18	650.6 Ω	Yes
80.4 °C	6.31 +/- 2.22	737 Ω	Yes
49.1 °C	10.88 +/- 4.30	1172 Ω	Yes-converging
33.4 °C	22.06 +/- 3.23	1793 Ω	Yes-converging
22 °C	31.48 +/- 5.19	2744.8 Ω	Convergence initiated

In order to determine a possible source of the sensitivity change in the porous silicon device, impedance sweeps were conducted across the pads and through the thickness of the wafer for a range of temperatures. These experiments revealed that the through impedance of the device was decreased from approximately 10,000 ohms (for the case of room temperature porous silicon) to approximately 3000 ohms for the case of silicon at 100°C. An inspection of the device's geometry illustrates why this effect is problematic. The separation distance between the two gold pads was approximately 3-4 mm. Conversely the thickness of the device was approximately 350 μm . Since the backside was uniformly coated with aluminum, the resistance across the backside length was negligible, and a secondary current pathway existed. As the impedance of the bulk silicon decreases, the ratio of current that traveled through the porous silicon decreased.

REFERENCES

- ⁱ G. Wang, Modification of vapor sensitivity in ellipsometric gas sensing by copper deposition in Porous Silicon, *Sensors and Actuators B*, 4263 (2002) 1-9
- ⁱⁱ S. Zangoie, R. Bjorklund, H. Arwin, Vapor Sensitivity of thin porous silicon layers, *Sensors and Actuators B* 43 (1997) 168-174
- ⁱⁱⁱ L Pancheri, C. Oton, Z. Gaburro, G. Soncini, L. Pavesi, Very sensitive porous silicon NO₂ sensor, *Sensors and Actuators B*, 6974 (2003) 1-3
- ^{iv} Gole, James L., DeVincentis, Julie A., Seals, Lenward Seals, Peter Lillenhei, S. M. Prokes, David Dickson, Chloride salt enhancement and stabilization of the photoluminescence from a porous silicon surface, *Physical Review B* 61-8 (February 2000) 6515-6531
- ^v S Prokes, W Carlos, L Seals, J Gole, Defect study of light-emitting HCl-treated porous silicon, *Physical Review B*, 62-3 (July 2000) 1878-1882
- ^{vi} J Gole, L. Seals, P Lillehei, Patterned Metallization of Porous Silicon from Electroless Solution for Direct Electrical Contact, *Journal of the Electrochemical Society*, 147-10 (2000) 3785-3789
- ^{vii} L Seals, J Gole, Laam Tse, P Hesketh, Rapid, reversible, sensitive porous silicon gas sensor, *Journal of Applied Physics*, 91-4 (February 2002) 2519-2523
- ^{viii} J. Gole, L. Seals, P Lillehei, Patterned Metallization of Porous Silicon from Electroless Solution for Direct Electrical Contact, *Journal of the Electrochemical Society*, 147-10 (2000) 3785-3789
- ^{ix} F. Sarry, M. Lumbreras, Discrimination of carbon dioxide and forane R134a using Figaro-type sensors TGS 832, *Sensors and Actuators B*, 57 (September 1999) 142-146

CHAPTER FIVE

CONCLUSIONS

The effort to characterize the porous silicon gas sensor has rendered both process and technology innovations. A novel parametric method for the analysis of a gas response has been designed, evaluated, and implemented. With this technique, small amplitude gas responses were successfully extracted from drifting baselines. This method was able to overcome common noise sources such as temperature and pressure. The total test time for sensor evaluation process was reduced from hours to less than 30 minutes. Finally, this technique has the potential to serve as a process improvement for a broad class of sensors spanning numerous functional areas.

Improvements in the device itself were demonstrated through an investigation of the performance metrics. The lower exposure limit to NH_3 for the porous silicon gas sensor was reduced from 50 ppm to 8.5 ppm. Stability was improved, yield increased, and unique selectivity to carbon monoxide was obtained. Furthermore, a process of electroless deposition of gold and tin was achieved, and the results further improved the device. In all, these efforts steer the porous silicon gas sensor closer to target commercial application as a rapid, reversible, portable environmental sensor.

APPENDIX A

FABRICATION PROCESS

Fabrication of the Porous Silicon Gas Sensor takes place in both the GT MiRC and the GT School of Physics. The sensors are constructed on a two-inch test-grade one-side polished p-type (100) wafer. The resistivity of the wafer is between 1 and 20 Ω -cm. Fabrication begins with the deposition of a conductive Aluminum layer on the unpolished side of the wafer₁. The presence of this coating enhances the uniformity of the PS-etch process₆. A Silicon Carbide layer is next deposited on the polished surface of the wafer₂. Photolithography is used to define a pattern on the Silicon Carbide with a protective coating of S1827 photoresist₃. A RIE plasma etch removes the unprotected Carbide, leaving windows to the exposed silicon wafer₄. The remaining photoresist is removed and the wafer is cleaned next, in preparation for the etching₅. An electrochemical Porous Silicon etch process produces a thin (0.1-10 μ m) layer in the windows of silicon exposed through the application of a current density₆. The reaction takes place in an electrochemical etching solution consisting of 0.1M HF, 0.1M H₂O, and 1M TBAP in MeCN with a Pt counter electrode. A second photolithographic procedure defines the location of electrodes on the etched Porous Silicon film₇. An electroless gold deposition is used to coat the pores with a thin layer of gold which provides better electrical contact₈. Ebeam evaporation deposits a 3000Å layer of Gold to provide a contact to the device via a probe station₉. Finally, the second masking layer is removed by a rinse in Methanol, thus forming individual conductometric devices.



1) DC sputterer coats backside of new wafer with Aluminum.



2) Unaxis PECVD deposits Silicon Carbide on wafer.



3) Mask #1 patterns the carbide over area to be PS-etched.



4) RIE removes Silicon Carbide from unmasked region.



5) Excess photoresist is removed.



6) Porous Silicon Etch creates gas-sensitive region.



7) Mask #2 patterns the electrodes for contact to sensor



8) Electroless Gold treatment makes good contact to PS.



9) E-beam deposits Ti/Au layer.



10) Methanol rinse removes photoresist and gold covering.

APPENDIX B

PROPOGATION OF UNCERTAINTY ANALYSIS

Governing Equation for Uncertainty Analysis

$$C_{tot} := \frac{V1 C1}{V1 + V2}$$

Partial derivative of function wrt V1

$$CV1 := \frac{C1}{V1 + V2} - \frac{V1 C1}{(V1 + V2)^2}$$

Partial derivative of function wrt V2

$$CV2 := - \frac{V1 C1}{(V1 + V2)^2}$$

Partial derivative of function wrt C1

$$CCI := \frac{V1}{V1 + V2}$$

Performing Uncertainty Analysis with experimental conditions

$$\omega4 := \sqrt{.0001 \left(1000 \frac{1}{V1 + 100} - \frac{1000 V1}{(V1 + 100)^2} \right)^2 + \frac{1000000 V1^2}{(V1 + 100)^4} + \frac{400 V1^2}{(V1 + 100)^2}}$$

Units Note: C1 ppm, V1 & V2 SCCM, omega1 SCCM, omega2 SCCM, Omega3 ppm, omega4 SCCM

Which can be simplified to:

$$\omega4 := 20 \sqrt{\frac{2500 + 12500 V1^2 + V1^4 + 200 V1^3}{(V1 + 100)^4}}$$

APPENDIX C

FEATURES OF TEST MATRIX

Device #	Impedance	Frequency	PL	PS Length	Light Gray	Black	Gp #	Treatments
3.2.1 # D	728	Flat	0.75	3 mm	0.5	0.5	1	EP # 4
3.2.1 # E	3440	Flat	0.25	2 mm	0.75	0.25	1	EP # 5
3.2.3 # 11	574	Flat	0	2 mm	0	0	1	
J 3.2.4 #7	1830	Flat	0.5	3 mm	0.5	0.5	1	
J 3.2.4 #9	718	Flat	0	3 mm	0.5	0.5	1	EP # 3
3.2.1 F	7930	Flat	0.5	3 mm	0.75	0.25	2	Treatment #5
3.2.1 # I	679	Flat	0.25	3 mm	0.5	0.5	2	Treatment #5, EL 2
2.2.4 # 2F	372	Flat	0.75	3 mm	1	0	2	Treatment #5
3.2.3 #4	145.6	Flat	0	poor liftoff	0.75	0.25	2	Treatment #5
3.2.3 #7	275	Flat	1	poor liftoff	0.5	0.5	2	Treatment #5
3.2.1 G	2530	Flat	0	3 mm	1	0	3	EL #3
3.2.3 #6	2760	Flat	0	3 mm	0.5	0	3	EL #3
PL #3	415	Unstable	1	3 mm	0	1	3	Device unfit for testing
3.2.3 #1	584	Flat	0.5	2 mm	0	0.5	3	Treatment #6, Tin EL #1
3.2.3 #10	224	Flat	0	poor liftoff	0	1	3	EL #2
3.2.1 # H	1400	Flat	0.5	2 mm	0.5	0.5	4	Treatment #3, EL #1
3.2.1 # B	3310	Flat	0	3 mm	1	0	4	Treatment #3, Tin #1
3.2.1 # C	623	Flat	1	3 mm	1	0	4	Treatment #3, Zn #2
3.2.3 #5	122.9	Flat	0	3 mm	0.75	0.25	4	Treatment #3, Zn #1
Wafer 13 #2	564	Flat	0.75	3 mm	0	1	4	Treatment #3
3.2.1 #A	1205	Flat	0.5	3 mm	0.5	0.5	5	Treatment #1, #4, EP # 1
PL #1	880	Flat	1	3 mm	0	1	5	Treatment #1, #4, pending
3.2.3 #8	305	Unstable	0	3 mm	1	0	5	Treatment #1, #4, ruined during EP
J 3.2.4 #4	1990	Flat	0.25	2 mm	0.5	0.5	5	Treatment #1, #4
J3.2.4 #6	796	Flat	1	2 mm	0.5	0.5	5	Treatment #1, #4, EP #2
3.2.3 #2	1442	Flat	0.5	3 mm	0.5	0	6	Treatment #6, EIPt batch 3
Wafer 13 #1	2360	Flat	0.75	3 mm	0	1	6	EL #2
J3.2.4 #1	453	Flat	0.25	3 mm	1	0	6	Treatment #6, TinEL #2, Treatment #8
3.2.3 #9	417	Flat	0	3 mm	0	0	6	Treatment #6
J 3.2.4 #8	5190	Flat	1	3 mm	0.5	0.5	6	Treatment #6

The preceding table provides features recorded for the porous silicon gas sensors that were grouped into a “test matrix.” The measurement criteria were:

Impedance - Measured with the impedance analyzer after manufacture with a 10mV AC wave

Frequency - Test to confirm that device was insensitive to frequency range from 100 – 50000 Hz

PL - Photoluminescence test evaluated with a ultraviolet light. 0 – No photoluminescence, 0.5 – partial photoluminescence, 1.0 – Brilliant photoluminescence

PS Length - Distance from one gold pad to the other on the surface

Light Gray/Black - Qualitative measure of appearance and damage on surface

Gp - Group number of devices. Similar devices had similar gas tests

Treatments - Provides a reference of specific cleaning treatments performed on individual devices

APPENDIX D

ORIGINAL TEST MATRIX

Device #	Ω	Test N2	CO B	CO A	NH3 B	NH3 A	NO B	NO A
3.2.1 # D	728							
3.2.1 # E	3440							
3.2.3 # 11	574							
J 3.2.4 #7	1830							
J 3.2.4 #9	718							
3.2.1 F	7930							
3.2.1 # I	679							
2.2.4 # 2F	372							
3.2.3 #4	145.6							
3.2.3 #7	275							
3.2.1 G	2530							
3.2.3 #6	2760							
PL #3	415							
3.2.3 #1	584							
3.2.3 #10	224							
3.2.1 # H	1400							
3.2.1 # B	3310							
3.2.1 # C	623							
3.2.3 #5	122.9							
Wafer 13 #2	564							
3.2.1 #A	1205							
PL #1	880							
3.2.3 #8	305							
J 3.2.4 #4	1990							
J3.2.4 #6	796							
3.2.3 #2	1442							
Wafer 13 #1	2360							
J3.2.4 #1	453							
3.2.3 #9	417							
J 3.2.4 #8	5190							
J 3.2.2 #2	538/628							
J 3.2.2 #3	630/820							
J 3.2.2 #5	2400/2470							
J 3.2.2 #6	2090/3000							
J 3.2.2 #8	3360/4680							
J 3.2.2 #9	2160/1370							

Description

Device # - Reference number for device in lab notebook

Ω – Measurement of resistance in ohms with a handheld Keithley multi-meter

Test N2- Nitrogen pulsing test as a reference for gas testing

B/A - Before (B) or after (A) an electroless or electroplating treatment

CO, NH₃, NO – The test gas for the experiment

APPENDIX E

LIST OF SUCCESSFUL ELECTROLESS COATINGS

Device #	Metal	Etch Name	Result
J3.2.4 #1	Electroless tin	TinEL #2	CO, NH3 Sensitivity
3.2.3 #1	Electroless tin	TinEL #2	CO, NH3 Sensitivity
3.2.1 #1	Electroless gold	EL 2	NH3 Sensitivity
3.2.3 #6	Electroless gold	EL 3	Slight NH3 Sensitivity
3.2.5 #4	Electroless gold	EL 6	NH3 Sensitivity